UNIVERSITY OF EASTERN PIEDMONT

"Amedeo Avogadro"

Department of Translational Medicine

PhD in Medical Sciences and Biotechnology

XXXVI Cycle

The identification of the PYRIN domain as mediator of IFI16-TLR4 interaction reveals a new class of endogenous inflammatory molecules

SSD: MED/07

Coordinator

Prof. Marisa Gariglio

Tutor

Prof. Marco De Andrea

Candidate:

Davide Lacarbonara

Table of contents

1. Abstract

Since the IFI16 protein was discovered in the early 1990s, it has been linked to a wide range of biological functions, such as cell cycle regulation, tumor suppression, apoptosis, DNA damage signaling, virus sensing, and virus restriction. In addition, a number of inflammatory diseases have been associated with abnormal IFI16 expression and release in the extracellular space. The current hypothesis is that overexpression of the IFI16 protein occurs in tissue compartments where it is not physiologically expressed during inflammation. As a result, IFI16 is released into the extracellular space, where it may function as a damage-associated molecular pattern (DAMP) that communicates with the Toll-like receptor 4 (TLR4) to initiate inflammation either on its own or in response to interactions with external molecules, including bacterial lipopolysaccharide (LPS). However, the precise molecular mechanisms underlying the extracellular function of IFI16 as DAMP remain to be elucidated. Here, human macrophages were used as target to define the proinflammatory activity of a panel of IFI16 recombinant domains or truncated proteins, along with the recombinant domains of other PYHIN family members. Moreover, surface plasmon resonance (SPR) experiments, 3D structure prediction and site-directed mutagenesis were used to identify the IFI16 moiety responsible for TLR4 binding and signaling. Collectively, our data provide compelling evidence that the proinflammatory activity of the IFI16 protein specifically lies within its N-terminal region and that the IFI16-PYRIN domain is involved in TLR4/MD2 binding and activation. Moreover, we expand previous knowledge by showing that the proinflammatory activity of the PYRIN domain is conserved among the PYHIN family members, and that specific amino acids located within the IFI16-PYRIN domain, and conserved across the family, are critically involved in their TLR4-mediated proinflammatory activity. These data strengthen the notion that specific PYRIN domains, including the one in the IFI16 N-terminus, behave as DAMP, and can be envisaged as targets of new drug candidates to be exploited for dampening the inflammatory response in different pathological settings.

2. Introduction

2.1 Innate immunity and the role of interferon

Maintaining homeostasis upon changes in the external and internal environments is a critical challenge for living organisms. Controlling variations in nutrition and water supply, physical stress, temperature changes, physiological stress, infections, and cancers are among them. The varieties of life and biological systems that can best deal with these obstacles have been chosen during billions of years of evolution. The removal of microorganisms and aberrant or damaged cellular material is a difficulty that all organisms undergo (Paludan et al., 2021). In addressing these challenges, the mechanisms for recognizing microbial structures play a crucial role. These mechanisms can be divided into two broad categories. First, there are hard-wired responses encoded by genes in the host's germ line, which comprehend pattern recognition receptors (PRRs) that bind unique pathogen-associated molecular patterns (PAMPs) shared by many microbes as well as toxins that are not present in the mammalian host. Included in PRRs are Toll-like receptors (TLRs), RIG-I-like receptors (RIG-Is), nucleotide-binding domain and leucine-rich repeat-containing receptors (NLRs), cyclic GMP-AMP (cGAMP) synthase, AIM2-like receptors (ALRs), and stimulator of interferon genes (STING) (Taguchi and Mukai, 2019).

Secondly, there are responses encoded by gene elements that somatically rearrange to assemble antigen-binding molecules with exquisite specificity for individual unique for each microbe, constituting innate immune response. Because the innate system's recognition molecules are widely expressed on a vast number of cells, this system is ready to respond quickly once an invading pathogen or toxin is met, and so comprises the primary host response (**Figure 1**) (Hillion et al., 2020). The second set of responses constitutes the adaptive immune response (not treated in this elaborate) (Chaplin, 2010).

In the innate immunity, when PRRs are activated, they initiate intracellular signaling cascades that result in the transcriptional production of proinflammatory cytokines, antiviral proteins and interferons (IFNs), that all work cooperatively to eliminate pathogens and infected cells. Concerning Interferons, these polypeptides, when released by infected cells, play three distinctive roles. They first generate cell-intrinsic antimicrobial states in infected and adjacent cells, limiting the transmission of infectious agents, notably viral infections. Second, they regulate innate immune responses by promoting antigen presentation and natural killer cell capabilities while suppressing pro-inflammatory pathways and cytokine generation (Ivashkiv and Donlin, 2014). Third, they stimulate the adaptive immune system, increasing the formation of antigen-specific T and B cell responses as well as immunological memory [(Katze et al., 2002);(Toshchakov et al., 2002)]. The IFN family consists of two main types of related cytokines: type I IFNs and type II IFNs. There are several type I IFNs all of which have significant structural similarity. These include IFN-α (which may be further classified into 13 distinct subtypes), IFN-β, IFN-δ, IFN-ε, IFN-κ, IFN-τ and IFN-ω1,2,3. In contrast, IFN-γ is the sole type II IFN. IFN-γ is a distinct cytokine from type I IFNs, but it was first categorized as an IFN because of its capacity to 'interfere' with viral infections, which is compatible with the original description of IFNs (Platanias, 2005). Type I and II IFNs bind to different cell-surface receptors found on the majority of cell types and promote gene expression via pathways involving the protein tyrosine kinases JAKs and STATs (signal transducers and activators of transcription) (**Figure 2**).

The binding of type I IFNs to their heterodimeric receptor IFNAR activates the receptor-associated protein tyrosine kinases JAK1 and TYK2, leading to activation of STAT1 and STAT2 and their interaction with the IFN transcription factor IRF9, resulting in the formation of the heterotrimeric complex IFN-stimulated gene factor 3 (ISGF3). ISGF3 binds to interferon-sensitive response elements (ISREs) in DNA (with the consensus sequence TTTCNNTTTC) and activates ISGs,

including genes producing antiviral proteins like Mx1 and OAS, as well as transcription factors like interferon-regulatory factors (IRFs). In the other hand, type II IFNs (*i.e.* IFN-γ) binds to its receptor called interferon gamma receptor 1 and 2(IFNGR1 and IFNGR2), it activates JAK1 and JAK2, as well as STAT1 homodimers. STAT1 binds to a specific DNA region known as a gamma-activated site (GAS; consensus sequence TTCNNNGGA) and directly activates a subset of ISGs, including chemokines like CXCL10 and transcription factors like IRFs. Given their unique basic signaling pathways type I and type II IFN signatures should be easily identifiable, revealing which IFNs are driving gene expression and, by extension, disease etiology. (Barrat et al., 2019). According to research anomaly-expressed IFN-Is and/or type I IFN-inducible gene signatures have been connected to pathophysiology, clinical symptoms, and disease activity in individuals with autoimmune disease (Jiang et al., 2020).

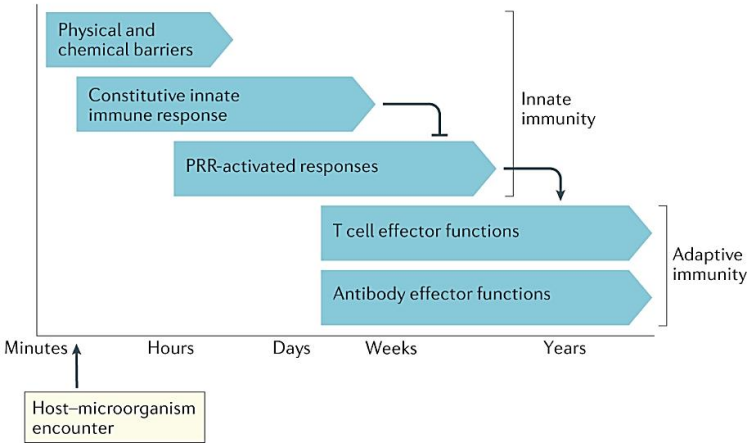

Figure 1. The relationship between time and immune response. Physical and chemical barriers provide a first line of defense. Constitutive innate immune systems activate as soon as a danger signal is recognized and use non-inflammatory processes that operate independently of PRRs to destroy dangerous bacteria and host molecules. This stops the infection from spreading and the buildup of PAMPs, restricting the activation of PRR-based inducible innate immune responses. When PRR-based immunity is engaged because of PAMP levels above a particular threshold, inflammation occurs, which promotes activation of the adaptive immune response mediated by T cells and antibodies. [Adapted from Paludan et al., 2021]

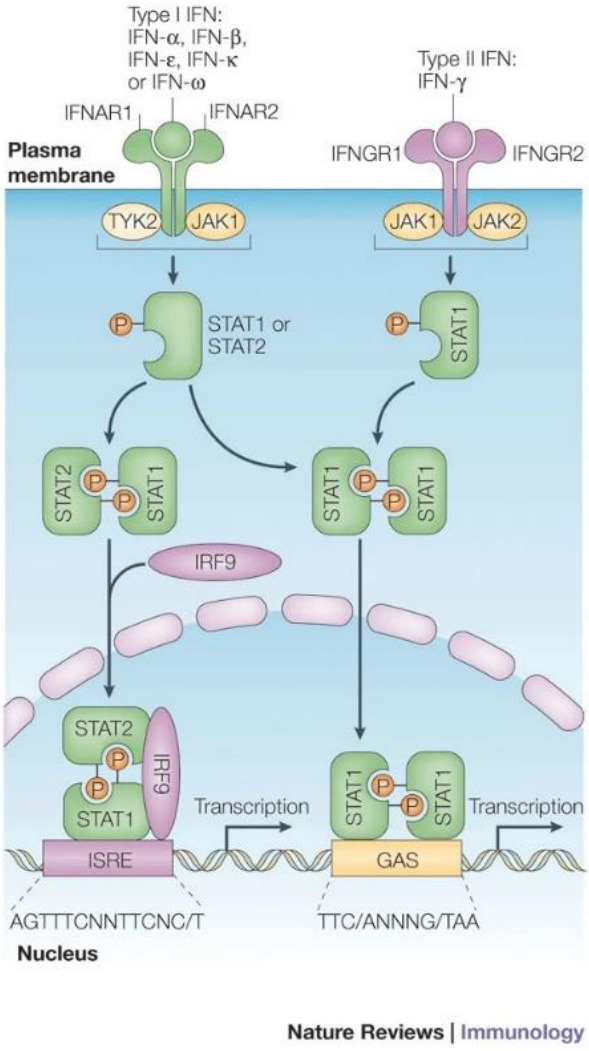

Figure 2. Signal transduction pathways of interferons (IFNs) on target cells. Distinct types of interferons bind to distinct receptors. Type II interferon receptors are tetramers, whereas types I are dimers [Adapted from Platanias 2005**]**

2.2 Toll-like receptors: a focus on the TLR4/MD2 pathway

The understanding of the ways the innate immune system uses to identify microbial components and its crucial function in the host's defense against infection has advanced quickly during the last ten years. The discovery of the Toll-like receptors (TLRs) in the mid-1990s contradicted the early theory that the innate immune system recognized microbes in an indiscriminate manner. Instead, it became clear that the innate immune system functions selectively, depending on germline-encoded pattern-recognition receptors (PRRs), including TLRs, which have evolved to identify pathogen-associated molecular patterns (PAMPs).

In detail, TLRs are type I transmembrane proteins containing ectodomains with leucine-rich repeats—that facilitate PAMPs recognition— transmembrane domains, and an intracellular Toll-interleukin 1 (IL-1) receptor domain (TIR) that serves as a platform for the recruitment of downstream signaling molecules (Balka and De Nardo, 2019). Humans and mice contain 10 and 12 functional TLRs, respectively, with TLR1-TLR9 being preserved in both species. Following the identification of the TIR domain-containing adaptor protein MyD88, TLR signaling pathways were thoroughly investigated. The discovery of further TIR domain-containing adaptors later on has demonstrated that different TLRs attract different adaptor molecules, eliciting immune responses that are specifically shaped on the microbe causing the infection. Toll-like receptor 4 (TLR4), in particular, was discovered as the long-sought receptor that reacts to bacterial lipopolysaccharide (LPS), a component of gram-negative bacteria's outer membrane that may induce septic shock (Kawai and Akira, 2010).Since then, various studies have identified a large number of other TLR4 agonist, both pathogen-derived as well as endogenous, such as HSP60, beta-amyloid, α-synuclein, fibrinogen, HMGB1, opioids and IFI16 [(Tian et al., 2013); (Apetoh et al., 2007); (Zhang et al., 2020); (Hughes et al., 2020); (Leavy, 2013); (Iannucci et al., 2020); (Long et al.,

2022)]. Considering LPS as the paradigmatic ligand of TLR4, the pathway shows multistep process involving different proteins (**Figure 3**). Human TLR4 alone, however, is not capable of sensing the presence of LPS (Akashi et al., 2000). The lipopolysaccharide-binding protein (LBP) was the first recognized actor in the recognition process [(Schumann et al., 1990); (Tobias et al., 1986)]. Extracellular LBP makes direct connections with the bacterial outer membrane (or LPS micelles) and changes the outer membrane, allowing the protein CD14 to extract a single molecule of LPS (Gioannini et al., 2004). CD14 is a free soluble extracellular protein or a glycosylphosphatidylinositol (GPI)-anchored protein found in plasma membrane nanodomains rich in cholesterol and sphingolipids known as rafts, which are thought to be TLR4 activation sites. TLR4-TLR4 dimerization happens at this stage as CD14 transfers LPS to Myeloid differentiation factor 2 (MD2), a key mediating protein (Akashi et al., 2000)**.** Furthermore, contact with the lipid A moiety of LPS causes structural modifications in MD2, generating hydrophilic connections between MD2 and TLR4, further stabilizing the newly formed complex. Indeed, a crystallographic analysis of the human TLR4/MD-2 complex with LPS bound revealed that five of the six acyl chains of LPS are buried in the hydrophobic pocket of MD-2, while the sixth interacts with TLR4 of another TLR4/MD-2 complex, and that dimerization of the TLR4/MD-2 complexes is strengthened by ionic bonds between the phosphate group of lipid A and the neighboring TLR4 molecule (Ciesielska et al., 2021). Upon TLR4-TLR4 dimerization, TIR domain containing adaptor protein (TIRAP) detects the TLR4 cytosolic Toll/IL-1R (TIR) domain of TRL4 C-term (Horng et al., 2001). TIRAP is a phosphoinositide-binding protein which contains a TIR domain and leads to the assembly of a supramolecular organizing center named myddosome (Kagan et al., 2014). TIRAP functions as a sorting adaptor that recruits MyD88 to TLR4 through its ability to interact with phosphatidylinositol-4,5-bisphosphate (PtdIns(4,5)P2), a component of the cellular membrane (Kagan and Medzhitov, 2006). From a molecular point of view, the TIR domain of TIRAP interacts

with the TIR domain of TLR4 forming a homodimer interaction (Valkov et al., 2011). This interaction is facilitated by tyrosine phosphorylation of TIRAP by several tyrosine kinases, including Bruton's tyrosine kinase (BTK) (Rajpoot et al., 2021). The homo- and heterotypic TIR–TIR domain interactions play a pivotal role in the assembly of the TLR signalosomes and in initiation of the signaling pathway, in fact they are central also in the binding between TIRAP and MyD88 (Ohnishi et al., 2009). Specifically, the adapter protein myeloid differentiation primary response protein 88 (MyD88) is a modular protein. Along with a TIR domain, it contains a death domain (DD) by which it recruits the IRAKs to the receptor complex via homotypic DD interactions. Activation of the IRAKs involves auto- and cross-phosphorylation, followed by K63-ubiquitination mediated by Pellino-3 (Gay et al., 2011). At this stage, the complex formed by TIRAP, MyD88, and multiple IL-1 receptor-associated kinases (IRAKs) are the proteins is called myddosome. The assembled myddosome recruits E3 ubiquitin ligase TRAF6, which triggers a signaling cascade involving TAK1 kinase and leading, through the phosphorylation and activation, among different protein, IκB kinases α/β (IKKα/β), to nuclear translocation of the NF-κB transcription factor. In addition, downstream of TRAF6 and TAK1, MAP kinases are phosphorylated to activate transcription factors AP-1 and CREB which lead to the expression of pro-inflammatory cytokine (such as TNF and IL6) and anti-inflammatory (such as IL10) (Ciesielska et al., 2021). The MyD88-dependent signaling described until now, is followed by internalization of TLR4. During endocytosis, PtdIns(4,5)P_2 concentrations on the invaginating membrane drop precipitously, thereby releasing the TIRAP-MyD88 complex from the invaginating membrane, which will ultimately become an early endosome. Concurrently, CD14 facilitates the internalization of LPS-TLR4/MD2 from plasma membranes into endosomes (Zanoni et al., 2011). This pathway is entirely subject to CD14 and MD2 (Tan et al., 2015) and is not dependent on TLR4-TIR domains, even though CD14 may increase LPS endocytosis in the absence of TLR4

(Dunzendorfer et al., 2004). Thus, the Loss of the TIRAP-MyD88 complex allows the TRAM-TRIF complex to engage the TIR domain of TLR4 on early endosomes and induce the second phase of signaling from an intracellular location. Now, the so called Triffosome is formed and TLR4 is found in the endosome, with the adaptor molecules translocating chain-associated membrane protein (TRAM) and TIR-domain-containing adapter-inducing interferon (TRIF) (Yamamoto et al., 2003). By analogy with TIRAP, TRAM may also function as a sorting adaptor to recruit TRIF to TLR4. TRAM is targeted to the plasma membrane by myristylation, and the present model of TRAM activation is that it recruits TRIF to the plasma membrane, where TLR4 is located. Moreover, TRAM contains a bipartite sorting signal that controls its trafficking between the plasma membrane and endosomes. The formed triffosome recruits TRAF3, which catalyzes its own K63-linked polyubiquitination. This leads to the activation of the TBK1 and the non-canonical IKK, IKKε, which in turn phosphorylates IRF3 (Dhillon et al., 2019). Finally, this lead to the expression of genes encoding type I interferon and CCL5/RANTES. In summary, TLR4 triggered by LPS promotes two sequential signaling pathways depending on receptor redistribution: the MyD88-dependent signaling is induced by TLR4 localized to the plasma membrane, whereas the TRIF-dependent signaling is triggered by TLR4 internalized in endosomes. The two pathways result in coordinated synthesis of pro- and anti-inflammatory mediators, contribute to NLRP3 inflammasome activation, control cell metabolism, trigger adaptive immunological responses, and other cell type-specific reactions.

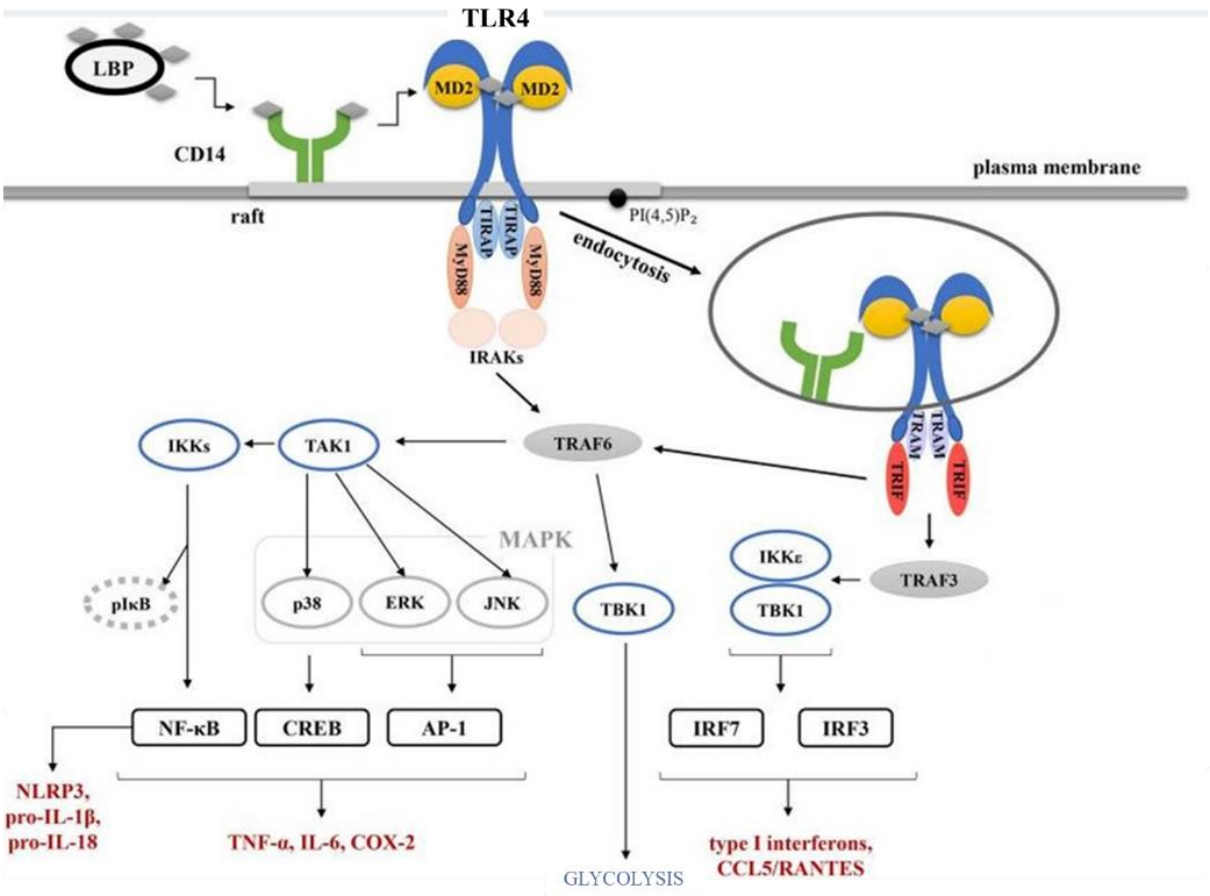

Figure 3. Paradigmatic LPS-induced TLR4 signaling pathway that promote inflammation. TLR4 stimulates the MyD88-signaling pathway at the plasma membrane, triggering the TRIF-dependent cascade after CD14-dependent endocytosis. TLR4 also contributes to the activation of the cytosolic NLRP3 inflammasome via activated NF-κB. [Adapted from Ciesielska et al., 2021]

2.3 The HIN200/PYHIN gene family

Interferons, previous described, have the property to regulate around 10% of the genes in the human genome (Schoggins, 2019), and most of them are indeed classified as IFN-stimulated genes. The HIN200/PYHIN (PYHIN hereinafter) gene family comprises most of them. Since the discovery of the first murine PYHIN gene in 1982 (*Ifi*202, coding for the p202 protein)in chromosome 1) (Samanta et al., 1982), a family of at least 13 genes in mice and four in humans have been cloned and described (Ludlow et al., 2005). The human PYHIN family members are: IFN inducible protein 16 (IFI16), myeloid cell nuclear differentiation antigen (MNDA), Absent in melanoma 2 (AIM2), and interferon-inducible protein X (IFIX); sometimes the PYRIN domain only protein 3 (POP3) has been also considered as a variant of the PYHIN family, which resulted from a HIN domain deletion (Khare et al., 2014) (**Figure 4**). In mouse, the most characterized proteins are p202, p203, p204, p205, p206, p207, Aim2/p210, and Mndal, plus several predicted proteins [(Fan et al., 2022)**;** (Cridland et al., 2012); (Landolfo et al., 1998); (Schattgen and Fitzgerald, 2011)**]**. PYHIN family is historically also named HIN200 because of the presence of either one or two consecutive 200-amino acid DNA binding HIN (for hematopoietic expression, interferon-inducible nature, and nuclear localization) domains (Ludlow et al., 2005). Although the overall structure of HIN domains is highly conserved, their superposition reveals significant flexibility in the loops in oligonucleotide/oligosaccharide binding (OB) folds [(Shaw and Liu, 2014); (Theobald et al., 2003)**]**. These HIN domains exhibit different surface charges, indicating distinct DNA-binding surfaces (Fan et al., 2022). Furthermore, the structural superposition of the HIN dsDNA complex reveals two distinctly different DNA-binding modes in the PYHIN family. To bind to dsDNA, AIM2 HIN, IFI16 HINB, p204 HINA, and HINB adopt the linker joining two OB folds and the

surrounding residues, whereas IFI16 HINA and p202 HINA use an opposing surface created by the loops of two OB folds that exhibited as well as a greater affinity for single-stranded DNA (ssDNA), the possibility to wrap, stretch, and form oligomers with ssDNA [(Fan et al., 2022); (Yan et al., 2008)]. With the exception of murine p202, the N-terminus of the PYHIN proteins contains a PYRIN domain. PYRIN has been identified in more than 20 human proteins with putative functions in apoptotic and inflammatory signaling pathways and it belongs to the Death Domain Fold (DDF) superfamily [(Liepinsh et al., 2003); (Liu et al., 2003); (Steward et al., 2009); (Bürckstümmer et al., 2009)]. DDF is a highly conserved protein interaction domain spanning approximately 90 amino acid residues (Stehlik, 2007) consisting of six anti-parallel alpha helices arranged in a Greek key structure (Steward et al., 2009). PYRIN is implicated in homo-oligomerization interaction (Yi, 2017); (Lum et al., 2019) and it is frequently involved in inflammation and immune responses (Piao et al., 2019). Especially, the engagement of PYRIN during stress stimuli leads to the assembly of an inflammasome, and the subsequent activation of caspase-1 and release of IL-1β and IL-18. An important step in this process is the recruitment of ASC to PYRIN. Via its N-terminal PYRIN domain, ASC enters a PYRIN-PYRIN homotypic interaction with PYRIN, which induces its oligomerization of micrometer-sized assemblies (Schnappauf et al., 2019). The PYHIN proteins have been demonstrated to localize to the nucleus and the cytoplasm. IFI16, IFIX, MNDA and p204 contain either a monopartite or bipartite nuclear localization sequence (NLS) and are predominantly found in the nucleus (Ludlow et al., 2005). Following activation, these proteins can be delocalized from the nucleus to the cytoplasm. AIM2 and p202, on the other hand, lack a NLS and are mostly, if not only, found in the cytoplasm. Because of their tissue-specific inducibility by IFN treatment, the PYHIN proteins have been linked to the regulation of growth and cell differentiation. The IFI16, p202, and p204 nuclear phosphoproteins are rather well defined in terms of their function in IFN action: these proteins have been shown to contribute in cell cycle

progression suppression, differentiation regulation, and cell survival. In general, PYHIN proteins are assumed to operate as scaffolds for the assembly of large protein complexes involved in transcriptional control (Ludlow et al., 2005). Finally, due to their ability to act as a new class of pattern recognition receptors (PRRs), some PYHIN proteins, including AIM2, IFI16 and p204, have been recently grouped as AIM2-like receptors (ALRs). PRRs act as sensors, detecting signals of infection or tissue damage in the extracellular and intracellular compartments. These PRRs, include the Toll-like receptors (TLRs), the retinoic acid inducible gene-like receptors (RLRs), the nucleotide oligomerization domain-like receptors (NLRs), and the AIM2-like receptors (ALRs) [(Kawai and Akira, 2009); (Unterholzner et al., 2010); (Gray et al., 2016); (Caneparo et al., 2018)].

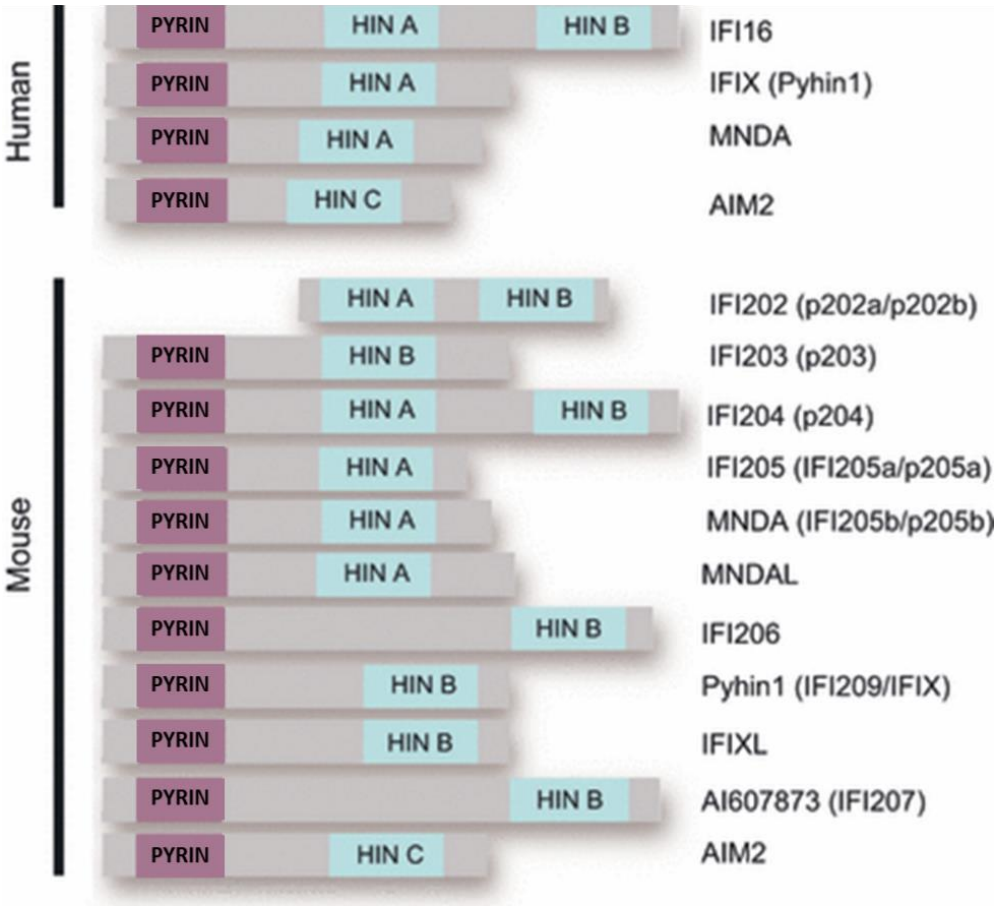

Figure 4. The human and murine PYHIN protein families. The PYHIN proteins consist of an N-terminal PYRIN domain and one or more HIN-200 domains which can be one of 3 subtypes (HINA, HINB, or HINC) based on their sequence [adapted form Schattgen and Fitzgerald, 2011].

2.4 The human interferon-inducible protein 16

The human interferon-inducible protein 16 (IFI16) was discovered in 1994, coded by a gene that was constitutively expressed in human lymphoid cell lines and inducible in myeloid cell lines following IFN-γ treatment or differentiation stimuli (Trapani et al., 1994). IFI16, like the other members of the PYHIN family, has a PYRIN domain at its N-terminus, which is well-known for promoting homotypic protein interactions **(Figure 5)**. The presence of the PYRIN was originally associated with a role of the protein in apoptosis, since it may regulate the activity of specific nuclear transcription factors that are involved in cell death commitment. Characteristically, IFI16 also contains the HINA and HINB domains, which are separated by a 116 amino-acid serine-threonine-proline (S/T/P) rich spacer **(Figure 5)**. The length of this spacer is controlled by alternative mRNA splicing, which results in three IFI16 isoforms called A, B, and C, respectively. In human fibroblasts, epithelial cells, keratinocytes, macrophages, and T cells, the B isoform is the most prevalent (Jakobsen and Paludan, 2014). IFI16 is expressed also in other cells, such as in CD34+ myeloid precursor cells and is seen in high concentrations in monocyte progenitors, peripheral blood monocytes, and throughout lymphoid development (Dawson et al., 1998). Furthermore, immunohistochemical analysis of normal human tissues indicated that IFI16 is expressed in a highly restricted pattern in selected cells within certain organs [(Gariglio et al., 2002); (Wei et al., 2003)]. Indeed, IFI16 has been found in epithelial cells of the skin, gastrointestinal system, urogenital tract, and breast glands and ducts. Its expression was shown to be prominent in stratified squamous epithelia, especially in basal cells in proliferative compartments, although it gradually diminishes in a more differentiated supra-basal compartment. Connective tissue staining was limited to scattered fibroblasts in the underlying dermis. Furthermore, IFI16 was found in all vascular endothelial cells from both blood and lymph channels.

IFI16 is an important player involved in innate immunity along with inhibition of cell cycle progression and in the regulation of apoptosis [(Caposio et al., 2007); (Li et al., 2021)**]**. Overexpression of IFI16 can lead to reduced cell proliferation and arrest in cell cycle progression at the G1-S phase transition. The interaction of IFI16 with p53 and pRb appears to cause IFI16-mediated growth arrest [(Aglipay et al., 2003); (Liao et al., 2011)]. Indeed, prostate cancer cell lines harboring functioning p53 and pRb were much more susceptible to IFI16's antiproliferative activities (Xin et al., 2003). In medullary thyroid cancer cells, IFI16 has also been identified as an important growth-specific effector of the cell extrinsic growth-inhibitory pathway of Ras/Raf signaling (Kim et al., 2005). Finally, IFI16 expression has been discovered to be altered in a variety of human cancers [(Azzimonti et al., 2004); (Fujiuchi et al., 2004); (Xin et al., 2003)]. In vitro experiments, including chemotaxis, matrigel invasion, tube morphogenesis, and cell cycle progression, have shown that IFI16 overexpression inhibits tube morphogenesis and proliferation of human endothelial cells (Raffaella et al., 2004). Overall, these findings suggest that IFI16 plays a role in the control of cell proliferation, differentiation, and angiogenesis. As mentioned before, IFI16 has a pivotal role in innate immunity and inflammation. Not only IFN-γ, but also other pro-inflammatory cytokines like IL-1b and TNFa, can considerably increase IFI16 expression (Mondini et al., 2007). Anti-inflammatory cytokines (*e.g.*, IL-4, IL-10, IL-13, and IL-17), on the other hand failed to stimulate IFI16 expression. The physiologic nuclear localization of IFI16 is regulated by a bipartite nuclear localization sequence (NLS) located at the protein's N-terminus (Li et al., 2012). In contrast, stress stimuli like UVB irradiation of human keratinocytes have been demonstrated that can promote the IFI16 translocation from nucleus to cytosol and eventually in extracellular space [(Cao et al., 2016); (Costa et al., 2011)]. IFI16 is peculiar due to the fact that it can shuttle between the cytoplasm and the nucleus and detect DNA from a variety of viruses, including dsDNA from herpes simplex virus type 1 (HSV-1), Kaposi sarcoma-associated herpesvirus (KSHV), and

human cytomegalovirus (HCMV) (Dell'Oste et al., 2015), and ssDNA or dsDNA from bacteria, [(Li et al., 2012); (Veeranki and Choubey, 2012)].

Overall, IFI16 is found mostly in the nucleus in many cells, functioning as a DNA sensor to identify pathogenic DNA and subsequently activating cytoplasmic inflammasome and innate signaling pathways to initiate an immunological response against pathogen invasion. Mechanistically, upon HSV-1 infection, IFI16 mainly detects HSV-1 genomic DNA in the nucleus and then translocate to the cytoplasm where it cooperates with cyclic GMP-AMP synthase (cGAS) to activate the endoplasmic reticulum protein stimulator of interferon genes (STING) to induce the expression of type I IFN through activating TBK1-IRF3 and NF-κB signaling pathways [(Almine et al., 2017)**;** (Iqbal et al., 2016)]. Furthermore, HSV-1 and other DNA viruses do not consistently increase IFI16 expression at the late stage of viral infection, and STING overexpression enhances IFI16 protein degradation at the late stage of infection. Both inducible and overexpressed IFI16 degradation are inhibited by the proteasome inhibitor MG132. These findings suggest that an internal mechanism regulates IFI16 accumulation to prevent excessive or continuous activation. It has been shown that STING, an IFI16 downstream adaptor protein, adversely controls the IFI16 protein level by promoting its K48-linked ubiquitination and degradation (Li et al., 2019). However, the exact pathways for IFI16-mediated nuclear pathogenic DNA detection, as well as the STING and inflammasome activation in the cytoplasm remain partially unexplored. During KSHV infection, it seems that the IFI16 mechanism of action is different. In this case, nuclear IFI16 detects and binds viral dsDNA before recruiting ASC and procaspase-1 to form an active inflammasome. Following that, the IFI16-inflammasome translocate to the cytoplasm, where the inactive procaspase-1 is then proteolitically converted into activated caspase-1 and where cleavage of IL-1 and IL-18 occur [(Kerur et al., 2011); (V. V. Singh et al., 2013)]. However not only the viruses nature can trigger a different pathway but also the nature of the cells. Indeed, while STING is

activated in macrophages and keratinocytes in response to viral infection, IFI16 increases cyclic guanosine monophosphate-adenosine monophosphate (cGAMP) production by cGAS only in macrophages, indicating cell specific roles for IFI16 in cooperating with the cGAS pathway. In CD4+ T cells, the HIV proviral DNA detection by IFI16 follows a different route. In this case, IFI16 forms an inflammasome with ASC to induce caspase-1-dependent pyroptotic cell death, leading to abortive infection of these cells and enhancing clinical development of AIDS (Monroe et al., 2014). Indeed, silencing of IFI16 or ASC with shRNA or inhibiting caspase-1 save CD4+ T cells from death. This finding might explain why CD4+ T cells die during HIV infection. As a transcriptional regulator, IFI16 can also limit viral genomic replication via epigenetic changes. By regulating restrictive histone modifications, IFI16 enhances the loading of nucleosomes and the insertion of heterochromatin marks on infected cell protein 0 (ICP0)-null HSV-1 chromatin to limit viral replication [(Johnson et al., 2014); (Orzalli et al., 2013)]. Upon KSHV infection and latency, IFI16 recruits the H3K9 methyltransferase SUV39H1 and GLP to the KSHV genome for silencing the KSHV lytic genes (Roy et al., 2019). Similarly, after HPV and HSV-1 infection, IFI16 increases the addition of heterochromatin marks and the removal of euchromatin marks on viral chromatin at both early and late promoters, hence limiting viral replication and transcription [(Lo Cigno et al., 2015); (Sodroski and Knipe, 2023)]. Finally, as a restriction factor, IFI16 prevents the transcription factor Sp1 from binding to the promoter region of the viral DNA polymerase gene (UL54), limiting viral genome replication during HCMV infection (Gariano et al., 2012). All in all, IFI16 may inhibit viral infections through four different mechanisms: 1) activation of the cGAS-STING-IFN pathway; 2) formation of inflammasomes; 3) epigenetic silencing of viral promoters, and 4) restricting access to host components essential for viral replication such as Sp1. This helps to explain why IFI16 is such a common target of immune evasion by a variety of viruses [(Chan and Gack, 2016); (Dell'Oste et al., 2015)]. Indeed, the HCMV protein pUL83 binds IFI16 and

prevents IFI16 oligomerization, blocking the STING-TBK1-IRF3 pathway from being activated (Li et al., 2013), whereas the protein pUL97 promotes IFI16 phosphorylation and delocalization to the cytoplasm of HCMV-infected cells (Dell'Oste et al., 2014). HSV ICP0 targets IFI16 for degradation [(Orzalli et al., 2012); (Cuchet-Lourenço et al., 2013)], whereas HPV E7 recruits the E3 ligase TRIM21 to ubiquitinate and degrade IFI16 to inhibit IL-1 production and pyroptosis in Hela and HaCaT cells (Song et al., 2020).

Out of all the many IFI16 functions that have been previously described, one that has recently been discovered by our group is that IFI16 behaves as a DAMP triggering inflammation through Toll-like receptor 4 (TLR4) activation (Iannucci et al., 2020). As mentioned before, IFI16 can translocate in the extracellular environment following stress stimuli (i.e., UVB irradiation or bacterial/viral infection) or upon tissue inflammation. Here, alone or upon binding to subtoxic concentrations of strong TLR4-activating lipopolysaccharide (LPS) variants, IFI16 can bind TLR4 and induce inflammation (Iannucci et al., 2020). This opens a new perspective in the study of extracellular IFI16, its potential role in autoimmune and autoinflammatory diseases, and how to exploit it as a therapeutic target.

Figure 5. Schematic illustration of IFI16 protein structure. Residues 1-83 constitute the N-terminal PYRIN domain (dotted box). The solid-shaded boxes denote the HINA (residues 192-393) and the HINB (residues 515-710) domains. Diagonal stripped bars indicate the S/T/P-rich seven amino acid repeat motifs between the two HIN domains, resulting from alternative splicing of the gene. Vertical bars indicate the nuclear localization sequence (NLS). The conserved MFHATVAT motifs are also shown. Numbers located below each diagram represent amino acid positions (Adaptation from Dell'Oste et al., 2015)

2.5 Damage-associated molecular patterns - DAMPs

One of the essential properties of the immune system, leading to immunological responses against pathogens, is the ability to discriminate between "self" and "non-self". However, the innate immune response can be engaged even when there is no infection, as introduced in 1994 by Polly Matzinger with the so-called "danger theory" which claimed that danger signals from stressed or damaged cells can trigger immune responses (Matzinger, 1994). This notion led to the identification of a variety of endogenous molecules generated after tissue injury, which were identified as damage-associated molecular patterns (DAMPs) (Land, 2003). DAMPs are ordinarily sequestered intracellularly and hence remain unrecognized by the immune system under normal physiological settings. However, dying cells following cellular stress or damage might release these molecules into the extracellular environment, independent of pathogen infection, resulting in sterile inflammation (Chen and Nuñez, 2010). Like pathogens, DAMPs may in turn activate both non-immune cells, such as epithelial cells, endothelial cells, and fibroblasts, as well as innate immune cells, such as neutrophils, macrophages, and dendritic cells (DCs). Once activated, these cells produce a variety of cytokines and chemokines, which attract inflammatory cells and trigger adaptive immune responses **(Figure 6)** (Gong et al., 2020). Furthermore, certain DAMPs can directly activate adaptive immune cells. Although sterile inflammation is necessary for tissue repair and regeneration, unresolved chronic inflammation is harmful to the host and can result in metabolic disorders, neurological diseases, autoimmune diseases, and cancer. Numerous novel DAMPs have been found in distinct damage conditions throughout the last 20 years and their number is still increasing. Furthermore, DAMPs differ widely depending on the kind of cell (epithelial or mesenchymal) and wounded tissue. They can arise from extracellular matrix degradation processes during tissue injury and include hyaluronan, biglycan and tenascin C, among

the others, or from intracellular compartments, as in the case of high-mobility group box 1 (HMGB1), histones, S100 proteins, heat-shock proteins (HSPs), oxidized phospholipids (oxPAPC,) and plasma proteins (e.g., fibrinogen, Gc-globulin, serum amyloid A or SAA) [(Tsung et al., 2005); (Schaefer, 2014); (Smiley et al., 2001); (Zhou and Binder, 2014); (Sokolove et al., 2010); (Sohn et al., 2012); (Ye and Sun, 2015); (Zanoni et al., 2017)]. A list of well-characterized DAMPs, along with their origin and receptors, is shown in **Table 1** (Roh and Sohn, 2018). Along with the discovery of new DAMPs, numerous related receptors have been also discovered. As a major broad distinction, released nucleic acids can activate transmembrane TLR3, TLR7, TLR8 and TLR9, whereas released intracellular proteins can activate mostly TLR2 and TLR4. Among these, TLR4 is of special importance since it can be bound and activated by a large number of DAMPs. As a consequence, several therapeutic approaches are being developed to inhibit TLR4 activation in a variety of diseases [(Garcia et al., 2020); (Romerio and Peri, 2020)]. Tenascin-C, an extracellular matrix glycoprotein linked with tissue damage and fibrotic activity (Ummarino, 2016), has been shown to stimulate the creation of pro-inflammatory cytokines in macrophages via its fibrinogen-like globe (FBG), and TLR4 neutralizing antibodies, genetic deletion of TLR4, or production of a dominant negative MyD88 mutant, totally abrogate Tenascin-C proinflammatory activity (Midwood, 2009). Subsequential analyses have also identified tenascin-C specific sites that directly and cooperatively interact with TLR4 through its fibrinogen-like globe domain and (Zuliani-Alvarez et al., 2017). Levels of Tenascin-C and the delivered persistence state of inflammation are elevated in Systemic sclerosis (SSc) skin and in circulation (sera) making it a possible biomarker of skin and lung fibrosis in SSc and related diseases[((Bhattacharyya et al., 2022)**;** (Bhattacharyya et al., 2016)].

In 1973, Ernest Johns, Graham Goodwin and colleagues extracted a set of nonhistone proteins from calf thymus chromatin (Goodwin and Johns, 1973). Subsequently, these proteins were named “high

mobility group" (HMG). Since then, HMGB1 has become one of the most studied DAMPs able to bind TLR4/MD2 (Yang et al., 2010). HMGB1 proinflammatory activity was also demonstrated in necrotic wild-type (WT) or HMGB1-knockout (HMGB1-KO) cells, demonstrating that TLR4 activation was not caused by bacterial contaminants in the recombinant protein. Surface plasmon resonance (SPR) analysis revealed that the HMGB1-TLR4-MD2 interaction is initiated by HMGB1-TLR4 binding via the HMGB1 A-box domain (high affinity and slow off-rate), and then the HMGB1 B-box domain binds to MD2 (low affinity but extremely slow off-rate) once in proximity (He et al., 2018). Despite this, HMGB-1 is a pleiotropic DAMP because it binds to and activate a variety of receptors, including TLR2 and a non-PRR, namely the receptor for advanced glycation end products (RAGE, (Yang et al., 2020). The evidence that HMGB1 can bind also a non-PRR (unlike PAMPs), suggested that it may be detected by a variety of receptors to trigger inflammation. DAMPs can stimulate the innate immune response because, following an injury, they contribute to support tissue repair and regeneration [(Pandolfi et al., 2016); (Vénéreau et al., 2015)]. However, the lack of inflammation control may lead to autoimmune disease. For instance, a wide range of endogenous TLRactivators, including heat shock proteins, HMGB1, and Tenascin-C, has been observed in the synovia of rheumatoid arthritis (RA) patients but not in those from patients with normal joints or in non-inflamed synovia from osteoarthritis (OA) patients [(Baillet et al., 2010); (Goldstein et al., 2007); (Midwood et al., 2009)]. Moreover, again high levels of HMGB1 and Tenascin-C circulate in the serum of septic patients [(Andersson and Tracey, 2003); (Li and Lu, 2021)], and high serum concentrations of DNA-containing immune complexes are associated with systemic lupus erythematosus (SLE) (Tian et al., 2007). Endogenous TLR activators are often associated with disease activity. In *in vivo* experimental inflammatory disease models, where high levels of circulating DAMPs were not found, the administration of exogenous DAMPs was sufficient to initiate inflammation. As an example, intra-articular injection of the TLR4

activators tenascin-C has been shown to induce joint inflammation in wild type but not in TLR4-null mice [(Gondokaryono et al., 2007); (Midwood et al., 2009)]. Interestingly, blocking DAMP activity using neutralizing antibodies, small compounds, or genetic deletion can improve disease *in vivo*, indicating that DAMP play a critical role in promoting chronic inflammation and pointing to DAMP inhibition as a necessary therapeutic intervention.

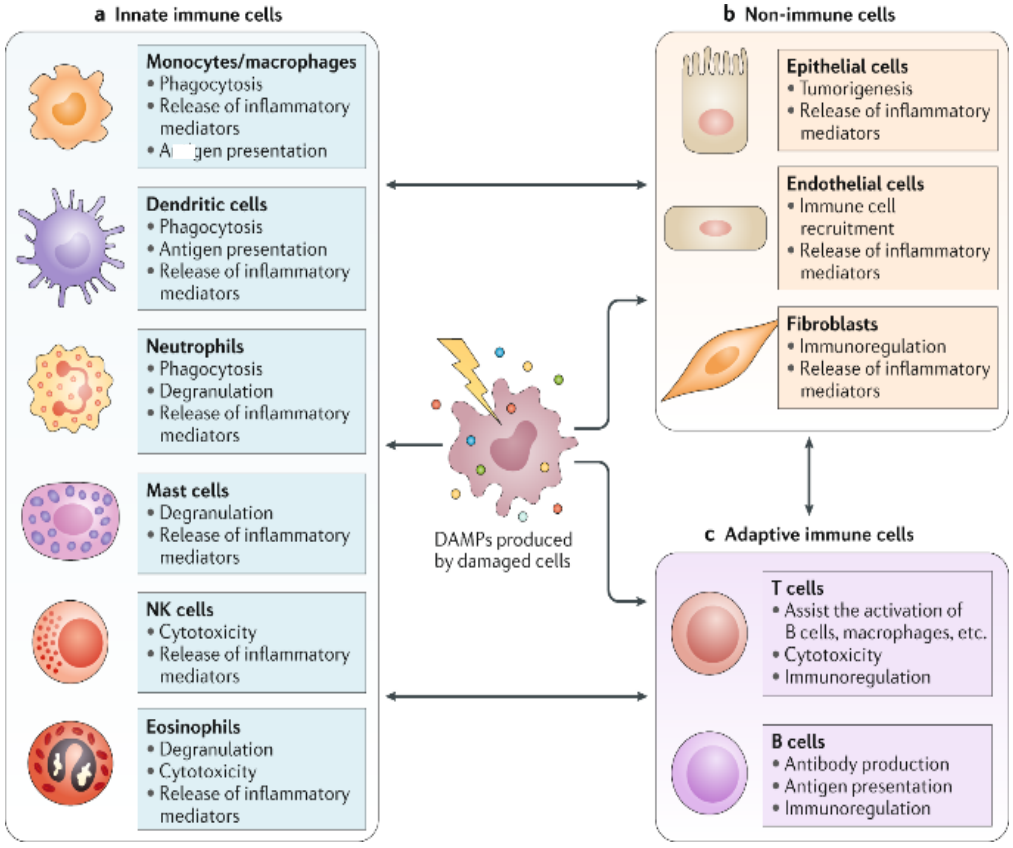

Figure 6. Damage-associated molecular patterns (DAMPs) can initiate innate and adaptive immune responses by targeting various types of cells [adapted from Gong et al., 2020]

Origin		Major DAMPs	Receptors
Extracellular matrix		Biglycan	TLR2, TLR4, NLRP3
		Decorin	TLR2, TLR4
		Versican	TLR2, TLR6, CD14
		LMW hyaluronan	TLR2, TLR4, NLRP3
		Heparan sulfate	TLR4
		Fibronectin (EDA domain)	TLR4
		Fibrinogen	TLR4
		Tenascin C	TLR4
Intracellular compartments	Cytosol	Uric acid	NLRP3, P2X7
		S100 proteins	TLR2, TLR4, RAGE
		Heat shock proteins	TLR2, TLR4, CD91
		ATP	P2X7, P2Y2
	Nuclear	Histones	TLR2, TLR4
		HMGB1	TLR2, TLR4, RAGE
		HMGN1	TLR4
		IL-1α	IL-1R
		IL-33	ST2
		SAP130	Mincle
		DNA	TLR9, AIM2
		RNA	TLR3, TLR7, TLR8, RIG-I, MDA5
	Mitochondria	mtDNA	TLR9
		TFAM	RAGE
		Formyl peptide	FPR1
		mROS	NLRP3
	ER	Calreticulin	CD91
	Granule	Defensins	TLR4
		Cathelicidin (LL37)	P2X7, FPR2
		EDN	TLR2
		Granulysin	TLR4
	Plasma membrane	Syndecans	TLR4
		Glypicans	TLR4

ER, endoplasmic reticulum; EDN, eosinophil-derived neurotoxin.

Table 1. List of the most characterized DAMPs and their receptors [adapted from Roh and Sohn, 2018]

2.6 IFI16 as a DAMP in autoinflammatory/autoimmune diseases

As described, type I IFN have several activities, including pathogenetic roles in the beginning and maintenance of autoimmune diseases. Abnormally expressed type I IFNs and/or type I IFN-inducible gene signatures have been connected to pathophysiology, clinical symptoms, and disease activity in individuals with autoimmune illnesses (Jiang et al., 2020). Indeed, high IFN serum levels and increased expression of IFN-stimulated genes due to an abnormal response to self-DNA recognition process have been found (Fu et al., 2022). This lead to the assumptions that the IFN-inducible PYHIN proteins have a role in the etiology of autoimmune and autoinflammatory diseases. Caneparo *et al*. found abnormal IFI16 expression (overexpression or de novo expression) in colonic biopsies of inflammatory bowel disease (IBD) patients [*i.e.* Crohn's disease (CD) and ulcerative colitis (UC) patients] compared to healthy controls [(Caneparo et al., 2016);. IFI16 is usually expressed in endothelium and inflammatory cells in the intestine lamina propria, however in IBD patients, colonic IFI16 expression is significantly greater and visible also in epithelial cells. Systemic lupus erythematosus (SLE) is another condition with abnormal IFI16 expression [(Costa et al., 2011); (Mondini et al., 2007); (Awad et al., 2023); (Fu et al., 2022)]. Indeed, the distribution pattern of IFI16 in the skin differed significantly between SLE patients and healthy donors. IFI16 expression was limited to the nucleus in normal skin, with keratinocytes showing clear positive staining. In contrast, in SLE biopsies, IFI16 staining in keratinocytes was stronger and intense positive in nuclei but it was also found in the upper epidermal layers, indicating a keratinocyte specific cytoplasmic IFI16 translocation in pathological setting. Furthermore, increased expression levels of IFI16 were observed also in PBMC from SLE patients. Expression of IFI16 were found to be closely associated with SLE Disease Activity Index (SLEDAI) scores and anti-dsDNA antibody titres (Fu et al., 2022). Finally, substantial evidence suggests that abnormal IFI16

expression can be found in the skin of patients with systemic sclerosis (SSc) (Mondini et al., 2006) or psoriasis [(Cao et al., 2016); (Chiliveru et al., 2014); (Tervaniemi et al., 2016)], as well as salivary epithelial cells and infiltrating lymphocytes of Sjögren's syndrome (SjS) patients. The localization of IFI16 became fundamental to investigate its implication in autoimmune disease. Several studies have found that IFI16 is mislocalized from the nucleus to the cytoplasm and eventually released in response to viral infection, stress, or pathological circumstances [(Antiochos et al., 2019)**;** (Bawadekar et al., 2015)**;** (Orvain et al., 2020)]. In particular, it has been demonstrated to be released into the exosomes of cells infected with Epstein-Barr virus (EBV) or KSHV [(Ansari et al., 2013); (Vivek Vikram Singh et al., 2013)]. Similarly, during the late stages of HCMV infection, IFI16 is hijacked and integrated into freshly constructed egressing virion particles before exiting the host environment (Dell'Oste et al., 2014). Furthermore, after UVB exposure, IFI16 mislocalization and release was seen in experimental models of keratinocyte monolayers and human skin explants (Costa et al., 2011). Finally, serum circulating IFI16 has been found in a variety of autoimmune diseases including SSc, rheumatoid arthritis (RA), SLE, SjS, and psoriatic arthritis (PsA) [((Alunno et al., 2015); (Alunno et al., 2016); (De Andrea et al., 2020); (Gugliesi et al., 2013)].

The extracellular presentation of a protein that is normally only expressed in the nucleus of cells induces the production of autoantibodies. Indeed, IFI16 autoantibodies have been found in a number of autoimmune/autoinflammatory conditions. Firstly, Seelig *et al.* discovered anti-IFI16 antibodies in a serum containing antinuclear antibodies (ANAs), anti-SSA/Ro, and anti-SSB/La autoantibodies (Seelig et al., 1994). These researchers discovered anti-IFI16 antibodies in 29% of 374 SLE patients' sera using immunoblotting on recombinant IFI16 produced as an MS2-polymerase fusion protein). Moreover, Antiochos *et al.* demonstrated that IFI16 autoantibodies present in SLE are frequently associated with anti-AIM2 and anti-dsDNA antibodies, introducing

the concept that also the PYHIN members could be implicated in the pathogenesis of autoimmune diseases (Antiochos et al., 2022)**.** In this regard, Uchida *et al.* discovered anti-IFI16 antibodies in 70% of patients with both primary and secondary SjS using a different approach, such as serological antigen analysis by recombinant cDNA expression cloning (SEREX) (Uchida et al., 2005). Instead, for SSc patients, solid-phase enzyme-linked immunosorbent assay (ELISA) has been used and thanks to recombinant purified His-tagged IFI16 protein as antigen, Mondini *et al.* identified anti-IFI16 antibodies in 21% of the ill patients (Mondini et al., 2006). By using the latter technique, anti-IFI16 autoantibodies were then found SLE (Caneparo et al., 2013), SjS [(Alunno et al., 2015); (Baer et al., 2016)], in IBD (Caneparo et al., 2016), RA (Alunno et al., 2016), and PsA (De Andrea et al., 2020) patients. Overall, these findings suggest that IFI16 has a damaging role in autoimmune/autoinflammatory diseases providing reasons for further research into IFI16 extracellular activity.

2.7 Herpes simplex viruses (HSV)

Herpesviruses are a group of viruses that are extremely invasive and extensively distributed, infecting humans and other vertebrates. They have a large double-stranded DNA genome, stringent host specificity, and the ability to establish latency and lifetime persistence following spontaneous reactivation (Fields, 2013). Herpesviruses are classified into three subfamilies based on shared biological traits and gene sequences: alpha-, beta-, and gamma-herpesvirinae. In particular, herpes simplex virus type 1 (HSV-1) is a member of the Alphaherpesvirinae subfamily and it is neurotropic human pathogen that is transmitted mainly by intimate contact between infected and susceptible individuals, and that causes labial, ocular, or genital infections. Primary infection usually occurs during childhood: an estimated 3.7 billion people under age 50 (67%) are infected with HSV-1 worldwide [(Word health organization data update April 2023); (Gopinath et al., 2023)]. It has a linear double-stranded DNA (dsDNA) genome which contains ~80 genes (Macdonald et al., 2012). Electron microscopy (EM) and electron tomography (ET) studies have revealed that virus particles have a spherical shape, with diameter ranging from 155 to 240 nm, each containing an icosahedral capsid with a diameter of 125 nm, which contains the viral DNA (Laine et al., 2015). Outside the capsid HSV-1 has a characteristic particle structure that implicates proteinaceous tegument layer, and a lipid envelope which contains glycoproteins (**Figure 7**). In addition to preserving the genome, the capsid aids in the retrograde trafficking in the host cell, the release of the viral genome into the host cell nucleus, and the mediation of nascent capsid egress from the cell nucleus. Capsids are made up of the primary capsid protein, VP5, as well as the UL6 portal complex, VP23, VP19C, VP26 and other VP protein reported in **Figure 7**. Finally, higher occupancy of the capsid-vertex-specific component (CVSC) contains UL17, UL25, and the suspected UL36 proteins (pUL36) and UL37 protein (pUL37), which are positioned around the exterior of each capsid vertices and have

been linked to DNA packing and capsid maturation (Wang et al., 2018). Virus binding and entry into host cells are mediated by specific interactions between viral glycoproteins (gB, gC, gD, and the gH/gL complex) and receptors on target cells, such as the herpesvirus entry mediator (HVEM), heparan sulfate moieties, and the cell-adhesion proteins nectin-1 and nectin-2 **(Figure 8)** [(Hilterbrand and Heldwein, 2019); (Marcocci et al., 2020)]. Initial attachment to the plasma membrane occurs through binding of glycoprotein B (gB) and gC to glycosaminoglycans (GAG). Although HSV gG binds to GAGs, its significance in viral attachment is unknown. Following binding to GAGs, gD interacts with various entrance receptors, including herpesvirus entry mediator (HVEM), nectin-1 and -2, and 3-O-sulfated HS. Several studies have found that interactions between gB and immunoglobulin-like type 2 receptor α (PILRA), myelin-associated glycoprotein, and non-muscle myosin IIA have a role in HSV entrance [(Satoh et al., 2008); (Suenaga et al., 2010)]. HSV-1 gH/gL interactions with certain integrins result in HSV-1 entrance via endocytosis. The receptors' expression varies between tissues and cell types, altering viral tropism. HVEM and nectin-1, for example, appear to be the primary receptors in the cornea and nervous system, respectively. HSV-1, however, requires HVEM to infect the mouse cornea, but HSV-2 does not. Mice missing HVEM and nectin-1 are resistant to HSV-1 and HSV-2 infection, demonstrating the importance of these receptors in HSV infection (Zhu and Viejo-Borbolla, 2021). Interaction with cellular receptors promotes gD to bind to a gH/gL heterodimer and expose the gB fusion peptide, resulting in viral and cellular membrane fusion (Hilterbrand and Heldwein, 2019). Following viral internalization, fusion can occur at the plasma membrane or within vesicles. Following fusion, certain tegument proteins, such as VP16, detach from the capsid and proceed to the nucleus independently, whilst others stay anchored [(Aggarwal et al., 2012); (Wolfstein et al., 2005); (Musarrat et al., 2021)]. Inner tegument proteins interact with motor proteins such as dynein, dynactin, and kinesin to assist capsid movement on microtubules toward the nucleus (Radtke et al.,

2010). The majority of data indicates that pUL36 and pUL37 are the most critical viral proteins involved in nuclear targeting essential for genome import into the nucleus (Richards et al., 2017). Nuclear pores allow the viral linear DNA genome to enter the nucleus (Brandariz-Nuñez et al., 2019). HSV genes are transcribed by cellular RNA polymerase II and viral proteins. During lytic replication, gene expression follows a sequential cascade. In the absence of de novo viral protein synthesis, immediate early (IE) genes - infected cell protein (ICP) 0, ICP4, ICP22, ICP27, ICP47, and unique short (US) 1.5 - are expressed. The tegument protein VP16, in collaboration with host cell factor 1 (HCF-1) and octamer binding protein-1 (Oct-1) creates a complex that binds to the promoter of IE genes, promoting their expression (Wysocka and Herr, 2003). One of the functions of IE genes is to promote the transcription of early (E) genes, the products of which include several proteins involved in DNA replication via the rolling circle process. Late (L) genes are expressed after DNA replication. Many L genes encode structural proteins that aid in viral assembly. The nucleus is the only location where viral transcription, DNA replication, capsid assembly, and DNA encapsidation occur. Importin alpha along with other cellular proteins are necessary for effective nuclear import of viral proteins as well as capsid assembly and egress (Döhner et al., 2018). Mature capsids with viral DNA exit the nucleus via an envelopment-deenvelopment mechanism (Johnson and Baines, 2011). In brief, the inner nuclear membrane provides the capsid with a main envelope. This envelope is lost when the capsid fuses with the outer nuclear membrane and is released into the cytoplasm. This mechanism is mediated by the nuclear egress complex generated by pUL31 and pUL34, which interacts with viral and cellular proteins such as lamin A/C [(Liu et al., 2014); (Liu et al., 2015); (Wu et al., 2016)]. Cytosolic capsids obtain more inner tegument proteins after exiting the nucleus, whereas outer tegument proteins and viral membrane proteins are integrated at the membrane compartments of trans-Golgi network vesicles and endosomes (Turcotte et al., 2005). Certain tegument proteins are debated to be integrated into the capsid inside the nucleus

[(Bucks et al., 2007); (Trus et al., 2007); (Donnelly and Elliott, 2001)]. Inner tegument proteins, specifically pUL36, pUL37, and pUS3, bind with the capsid first, followed by outer tegument proteins (Owen et al., 2015). Capsids on microtubules are directed by pUL36 and pUL37 toward the location of secondary envelopment [(Kelly et al., 2014); (Ivanova et al., 2016)]. Moreover, other HSV proteins involved in secondary envelopment include pUL20 and gK [(Baines et al., 1991); (Jayachandra et al., 1997)]. HSV trafficking from the nucleus to the periphery requires pUL36 and pUL37 interacting with kinesin [(Lee et al., 2006); (Sandbaumhüter et al., 2013)]. However, the processes behind viral glycoprotein transport and integration are not well understood. This mechanism is especially crucial in highly polarized cells such as neurons. It is unclear whether completely encased capsids originate within the cell body or whether bare capsids and envelope proteins are delivered separately and envelopment occurs in the axons [(Diwaker and Wilson, 2019); (Kratchmarov et al., 2012)]. Recent studies reveal that pUL36 and pUL37 drive motility in the neuronal cell body but are unable to guide non-enveloped capsids to axons, in contrast to vesicles containing gD, which efficiently used axonal transport (Buch et al., 2017). According to these findings, only fully constructed virus particles may move from the cell body to the axon termini. Vesicles transport HSV particles to the plasma membrane, and when the vesicle fuses with the plasma membrane, the enveloped HSV exits the cell (Ahmad and Wilson, 2020).

HSV infection could cause both lytic (as described until now) and latent replication. During lytic replication, viral genes are strictly organized, resulting in the creation of infectious viruses, whereas during latency, there is minimal gene expression and no viral particle formation. Anyway, the viral genome is capable of reactivation, and returns to the infectious cycle periodically, particularly when it goes back to the epithelia of the initial site of infection and multiplies to induce cold sore, ocular herpes, or genital herpes. Since keratinocytes are the most common cell type in these epithelia, the molecular mechanisms involved in HSV entrance and transmission in these cells are crucial to

understand the virus's biology. The HaCaT cell line, a spontaneously immortalized aneuploid line that is unable to achieve terminal epidermal differentiation, has been one the most employed keratinocyte cell line in HSV-1 investigations (Kite et al., 2021).

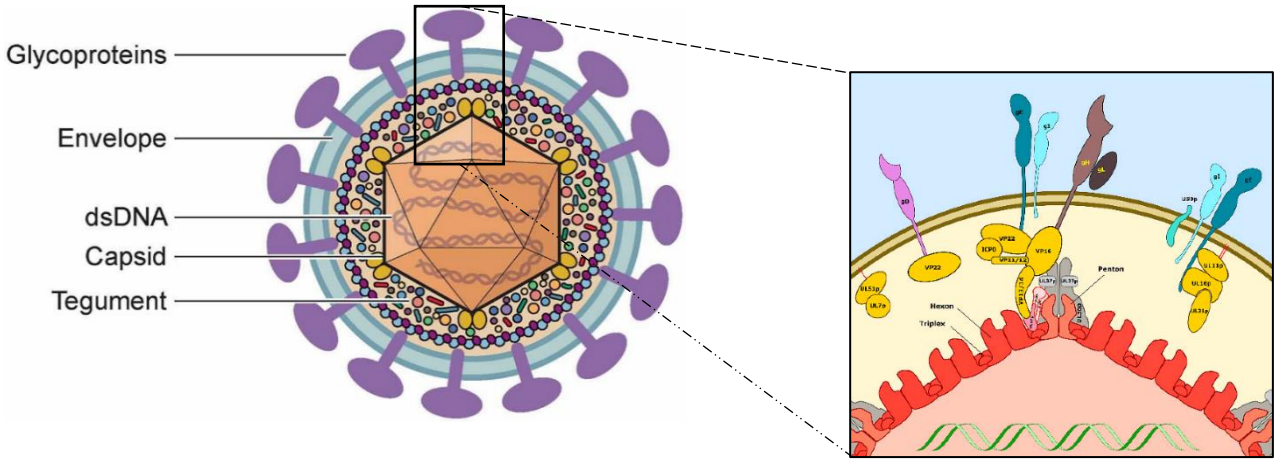

Figure 7. **The HSV1 virion**. Left: the linear double stranded DNA forms the core of the virion and is protected by the icosahedral capsid. The tegument, composed of many viral and cellular proteins, surrounds the capsid and connects it with the envelope, where the viral glycoproteins and other membrane associated proteins are embedded. Right: expanded view of a region of the capsid shell (red), inner- (gray), and outer- (yellow) tegument proteins and the envelope (dark brown bilayer). VP5 hexons and pentons are colored as in left-hand particle, and hexons, pentons, and triplexes are indicated. At the penton vertices, each copy of VP5 is connected to a UL36p dimer and to adjacent triplexes via a UL17p/$(UL25p)_2$ complex (for clarity the figure shows only two copies of VP5 at the vertex, and one copy of UL17p/$(UL25p)_2$). Envelope proteins gD, gE/gI, gH/gL, are shown embedded in the envelope bilayer such that their cytoplasmic tails project inward to connect with tegument proteins [Adapted from Zhu et al., 2021 and Ahmad et al., 2020]

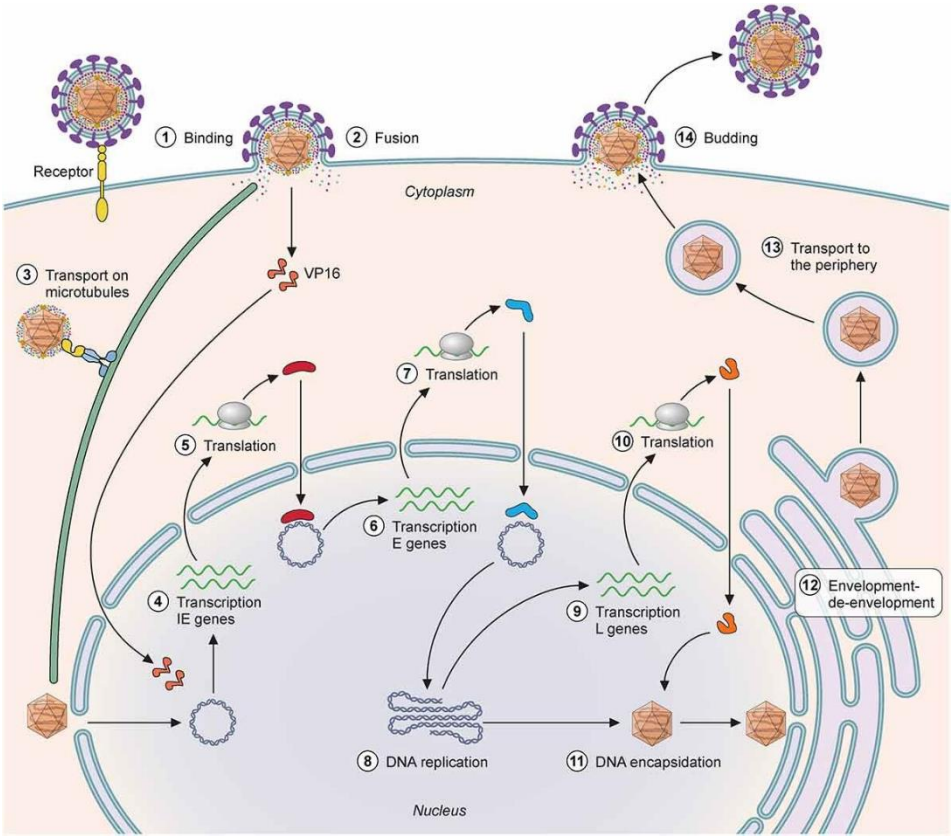

Figure 8. HSV1 cell cycle. 1) HSV glycoprotein interacts with cellular receptors and 2) endocytosis occur. Once the capsid fuses with the cellular membrane, it is led into the cytoplasm and then thanks the connection between UL36 and motor proteins, it moves to the cell nucleus via microtubules. 4) The tegument protein VP16, along with HCF-1 and Oct-1, enters the nucleus and initiates transcription of IE genes of viral linear DNA. 5) The IE genes are translated and participate in the transcription of E genes 6), which upon translation 7) are involved in viral genome replication 8). Once there are enough copies of viral genomes, the L gene products 9-10) promote DNA encapsidation 11). Capsids with DNA (called C capsids) mature and leave the nucleus by an envelopment-deenvelopment process 12), acquiring tegument and envelope (not shown) migrate to periphery of cytosol 13) and released in extracellular space 14) [Adapted from Zhu et al., 2021].

3. Aim of the study

Based on recent results obtained by our group and others, the autoinflammatory/autoimmune action of the nuclear protein IFI16 can be defined as follows (**Figure 9**): (1) IFI16 expression is aberrantly increased in damaged tissues of individuals with autoimmune/autoinflammatory illnesses due to abnormal response to type I IFNs and/or other proinflammatory/stress stimuli (Mondini et al., 2007); (2) IFI16 then delocalizes from nucleus to cytoplasm and (3) eventually is released into the extracellular space (Dell'Oste et al., 2014)**.** The released IFI16 protein leads to a breakdown in tolerance to self-antigens thus favoring the generation of specific anti-IFI16 autoantibodies (4a) [(Caneparo et al., 2013); (Alunno et al., 2015); **(**Baer et al., 2015**);** (McMahan et al., 2016)] moreover, the freely circulating IFI16 may act as a DAMP, alone or in combination with bacterial LPS, by binding the TLR4/MD2 complex (4b-c) (Iannucci et al., 2020). Finally, through the NF-kB pathway IFI16 can induce the production and the release of proinflammatory cytokine, thus amplifying (5-6) the injury of target cells (Bawadekar et al., 2015b)**.**

Altogether, these results clearly point out the role of extracellular IFI16 as a DAMP. However, the nature of such interaction remains poorly clarified. Therefore, this PhD project aimed to:

1) Mechanistically dissect the interaction between IFI16 and TLR4, using a panel of antibodies directed against either the N- or the C-terminal region of IFI16, along with a panel of IFI16 recombinant domains or truncated proteins spanning the whole IFI16 isoform from the N-terminus to the C-terminus;

2) Evaluate whether the pro-inflammatory activity of IFI16 could be extended to other PYHIN family members;

3) Identify the amino acids potentially involved in IFI16-TLR4/MD2 binding and

proinflammatory activity, through 3D structure prediction and site-specific mutagenesis;

4) By using human keratinocytes as cellular model, characterize different stress stimuli as triggers of IFI16 delocalization and extracellular release in vivo.

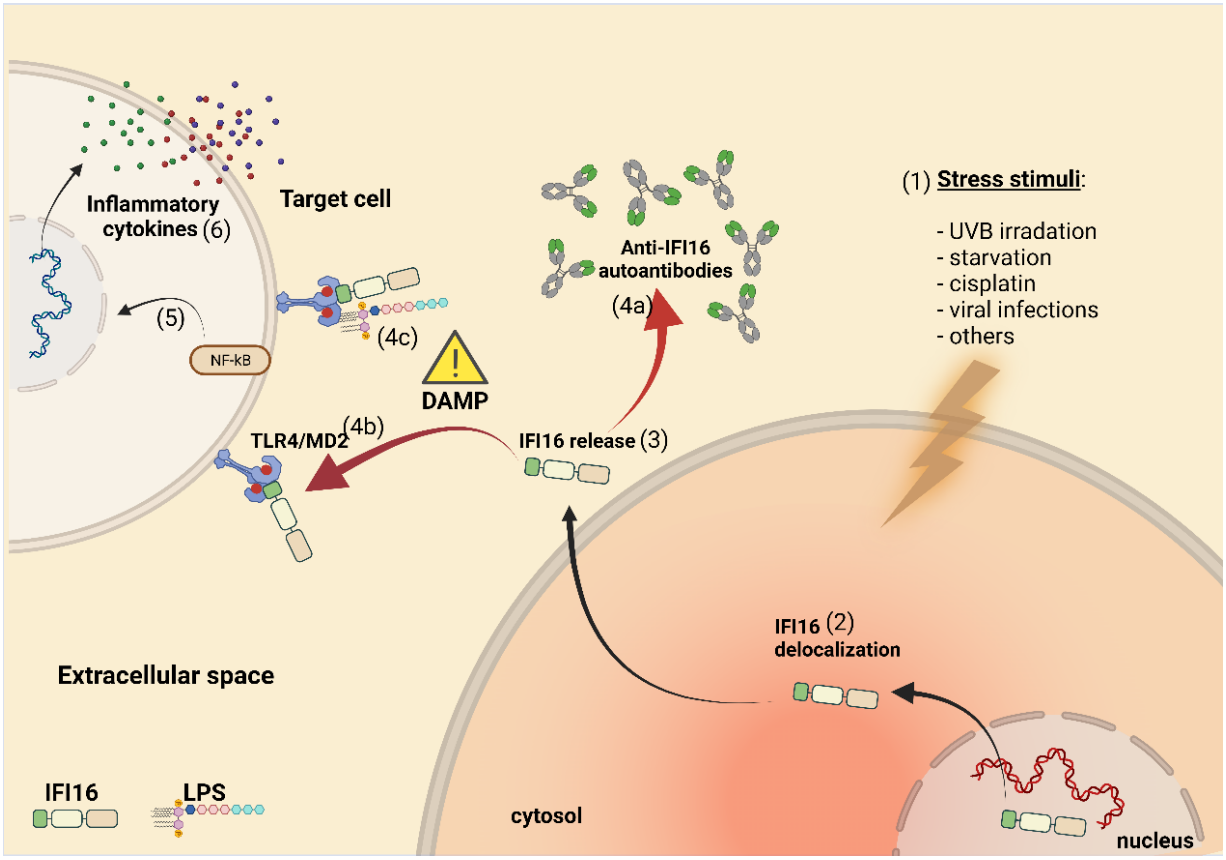

Figure 9. Schematic model underlying the mechanism of IFI16 release and DAMP-activity. Various stress stimuli (1) can promote the delocalization of IFI16 from nucleus to cytosol (2), which eventually results in its release in the extracellular space (3). Once released, circulating IFI16 can i) induce the production of autoantibodies (4a); ii) bind the TLR4/MD2 complex alone (4b) or in combination with bacterial lipopolysaccharide (4c). Once the binding occurs, an NF-kB-mediated signaling pathway (5) is induced leading to the production of pro-inflammatory. cytokines (such as TNF, IL6 and IL8) [Created by Biorender.com]

4. Materials and Methods

4.1 Reagents, antibodies, and recombinant proteins

LPS from Escherichia coli O111:B4 (LPS-EB), was purchased from InvivoGen. Bovine serum albumin Fraction V pH 7 (BSA) was purchased from Euroclone. The following antibodies were used: mAb anti-human TLR4 (sc-293072, Santa Cruz Biotechnologies), mAb anti-human TLR4 (sc-13593, Santa Cruz Biotechnologies), mAb anti- human TLR4 (mabg-htlr4, InvivoGen), rabbit polyclonal anti-MD2 (AHP1717T, Bio-Rad), mAb anti-β-actin (A1978, Sigma-Aldrich), rabbit IgG-HRP (A6154, Sigma-Aldrich,), mouse IgG-HRP (NA931V, GE Healthcare), streptavidin-HRP (E2886, Sigma-Aldrich,), mouse IgG- Alexa Flour 488 (A11001, Thermo Fisher Scientific), normal mouse IgG2a isotype control (sc- 3878, Santa Cruz Biotechnologies), anti-ICP27 (Virusys, P1113) and monoclonal anti-HSV1 ICP0 (H1A027-100, Virusys). Rabbit polyclonal anti-IFI16 N-term and C-term were produced as described previously (Gariglio et al., 2002). Briefly, N-terminus or C-terminus IFI16 cDNA from pBKS-IFI16 (kindly provided by J. Trapani, The Peter MacCallum Cancer Institute, Victoria, Australia) were cloned into a pGEX-4T-2 vector (Pharmacia, Uppsala, Sweden) to create an in-frame fusion protein with the GST coding region. The expression of N-terminus or C-terminus GST-IFI16 fusion protein in the Escherichia coli host AD202 was induced by treatment with 0.1 mM isopropyl-b-D-thiogalactopyranoside (IPTG) for 3 h. The bacterial cells were harvested by centrifugation, resuspended in cold lysis buffer (0.5 mg/ml lysozyme, 25 mM Tris-HCl, pH 7.9, 150 mM NaCl, 1 mM EDTA, 1 mM DTT, 10% glycerol, 0.2% Triton X-100 containing 2 mM PMSF, 50 mM pepstatin A, and 50 mM leupeptin as protease inhibitors) and lysed by sonication. Fusion proteins were purified from the cleared lysate by glutathione- Sepharose affinity chromatography. Antisera against IFI16 were raised by injecting

rabbits with the purified GST-IFI16 fusion proteins. The sera obtained after bleeding at 1 week after the fourth immunization were precipitated with ammonium sulfate at 45% saturation. The precipitate was then resuspended in phosphate-buffered saline (PBS) and purified on a protein A affinity column (Pharmacia) according to the specification of the supplier.

IFI16 mutated in PRYRIN domain (i.e., I17A, E85A, K64G, K34A, K86A and triple mutant K64G-K34A-K86A) and Pyrin of HIN200 family (i.e., hNLRP3, mAIM2, hAIM2, mIFI203, mIFI204, hMNDA, hIFIX, hASC) were purchased from GenScript in pET30a expression vector.

Human recombinant IFI16, IFI16 domains (i.e., PYRIN, HINA and HINB), and IFI16 variants lacking the HINB domain (i.e., IFI16ΔHINB) or the PYRIN domain (i.e., IFI16ΔPYRIN), Pyrin domain of HIN200 members and Mutated IFI16 in its Pyrin domain were produced as previously described (Bawadekar et al., 2015b-6-01). Briefly, the different coding regions were amplified from the full-length human IFI16 cDNA (isoform b) and cloned in a pET30a expression vector (Novagen) containing an N-terminal histidine tag. The expression of the proteins in the ClearColi® BL21(DE3) host (to ensure no endotoxin contamination) and the lysis of the bacteria, were performed as described above. Recombinant proteins were purified from the cleared lysate by nickel-affinity purification and stored at - 80°C in endotoxin-free vials. GST recombinant protein was expressed using pGEX-4T2 vector and purified according to standard procedures. The purity of the proteins was assessed by 12% SDS-polyacrylamide gel electrophoresis. Recombinant TLR4 protein and TLR4/MD2 complex (478-TR-050 and 3146- TM-050/CF, respectively) were purchased from R&D Systems.

4.2 Cell cultures, treatments and cells viability

Human leukemia monocytes (THP-1) and mouse macrophages (RAW264,7), both obtained from ATCC grown in RPMI 1640 Medium (Sigma- Aldrich) containing 10% of fetal bovine serum (FBS, Immunological Sciences) and 1% of penicillin/streptomycin/glutamine solution (PSG, Gibco) at 37°C and 5% CO2. Green monkie normal epithelial cells (VERO) were obtained from ATCC too but grown in DMEM (Euroclone) containing 10% of fetal bovine serum (FBS, Immunological Sciences) and 1% of penicillin/streptomycin/glutamine solution (PSG, Gibco) at 37°C and 5% CO2. human Keratinocytes (HaCaT) kindly provided by Dr. Leonie Unterholzner (Lancaster University), and HaCaT IFI16KO previously formed in our lab grown in the same condition as VERO cells. Brightfield picture for cells morphology was taken with Leica MC120 HD (DMi1) microscope and Las X leica software. UVB irradiations were performed as previously described (Costa et al., 2011). Briefly, UV irradiation was performed in PBS and provided by a UVB lamp (HD 9021; Delta Ohm S.r.l., Padova, Italy), which emits most energy within the UVB range (280–315 nm), with an emission peak at 312 nm. Irradiation intensity was monitored by a UVB irradiance meter cosine corrector with spectral range of 280–319 nm (LP 9021 RAD; Delta Ohm). Following irradiation with the required UVB dose, cells were incubated in complete medium for 16h at 37 °C in a humidified 5% CO2 atmosphere. The resulting cell culture supernatants were centrifuged to remove any cellular pellet and stored at -80°C for the following experiments. For treatments, cells were stimulated in complete medium with equimolar concentration of IFI16, PYRIN, HINA, HINB, IFI16ΔHINB, IFI16ΔPYRIN, and only Pyrin domain of human AIM2 (hAIM2), MNDA, and IFIX and mouse PYHIN proteins aim2 (mAIM2), p203, and p204 along with those of the human NLRP3 and ASC proteins. Moreover, we treat cells with recombinant IFI16 mutated in a

single ammino acid for Four different amino acid (plasmid provide by GenScrip) and with a triple-mutant all in equimolar way (111nM).

Additionally, cells were stimulated with hTNF (Biolegend) 50ng/ml and 100ng/ml for 24h and 48h. All treatments were carried out at 37°C and 5% CO2.

For TLR4 neutralization, THP-1 cells were pretreated with CLI-095 (Thermo scientific) during treatments with recombinant protein. For treatments with anti-IFI16 antibodies, IFI16 was incubated with rabbit polyclonal anti-IFI16 N-term or C-term for 1 h at RT before treatments.

After treatment with UVB, TNF, and after HSV-1 infection (see relative paragraph), the viability was measured using 5% of Alamar Blu for (biorad) 1h and LDH release assay (Roche) following kit protocol. Both assays have been measured the relative absorbance to Spark multimode microplate reader (Tecan).

4.3 Western blot and immunoprecipitation

Whole-cell extracts were prepared using RIPA lysis and extraction buffer (Thermo Fisher Scientific) with halt protease and phosphatase inhibitor (Thermo Fisher Scientific) on ice, and total protein concentration was quantified by Bradford Reagent (Sigma-Aldrich) measuring absorbance at 595 nm. Twenty µg of cell extracts, or 30 µl of cells culture supernatants (HaCaT)were separated by electrophoresis on 7.5% or 12% SDS-polyacrylamide gels (Bio-Rad), transferred to nitrocellulose membranes, blocked with 10% non-fat milk in tris-buffered saline-tween (TBST), and probed with specific primary antibodies O/N at 4°C. After being washed with TBST, membranes were incubated with specific HRP-conjugated secondary antibodies, and binding was detected by ECL (Thermo Fisher Scientific, Super Signal West Pico). Expression of β-actin or

GAPDH was used as protein loading control. Co-immunoprecipitation of TLR4 with interacting proteins was performed using the Dynabeads Protein G Immunoprecipitation Kit (ThermoFisher), according to the manufacturer's instructions with minor modifications. Briefly, after lysis of treated cells, 20 µg of total cell extracts were kept as the input control, while 90 µg of total cell extracts were incubated for 1 h at RT with 2.5 µg of anti-TLR4 antibody previously conjugated with magnetic beads. The resulting complexes were then washed, eluted, denatured, and subjected to Western blotting as described above. For DNase-treated cell extracts, DNase I (Sigma Aldrich) was added at a 1:10 dilution and incubated for 15 min at RT. Images were acquired, and densitometry of the bands was performed using Quantity One software (version 4.6.9, Bio-Rad). Densitometry values were normalized using the corresponding loading controls.

4.4 Quantitative real time PCR

Quantitative real-time PCR (qRT-PCR) was performed on a CFX96 Real-Time PCR Detection System (Bio-Rad) as previously described (Albertini et al., 2018). Briefly, total RNA was extracted using TRI Reagent (Sigma-Aldrich), and 1 µg was retrotranscribed using an iScript cDNA Synthesis Kit (Bio-Rad). Reverse-transcribed cDNAs were amplified in duplicate using SsoAdvanced Universal SYBR Green Supermix (Bio-Rad), up to 40 cycles of PCR. The human glyceraldehyde 3-phosphate dehydrogenase (GAPDH) gene, or the murine actin gene, were used as housekeeping gene to normalize for variations in cDNA levels. The relative normalized expression after stimulation as compared to control was calculated as fold change = $2^{-\Delta(\Delta CT)}$ where $\Delta CT = CT_{target} - CT_{GADPH}$ and $\Delta(\Delta CT) = \Delta CT_{stimulated} - \Delta CT_{control}$. Primer sequences are summarized in Table 2.

Table 2. List of primers used for qRT-PCR (h: human)

Gene	Forward (5' to 3')	Reverse (5' to 3')
hIL-8	ATGACTTCCAAGCTGGCCGTGGCT	TCTCAGCCCTCTTCAAAAACTTCTC
hTNF-α	GCCAGAGGGCTGATTAGAGA	TCAGCCTCTTCTCCTTCCTG
hIL-1β	TCCCCAGCCCTTTTGTTGA	TTAGAACCAAATGTGGCCGTG
hGAPDH	AACGTGTCAGTGGTGGACCTG	AGTGGGTGTCGCTGTTGAAGT

4.5 Cytokines measurement by ELISA

Cytokines secreted in culture supernatants after treatments were analyzed using human IL-6 DuoSet ELISA and human IL-8 DuoSet ELISA (all from R&D Systems) and human TNF-α DuoSet ELISA (all from R&D Systems) according to the manufacturer's instructions. Absorbance was measured using a Spark multimode microplate reader (Tecan).

4.6 Cloning, transformation, Transfection, Monitoring IFI16-mCherry

A chimera form of IFI16 were formed by cloning using mCherry dye plasmid provided by Addgene. pET30a vector that contains IFI16(already present in laboratory) was amplified by PCR using primers present in table below (Table 3). IFI16 (300ng) obtain purified form Agarose gel (1%) and mCherry plasmid (700ng) were digested with Restriction Enzyme BamHI e XhoI for 15min at 37°C and then using T4 ligase (Invitrogen) with molar ratio vector: insert of 1:2. Size check and second round of checking digestion was done and analyzed in Agarose gel. Then, *E.coli (clear coli)* transformation using thermal shock (42°C and ice) is done followed by 1h of resting.

The selection occurs in plate dishes with LB agar auditioned with Kanamycin (50ug/ml) as selection marker, overnight at 37°C incubation, it. After amplification of the colony, plasmid DNA was extracted and checked with digestion with Restriction Enzyme. Plasmid DNA of IFI16-mCherry chimera obtained has been used for HACAT cells transfection. Cells were transfected with specific Lipo3000 following kit protocol (thermo scientific) with lower amount of Lipo proposed and 2.5ug of DNA. Following 24h of resting cells were monitored before at FLoid™ Cell Imaging Station (Thermo Scientific) and then after cells treatment in IncuCyte (Sartoriuss) by setting acquisition plate every 30min.

Table 3. Primers for IFI16 cloning in mCherry vecor.

Gene	Forward (5' to 3')	Reverse (5' to 3')
IFI16-ORF	CCGCTCGAGATGGGAAAAAAATACAAG	CCGGGATCCGAAGAAAAAGTCTGGTGAAGT

4.7 Surface plasmon resonance analysis

The Biacore X100 (GE Healthcare) instrument was used for real-time binding interaction experiments. Recombinant TLR4 or TLR4/MD2 complex was covalently immobilized onto the surface of sensor CM5 (cat # BR100012, GE Healthcare) chips via amine coupling. TLR4 was diluted to a concentration of 10 μg/ml in 10 mM sodium acetate at pH 4.0, while TLR4/MD2 complex was diluted to a concentration of 20 μg/ml in the same buffer. Both proteins were injected on CM5 chips at a flow rate of 10 μl/min, upon activation of the carboxyl groups on the sensor surface with 7-min injection of a mixture of 0.2 M EDC and 0.05 M NHS. The remaining esters were blocked with a 7-min injection of ethanolamine. Taking into account the ligands (TLR4 or TLR4/MD2) and analytes (IFI16, HIN200 protein Members and IFI16 mutated) molecular

weights (MW) of 70 or 90 kDa, and 90, 10 or 100 kDa 15 kDa respectively, the appropriate ligand density (RL) on the chip was calculated according to the following equation: RL = (ligand MW/analyte MW) × Rmax × (1/Sm), where Rmax is the maximum binding signal and Sm corresponds to the binding stoichiometry. The target capture level of the TLR4 or TLR4/MD2 was 596.0 or 1223.9 response units (RUs), respectively. The other flow cell was used as a reference and was immediately blocked after the activation. Increasing concentrations of IFI16, IFI16 subdomain, HIN200 family members; IFI16 mutated were flowed over the CM5 sensor chip coated with TLR4 or TLR4/MD2 at a flow rate of 30 µl/min at 25°C with an association time of 120 s and a dissociation phase of 180 s. A single regeneration step with 50 mM NaOH was performed following each analytic cycle. All the analytes tested were diluted in the HBS-EP+ buffer (GE Healthcare). Recombinant IFI16 was covalently immobilized onto the surface of sensor CM5 chips via amine coupling as done for TLR4 and TLR4/MD2 complex. IFI16 was diluted to a concentration of 25 µg/ml in 10 mM sodium acetate at pH 4.0. The target capture level of IFI16 was 1926.6 response units (RUs). A single regeneration step with 50 mM NaOH was performed following each analytic cycle. The KDs were evaluated using the BIAcore evaluation software (GE Healthcare) and the reliability of the kinetic constants calculated by assuming a 1:1 binding model supported by the quality assessment indicators values. For the binding inhibition experiments, a fixed concentration of IFI16 (500 nM) was incubated with increasing concentrations of rabbit polyclonal anti-IFI16 N-term or C-term for 1 h at RT, diluted in HBS-EP+ buffer. IFI16–antibody complexes were injected over the TLR4/MD2 sensor chip surface for 120 s and allowed to dissociate for 180s. A single regeneration step with 50 mM NaOH was performed following each analytic cycle. Data were background-subtracted using the adjacent control flow cell and buffer-alone injections. The reported RUs were calculated using the BIAcore evaluation software.

4.8 Viruses and Plaque assay

The clinical isolate of HSV-1 was grown in Vero cells and titrated by standard plaque assay as described as follow. Vero cells were seeded at a density of $3*10_4$/well in a 96-well plate and inoculated 24 h later with 10-fold serial dilutions of the HSV-1 production. After 48 h, cells were fixed and stained with crystal violet solution, and plaques were counted on each well to determine the virus titer, which was determined by counting the number of immunostained foci on each well using the following formula: virus titer (PFU/ml) = number of plaques * 0.1 ml/dilution fold. UVB-inactivated HSV-1was prepared using double pulse of UVB light (1.2 J/cm2). For each experiment, $2x10^5$ HaCaT cells were seeded in 12-well plates and, after 24 h, infected with HSV-1 at MOI 1. The infection was stopped after 2h by changing the media. Cells were observed and samples collected at 2-4-6-24hpi, considering the time of infection as time zero.

4.9 Immunofluorescence microscopy

HaCaT cells (3x104) were seeded in triplicate on coverslips in 24-well plates and infected with HSV-1 at an MOI of 1. At the indicated time points, cells were fixed with 4% paraformaldehyde and then incubated for 1 h using appropriate dilutions of primary antibody in a dark humidified chamber at room temperature (RT), followed by secondary labeled antibody for 1h. DAPI (4',6'-diamodino-2phenylindole) (D1306, Thermo Fischer Scientific, Waltham, MA USA) was used to counterstain the nuclei. The following primary and secondary antibodies were used: monoclonal anti-HSV1 ICP0 (H1A027-100, Virusys) or in house-produced rabbit polyclonal IFI16 [**Gariglio et al., 2002**], goat anti-mouse IgG-Alexa Fluor 488 (A11001, Thermo Fisher Scientific) and goat IgG anti-Rabbit IGA-Alexa Fluor 568 (A-11011, Thermo Fisher Scientific). The coverslips were mounted with SlowFade Gold antifade reagent mounting media (Thermo Fischer Scientific), and

cells visualized using a Leica SP8 LIGHTNING Confocal Microscope (Leica Microsystems, Wetzlar, Germany).

4.10 Sequence alignment, mutagenesis and protein structure docking

Sequence alignments of the Pyrin domains were performed with the program MEGAX using the ClustalW algorithm. The primary amino acid sequences were obtained from UniProtKB with the following codes: IFI16 Q16666, MNDA P41218, AIM2 O14862, IFIX Q6K0P9, IFI203 O35368, IFI204 P0DOV2, mAIM2 Q91VJ1, NLRP3 Q96P20, ASC Q9ULZ3. The genes encoding the mutated variants of IFI16 at level of the PYRIN domain (i.e., I17A, E85A, K64G, K34A, K86A and triple mutant K64G-K34A-K86A), were purchased from GenScript in pET30a expression vector. Structure prediction of IFI16 PYRIN domain was performed using Robetta software (Kim et al., 2004). Protein-protein interaction has been simulated using the Haddock web server (van Zundert et al., 2016). The binary complex between C-term of TLR4 (fist 626 amino acids) or MD2 with PYRIN, obtained through the docking approach, were ranked based on the Haddock score, which represents a binding free energy–like value. Proteins 3D structures were evaluated and figures obtained using PyMOL software (The PyMOL Molecular Graphics System, Version 2.3.4).

4.11 Statistical analysis

All statistical analyses were performed using GraphPad Prism version 6.00 for Windows (GraphPad Software, La Jolla California USA, www.graphpad.com). The data are expressed as mean ± SD. For comparisons between two groups, means were compared using a two-tailed Student's t test. For comparisons among three groups, means were compared using one-way or two-way ANOVA followed by Dunnett's test. Differences were considered statistically significant at a P value < 0.05.

5. RESULTS

5.1 The proinflammatory activity of the IFI16 protein lies within its N-terminal region

We previously demonstrated that the IFI16 protein is a specific TLR4-ligand and that IFI16 *per se* or upon binding to LPS can trigger TLR4-mediated inflammation (Iannucci et al., 2020). To identify the region of IFI16 responsible for TLR4 activation, we took advantage of a panel of antibodies directed against either the N- or the C-terminal region of IFI16. Phorbol 12-myristate 13-acetate- (PMA)-differentiated human THP-1 cells (human macrophages hereinafter) were stimulated with 10 μg/ml of full-length IFI16, alone or pre-incubated for 1h at RT with increasing concentrations of anti-IFI16 antibodies. After 24h, total RNA was extracted and analyzed using qRT-PCR to assess the inflammatory reaction. As expected, and consistent with the data previously obtained (Iannucci et al., 2020**),** *TNFα, IL8,* and *IL1β* mRNAs were strongly upregulated when cells were treated with IFI16 alone compared to untreated cells (61-fold for *TNFα,* 97-fold for *IL8,* and 50-fold for *IL1β*, respectively) (**Figure 10A**). Interestingly, a concentration-dependent inhibition of IFI16-mediated *TNFα, IL8,* and *IL1β* upregulation was observed when the anti-N-term-IFI16 antibodies were pre-incubated with the IFI16 protein, reducing the transcriptional activation of around 85% when the highest concentration of antibody (10 μg/ml) was used. By contrast, no significant changes were observed when anti-C-term-IFI16 antibodies were pre-incubated with the recombinant IFI16 protein when compared to the protein alone. Consistent with the transcriptional data, TNF-α and IL-8 release in cell culture supernatants was strongly increased when the cells were stimulated with IFI16, and this effect was significantly inhibited in a concentration-dependent manner when anti-N-term-IFI16 antibodies, but not anti-C-term, were used (**Figure 10B**). Moreover, the inhibitory activity exerted by anti-N-term-IFI16 antibodies has

been further investigated by surface plasmon resonance (SPR) in order to validate the possible interference of the selected antibodies in the physical interaction between IFI16 and TLR4/MD2 receptor. Briefly, IFI16, alone or pre-incubated for 1h at RT with increasing concentrations of anti-IFI16 antibodies, flowed over a TLR4/MD2-coated chip. Consistent with the results obtained in the cellular assays, anti-N-term-IFI16 antibodies significantly inhibited IFI16 binding to the receptor in a concentration dependent manner, exhibiting approximately 75% and 45% of binding inhibition versus the control setting without antibodies when the highest or the lowest concentrations of antibodies— 500nM and 62.5nM, respectively— were used (**Figure 10C**). As expected, preincubation with anti-C-term-IFI16 antibodies did not impair IFI16 binding to the TLR4/MD2 receptor even at the highest concentrations used.

Collectively, our findings strongly suggest that the IFI16 N-terminal region is mainly responsible for the recognition and activation of the TLR4/MD2 complex.

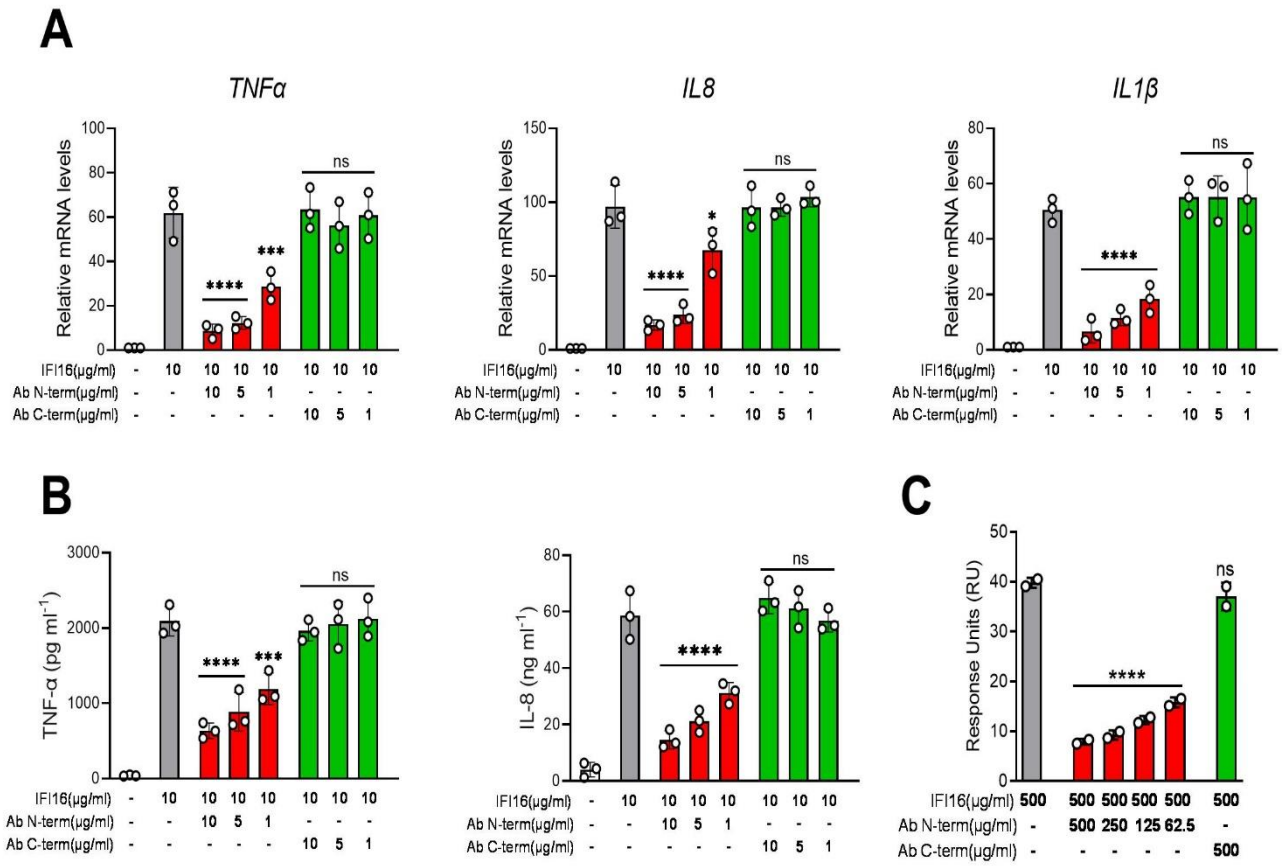

Figure 10. Antibody against the N-term region of IFI16 dampens the inflammatory response in human macrophages. (**A**) qRT-PCR analysis for TNF-α, IL-8, and IL-1β mRNA expression levels in human macrophages stimulated for 24 h with IFI16 alone (10 μg/ml) or pre-incubated for 1 h with the indicated amounts of anti-IFI16 polyclonal antibodies directed against either the N- or C-terminal region of the protein. Values are normalized to GAPDH mRNA and plotted as fold of induction over untreated cells. qRT-PCR data are presented as mean values of biological triplicates. (**B**) Protein concentration of TNF-α and IL-8 determined by ELISA in the culture supernatants harvested from human macrophages stimulated for 24 h as described in A. (**C**) Surface plasmon resonance (SPR) analysis of IFI16 binding to immobilized TLR4. Five-hundreds 500nM of IFI16 diluted in running buffer, alone or pre-incubated for 1h at RT with increasing concentrations (62.5 to 500 nM) of the anti-N-term-IFI16 antibody or with 500nM of anti-C-term antibody, were flowed over a TLR4/MD2-coated chip. Data are representative of three independent experiments, shown as the mean ± SD (* $p<0.05$, ** $p<0.01$, *** $p<0.001$; two-way ANOVA followed by Dunnett's test).

5.2 The PYRIN domain of IFI16 is involved in TLR4/MD2 binding and activation

To map the IFI16 domain that is involved in TLR4/MD2 binding and activation, we generated a panel of IFI16 recombinant domains spanning the whole protein from the N-terminus to the C-terminus that comprises the PYRIN, HINA or HINB domains as well as truncated IFI16 proteins that lack either the PYRIN or HINB domains (IFI16ΔPYRIN or IFI16ΔHINB, respectively) (**Figure 11A**). The human macrophages were stimulated with 10 μg/ml of IFI16, or equimolar concentrations of IFI16 domains or truncated proteins, and total RNA was extracted 24h later and analyzed using qRT-PCR to assess the inflammatory reaction. Consistent with **Figure 11A** and our previous work (Iannucci et al, 2020), *TNFα, IL8,* and *IL1β* mRNAs were significantly upregulated when IFI16 or the IFI16ΔHINB truncated protein were used (**Figure 11B**). By contrast, this proinflammatory activity dropped when the IFI16ΔPYRIN protein was used (from 57- to 10-fold for *TNFα,* from 113- to 20-fold for *IL8,* and from 48- to 5-fold for *IL1β* respectively, compared to untreated cells). Interestingly, out of the three IFI16 domains, only the PYRIN domain retained the ability to upregulate the expression levels of *TNFα, IL8,* and *IL1β* mRNAs, although at a lower extent when compared to the full-length protein (37-fold for *TNFα,* 66-fold for *IL8,* and 38-fold for *IL1β* respectively, compared to untreated cell). Consistently, TNF-α and IL-8 protein levels were significantly increased in the culture supernatants of the cells treated with IFI16, PYRIN or IFI16ΔHINB but not when cells were stimulated with the IFI16ΔPYRIN truncated protein or the HINA or HINB domains, compared to untreated cells (**Figure 11C**). As already reported for the full-length protein (Iannucci et al, 2020), the observed proinflammatory activity was TLR4 dependent, being inhibited by the addition of the TLR4 antagonist CLI-095 (**Figure 11C**).

Next, SPR analysis was performed to ascertain that the PYRIN domain was exclusively able to interact with the TLR4/MD2 receptor complex. To this end, increasing concentrations of the IFI16

protein, the truncated forms, or the single domains were flowed over a TLR4/MD2-coated chip. As shown in **Figure 11D**, we found that both IFI16ΔHINB and the PYRIN domain bound the TLR4/MD2 receptor complex with an affinity (K_D=7.8*10^{-8} and 4.1*10^{-6}, respectively) that was comparable to that displayed by the full-length protein (K_D=1.7*10^{-7}). Both HINA and HINB domains still retained binding affinity for the TLR4/MD2 complex but to much lower extent when compared to the full-length protein (K_D=1.6*10^{-4} and 3.2*10^{-5}, respectively). As expected, the binding to TLR4/MD2 complex was completely lost when the IFI16ΔPYRIN protein was probed.

The binding activity of the PYRIN domain to the TLR4 receptor was then confirmed *in vivo* using co-immunoprecipitation experiments. Human macrophages were treated for 1h with IFI16, the PYRIN domain, or left untreated, and after that the cell lysates were incubated with anti-TLR4 antibodies pre-adsorbed on protein G beads. Subsequently, SDS-PAGE and immunoblotting were used to detect the presence of TLR4, or the recombinant proteins in the immunoprecipitated protein complexes. As shown in **Figure 11E**, the protein bands corresponding to IFI16 and PYRIN domain were found when cells were treated with relatives' recombinant protein. The specificity of the interactions was confirmed by the absence of any bands in untreated cells

Taken together, our findings strongly suggest that the PYRIN domain of the IFI16 protein, through its interaction with the TLR4 receptor, is necessary and sufficient to induce a proinflammatory phenotype in target cells, *e.g.,* human macrophages, as demonstrated by the transcriptional activation and release of proinflammatory cytokines.

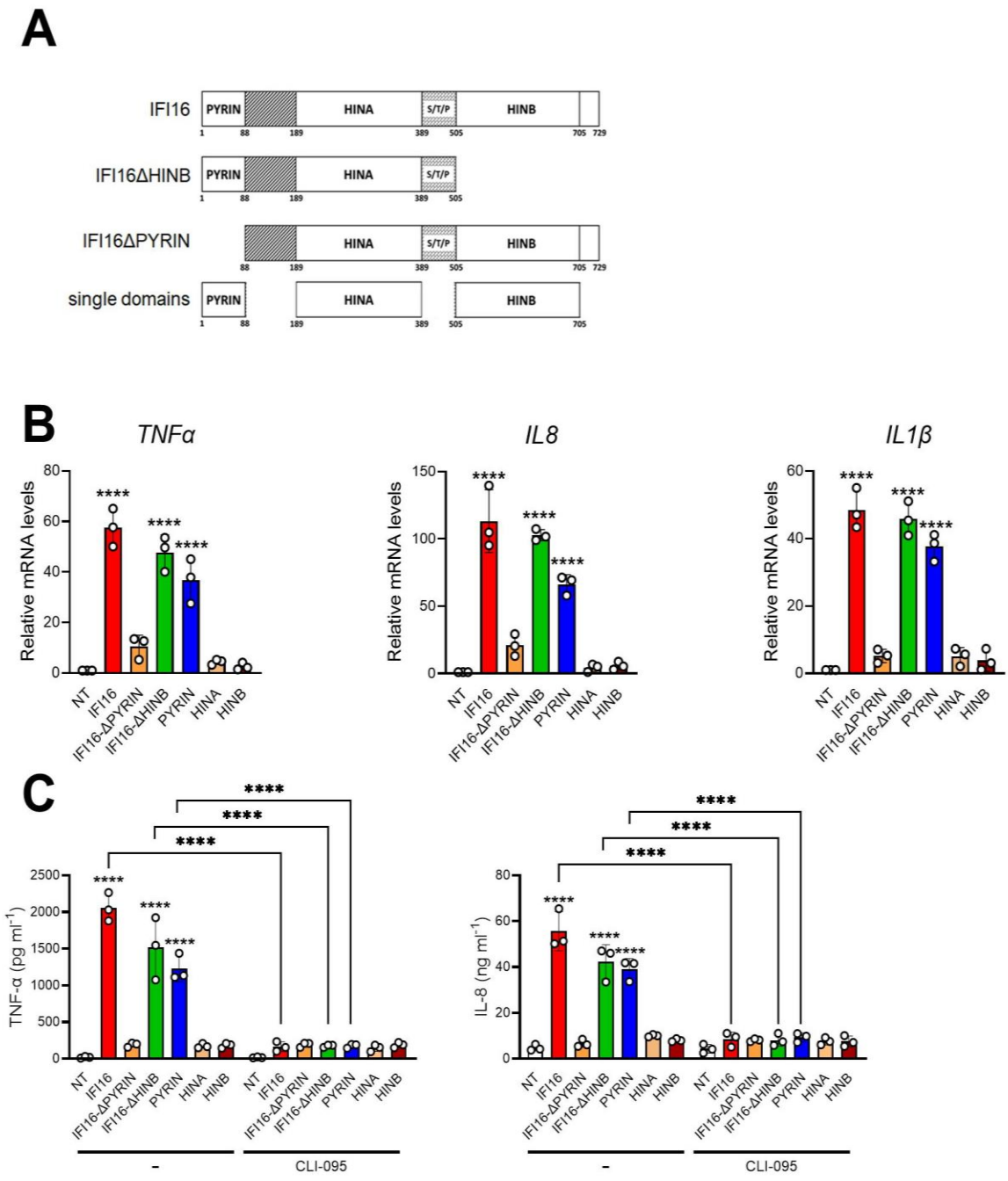

Figure 11. The PYRIN domain of IFI16 mediates TLR4 activation and pro-inflammatory activity. **A**) Schematic representation of the full length (IFI16), truncated forms IFI16DHINB and IFI16DPYRIN, and recombinant IFI16 single domains used in this study. Numbers represent the amino acid positions based on the NCBI Reference Sequence NP_005522. (**B, C**) Human macrophages were stimulated with equimolar concentrations (111nm) of IFI16 domains or truncated proteins and **B)** total RNA or **C**) culture supernatants were analyzed to assess the inflammatory reaction. Cytokines were significantly upregulated only when IFI16, PYRIN domain or the IFI16ΔHINB truncated protein were used, and similar results were obtained when TNF-α and IL-8 release was tested in ELISA. This proinflammatory activity was TLR4-dependent, being inhibited by the addition of the TLR4 antagonist CLI-095. Data are representative of three independent experiments, shown as the mean ± SD (* $p<0.05$, ** $p<0.01$, *** $p<0.001$; one-way ANOVA followed by Dunnett's test). Continue next page

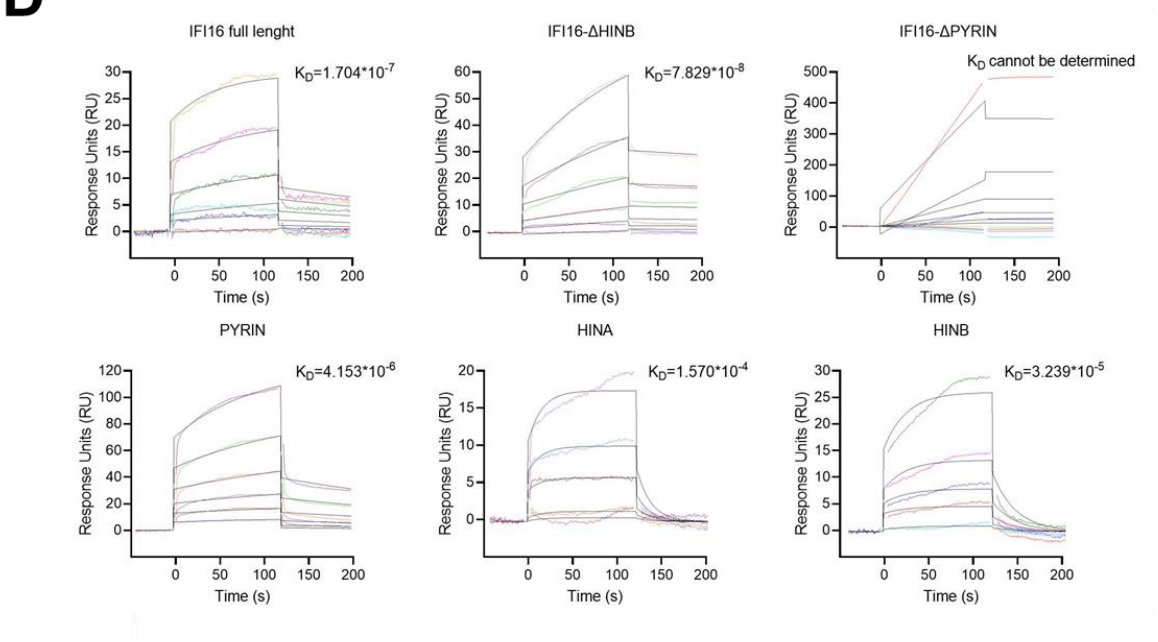

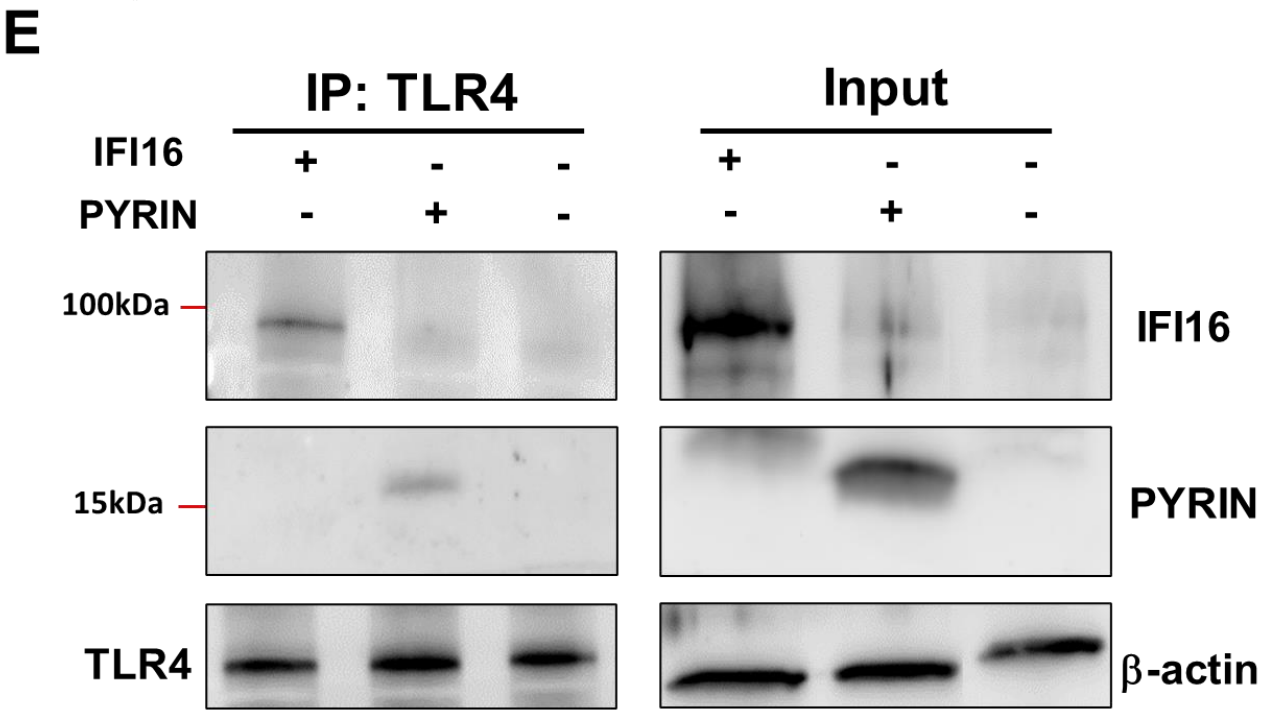

D) Surface plasmon resonance (SPR) analysis of IFI16 domains binding to immobilized TLR4/MD2. After immobilization of TLR4/MD2 on the CM5 sensor chip surface, increasing concentration of full length IFI16, PYRIN domain, IFI16ΔPYRIN, HINA or HINB domains (20–800 nM) diluted in running buffer were injected over immobilized complex. Data are representative of three different experiments, and for each analysis the dissociation constant (K_D) value is shown. **E)** Human macrophages were stimulated for 1h with full-length FI16 or the PYRIN domain (30ug/ml). Total cell extracts were subjected to immunoprecipitation using a TLR4 monoclonal antibody. Immunoprecipitated (left, IP:TLR4) and whole-cell lysates (right, Input) were analyzed by immunoblotting with anti-N-term-IFI16 (recognizing both flIFI16 and the PYRIN domain) or anti-TLR4 antibodies. β-actin protein expression was used for protein loading control. Data are representative of three independent experiments with similar results.

5.3 The proinflammatory activity of the PYRIN domain is conserved among the PYHIN family members

The results so far described prompted us to investigate whether the proinflammatory activity of the IFI16 PYRIN could be extended to the other members of the PYHIN family or even to other proteins that also harbor a PYRIN domain, such as the NOD-, LRR- and PYRIN domain-containing protein 3 (NLRP3), and the apoptosis-associated speck-like protein containing a CARD (ASC). To this end, we generated the recombinant PYRIN domains of other representative human AIM2 (hAIM2, hereinafter), MNDA, and IFIX and mouse PYHIN proteins aim2 (mAIM2, hereinafter), Ifi203, and Ifi204 along with those of the human NLRP3 and ASC proteins. Then, equimolar concentrations of these PYRINs were used to stimulate human macrophages for 24h and then total RNAs were extracted and analyzed by qRT-PCR for the expression of proinflammatory cytokine genes. As shown in **Figure 12A**, *TNFα, IL8,* and *IL1β* mRNA expression levels were significantly upregulated when the cells were stimulated with all the PYRIN domains of the PYHIN proteins (> 40-fold for all the three cytokines when compared to untreated cells under any condition), being very similar to those reported upon exposure to the IFI16-PYRIN domain, even when murine proteins were used. Notably, we didn't observe any significant upregulation of the proinflammatory cytokines when the cells were stimulated with the NLRP3-PYRIN or with the ASC-PYRIN, compared to untreated cells. Enhanced release of TNF-α and IL-8 was also shown in the culture supernatants of the cells stimulated with the PYRIN domain from the PYHIN family members but not in those of the cells exposed to the NLRP3-PYRIN or to the ASC-PYRIN (**Figure 12B**). Importantly, the small-molecule TLR4 antagonist CLI-095 was able to block the proinflammatory activity elicited by the PYRIN domain of the PYHIN family members confirming their function through the canonical TLR4/MD2 pathway.

Noteworthy, similar results were obtained when murine macrophages (*i.e.*, RAW264.7) were used as target cells. Indeed, as shown in **Figure 12C**, both human and murine PYHIN PYRIN domains were able to induce TLR4-dependent TNF-α release in cell culture supernatants of murine macrophages, while the NLRP3-PYRIN or the ASC-PYRIN did not. Next, to confirm that the proinflammatory activity exerted by the PYRIN domain derived from the PYHIN family members but not by other PYRIN domain derived from other families, *e.g.* NRLP3, consistently involved the TLR4/MD2 complex, increasing concentrations of hAIM2-PYRIN (human PYHIN), Ifi203-PYRIN (murine PYHIN) or NRLP3-PYRIN (non-PYHIN) were used to run SPR analyses on a sensor chip coated with TLR4/MD2. As expected, high affinity binding between both hAIM2 and Ifi203 PYRIN domains and TLR4/MD2 complex was found with a K_D comparable to that observed with IFI16-PYRIN ($K_D = 3.5*10^{-6}$ for hAIM2 and $K_D = 6.1*10^{-6}$ for Ifi203). By contrast, NLRP3-PYRIN still retained binding affinity for the TLR4/MD2 complex but to much lower extent when compared to the hAIM2 and Ifi203 PYRIN domains ($K_D = 4.4*10^{-3}$) **(Fig 12D).**

Altogether, these findings clearly indicate that the PYRIN domains of the PYHIN family members specifically retain the ability to induce a TLR4-mediated proinflammatory phenotype in target cells. Remarkably, this activity is observed in both human and mouse PYHIN members, suggesting a conserved interaction mechanism between the two species.

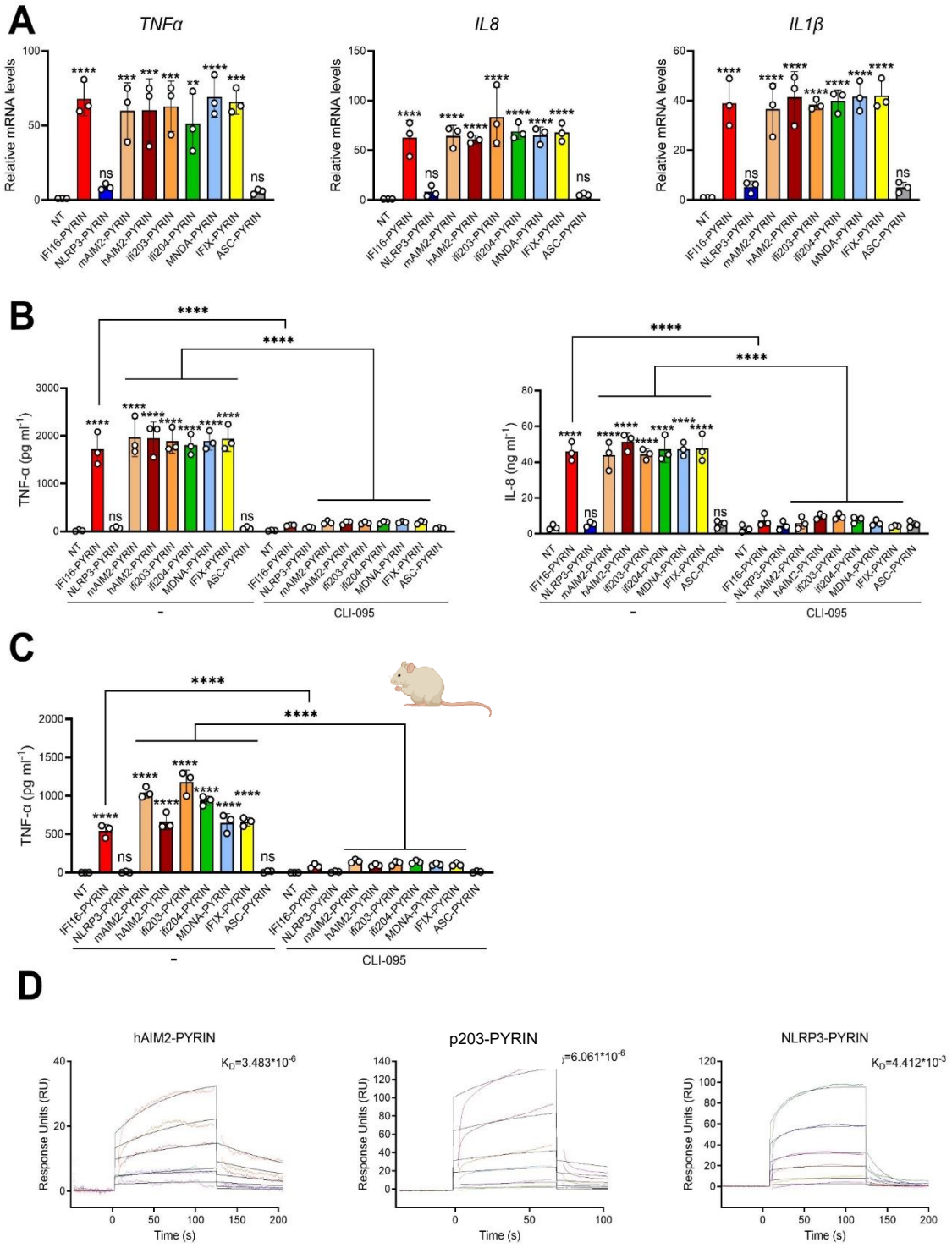

Figure 12. The proinflammatory activity of the PYRIN domain is conserved across the PYHIN family members. Equimolar concentrations of the PYRINs from different PYHIN family members, along with those from NLRP3 and ASC proteins, were then used to stimulate (**A, B**) human or **C**) mouse macrophages for 24h, with or without CLI-095 (TLR4 inhibitor, 5μM). Then, **A**) the relative amounts of TNF-a, IL8 and IL-1b mRNA were calculated through qRT-PCR analysis, and (**B, C**) TNFa and IL-8 release were measured through ELISA. Data are representative of three independent experiments, shown as the mean ± SD (* $p<0.05$, ** $p<0.01$, *** $p<0.001$; one-way ANOVA followed by Dunnett's test). **D**) Surface plasmon resonance (SPR) analysis of different PYRINs' binding to immobilized TLR4. After immobilization of TLR4/MD2 on a CM5 sensor chip surface, increasing concentration of the indicated PYRIN domains (20–800 nM) diluted in running buffer were injected over immobilized complex. Data are representative of three different experiments, and for each analysis the dissociation constant (K_D) value is shown.

5.4 Four amino acids located within the IFI16 PYRIN domain are critically involved in its TLR4-mediated proinflammatory activity

Having determined the TLR4-dependent proinflammatory activity of the PYHIN PYRIN domains, we chose IFI16-PYRIN as paradigmatic for the entire family to uncover the specificity of the interaction with the receptor at a structural level. To this end, we predicted its 3D structure taking advantage of *Robetta server* (Kim et al., 2004, **Figure 13A**) and used it to perform a molecular docking study with the extracellular portion of TLR4 (PDB:3FXI, **Figure 13B**) or with MD2 (PDB:2E56, **Figure 13C**) using High Ambiguity Driven protein-protein DOCKing (HADDOCK, van Zundert et al., 2016). In parallel, we performed sequences alignment of the PYHIN PYRIN domains, along with those of NLRP3 and ASC, to identify PYHIN-specific amino acids with similar chemical properties (**Figure 13D**). Notably, the integration of sequences alignment and molecular docking information, specifically considering i) the bindings length under 3Å, ii) the chemical nature of the amino acids involved, and iii) the characteristics of the PYHIN PYRIN domains, led to the identification of three residues in the IFI16-PYRIN that are potentially involved in the interaction with TLR4 — *i.e.,* Lys34, Lys64, and Lys86 (**Figure 13E**) and one potentially involved in the interaction with MD2 —*i.e.,* Glu85 (**Figure 13F**). Interestingly, the alignments between IFI16-PYRIN's projected 3D structure and those of NLRP3- and ASC-PYRIN using PyMOL software revealed that the amino acids in those positions are replaced not only by residues with different orientations but also shown an exeternal loop, that preventing the interaction with the TLR4 receptor (**Figure 14**). Moreover, NLRP3- and ASC-PYRIN structures are characterized by an extended loop that could interfere with the receptor binding by steric hindrance phenomena (respectively **Figure 14A** and **14B**). In particular, the loop moiety occupies the region that in

IFI16-PYRIN is designated to interact with TLR4 through electrostatic interaction involving Lys34 and Lys64.

To assess the significance of these predictions, and to confirm the contribution of these residues in activating the TLR4/MD2 receptor, a series of alanine mutations were constructed by site-directed mutagenesis of the identified polar residues, and the IFI16 mutants produced (namely, K34A, E85A, and K86A). Additionally, glycine mutagenesis was performed on the amino acid residue Lys64 (K64G mutant) to minimize the non-specific interaction that can occur with methyl group of alanine due to steric hindrance in its specific interaction background with TLR4. Finally, to validate the specificity of the interaction between PYHIN PYRIN domains and TLR4/MD2, alanine mutagenesis was also performed on a PYRIN superfamily conserved amino acid, in a region non predicted to be involved in the binding with the receptor —*i.e.*, Ile17— resulting in the I17A mutant. All the IFI16 mutants, including the triple mutant (K34A/K64G/K86A), were then used along with the IFI16 wild-type protein to stimulate human macrophages for 24h at equimolar concentrations. Interestingly, as shown in **Figure 15A** a significant decrease in TNF-α production was detected in the culture supernatants of cells treated with the aforementioned mutants except for the I17A mutant. Specifically, the decrease in TNF-α release was about 95%, 75%, and 90% for the K34A, K64G, and K86A mutants, respectively, compared to the IFI16 wild-type protein, indicating their potential direct involvement in the IFI16-TLR4 binding process. Consistently, the triple mutant showed a similar decrease in TNF production (about 85%). Additionally, the E85A mutant, carrying a substitution in the amino acid implicated in MD2 binding, resulted in a significant decrease in TNF-α production (about 65%, compared to IFI16 wild-type protein) even if less pronounced compared to the other mutations targeting the amino acids implicated in TLR4 receptor binding.

Next, SPR analysis was performed to establish the ability of each mutant to physically interact with the TLR4/MD2 receptor complex. To this end, increasing concentrations of the IFI16 mutants or the *wild type* form were flowed over the TLR4/MD2-coated chip. As shown in **Figure 15B**, we observed that the single mutations targeting the amino acids potentially involved in the interaction with TLR4 (K34A, K64G, and K86A) or MD2 (E85A) significantly affected the ability to bind the receptor, with consequences also in the kinetic of the interaction since the sensorgrams of the mutated variants do not reach the saturation levels representative of the steady state and the Kinetic constant measured is not statistically significative. Consistently, a similar picture was observed for the triple K34A/L64G/K86A mutant, while the I17A mutant still retained the high significantly affinity binding to the TLR4/MD2 receptor complex (K_D=1.7*10^{-7}) which was comparable to that observed with the wild type of form (K_D=4.2*10^{-6}).

Taken together, these findings confirm the specificity of the interaction between PYHIN PYRIN domains and TLR4/MD2, identifying specific amino acids in the PYRIN domain of IFI16 that are crucial for the interaction with its receptor complex.

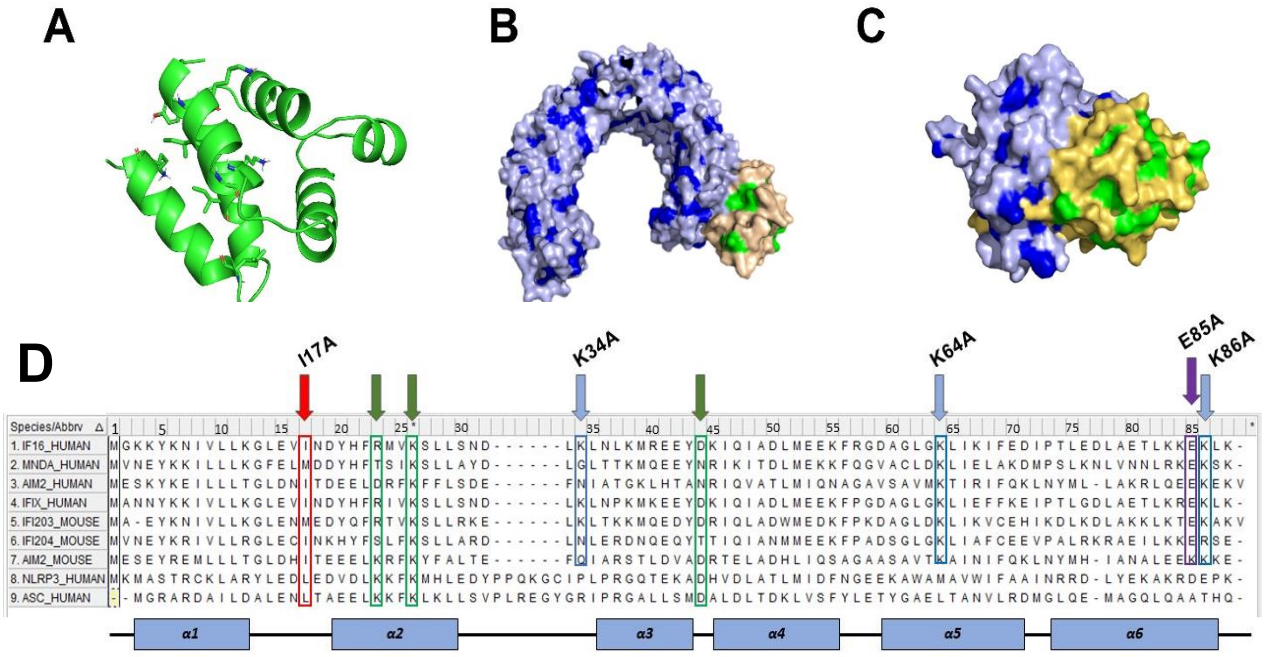

Figure 13. Caption on next page

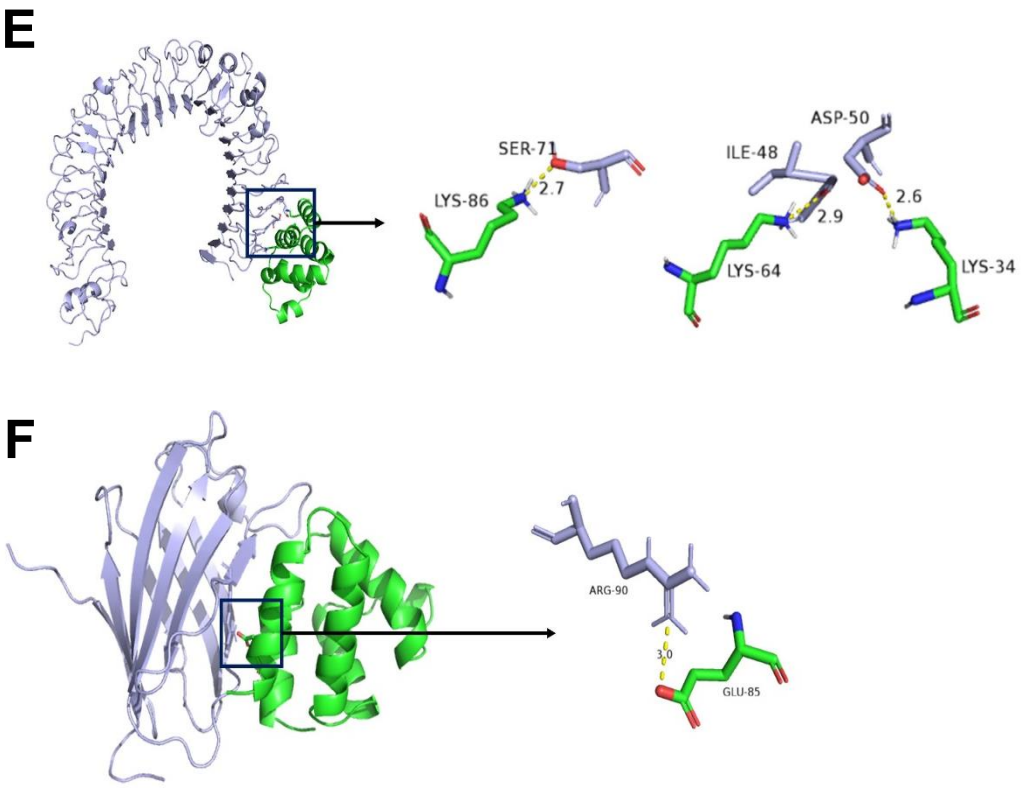

Figure 13. Structural analysis of the interaction moiety between the PYRIN domain of IFI16 and TLR4/MD2 complex. **A**) Predicted 3D structure of the IFI16 PYRIN domain using the Alphafold method (Jumper et al., Nature 2021). (**B, C**) Molecular docking analysis of the IFI16 PYRIN domain (green) and the extracellular portion of TLR4 (light blue) (PDB:3FXI, **B**) or with MD2 (PDB:2E56, **C**) using High Ambiguity Driven protein-protein DOCKing (HADDOCK, van Zundert et al., J. Mol. Biol., 2016). **D**) Alignment of the PYHIN PYRIN domains, along with those of NLRP3 and ASC, was performed using MEGAX and ClustalW algorithm to identify PYHIN-specific amino acids with similar chemical properties. Green arrows identify amino acids conserved across the different proteins, whereas light blue and purple arrows identify amino acids that are conserved only across the PYHIN family members and that were mutated (see Figure 6). The red arrow identifies the aminoacid which is conserved in all the proteins and that wasmutated as control. The six α helices of the PYRINs with known structures are also indicated. (**E, F**) Identification of the IFI16-PYRIN residues (green) potentially involved in the interaction with TLR4 (Lys34, Lys64, and Lys86, **E**) or MD2 *(*Glu85),(**F**) obtained by integrating the alignment and molecular docking information.

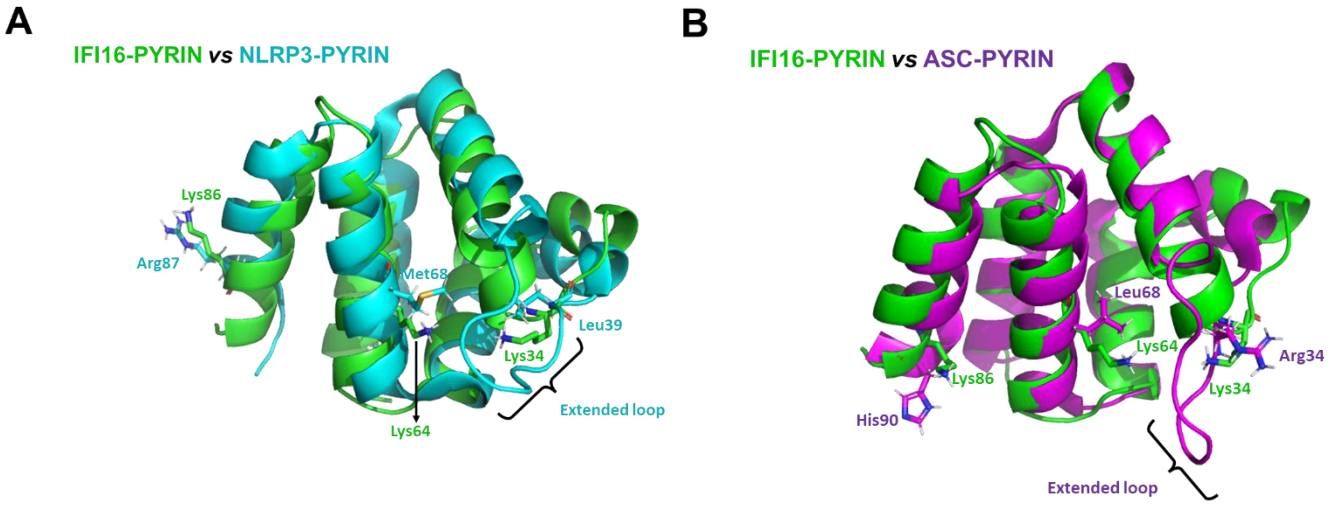

Figure 14. 3D structure alignment between the PYRIN domains of IFI16 and NLRP3 or ASC proteins. Superimposed alignments between the projected 3D structure of IFI16-PYRIN (green) and those of NLRP3-PYRIN (light blue, **A**) and of ASC-PYRIN (purple, **B**) using PyMOL software.

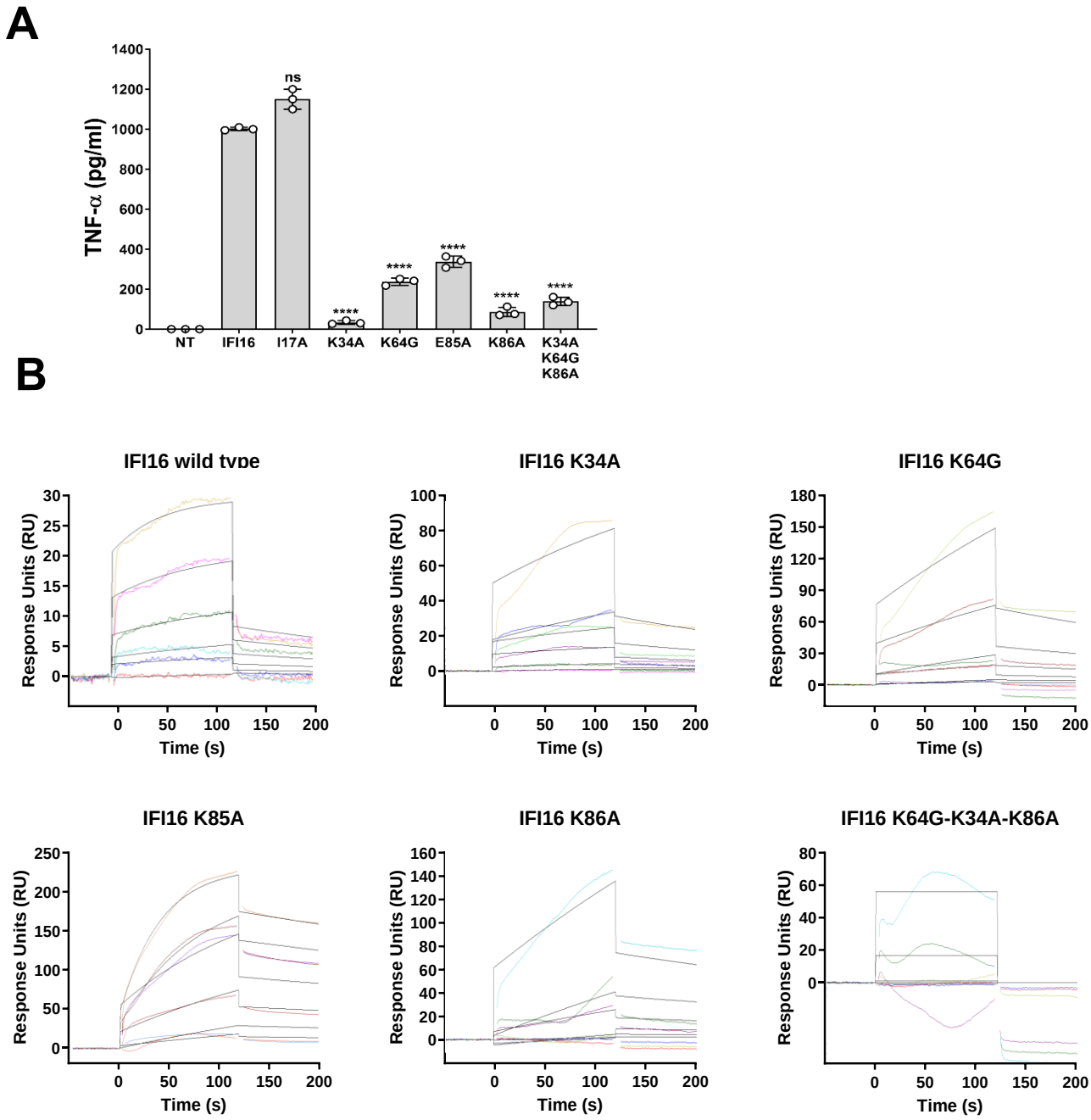

Figure 15. Four amino acids within the IFI16 PYRIN domain are critically involved in its TLR4-mediated proinflammatory activity. **A**) Equimolar concentrations (111mM) of the full-length IFI16 isoforms produced by site-directed mutagenesis of the amino acids in the PYRIN domain, as described in Figure 4, were used to stimulate human macrophages for 24h, along with the original isoform (IFI16 WT). Then, TNF-a release was measured through ELISA. Data are representative of three independent experiments, shown as the mean ± SD (* $p<0.05$, ** $p<0.01$, *** $p<0.001$; one-way ANOVA followed by Dunnett's test). **B**) The same mutants were also used to run surface plasmon resonance (SPR) analysis to immobilized TLR4/MD2. After immobilization of TLR4/MD2 on the CM5 sensor chip surface, increasing concentration of IFI16 *wt* and mutants (20–800 nM) diluted in running buffer were injected over immobilized complex. Data are representative of three different experiments, and for each analysis the dissociation constant (K_D) value is shown.

5.5 IFI16 is released in the extracellular milieu after stress stimuli.

The results described so far prompted us to evaluate the pathogenetic mechanism underlying IFI16 release. Since we have previously observed the occurrence of antibodies against IFI16 in the sera of patients with SLE, as well as UVB-induced IFI16 release in keratinocytes from SLE patients (Costa et al., 2011**)**, we reasoned that keratinocytes could represent a valuable model to characterize IFI16 release upon different stimuli. To this end, we took advantage of HaCaT cells, a spontaneously transformed immortal keratinocyte cell. We first confirmed that IFI16, normally restricted to the nucleus, can be induced to translocate in the extracellular milieu upon UVB-induced cell injury. Briefly, HaCaT were treated with different doses of UVB and then the presence of the protein in the culture supernatants was tested by immunoblotting. As shown in **Figure 16A**, IFI16 release was clearly both time- and dose-dependent, with maximum signals detected at 6hpt and upon 400-800J/m2 of UVB radiation, that were paralleled by a slight decrease of the intracellular protein. Analysis of LDH activity in the same supernatants confirmed that the extracellular presence of this soluble cytoplasmic protein as a consequence of cell death and lysis (Legrand et al., 1992) was barely detectable at 3hpt upon any irradiation doses even though start to increase at 6hpt with 200 and 400 J/m2 (~10% and ~20% of activity, respectively), when the IFI16 protein was already detectable. At higher irradiation dose (800J/m2), LDH activity increased dramatically in the extracellular medium, very likely due to cellular membrane rupture and the nonselective leakage of cytoplasmic proteins (**Figure 16B,** red bars). As further vitality control, we measured the cell viability and metabolic activity through the Alamar blue assay (Bonnier et al., 2015). As shown in **Figure 16B** (green bars), the metabolic activity decreasing compared with not treated cells was always not less than 75% regardless of the type of treatment, suggesting that IFI16 release could be associated to a partial active mechanism.

To follow the localization of IFI16 after UVB irradiation, we generated a chimera form where the full-length protein was fused with a mCherry fluorescent dye. Stable IFI16-knockout human keratinocytes (HaCaT IFI16KO cells) were transfected with IFI16-mCherry plasmid and then, after 48h, cells were irradiated with 400J/m2 of UVB and inserted in the Incucyte system. In IFI16-mCherry-transfected cells the fluorescent signal clearly spread and increase in the surrounding cells after 18h of incubation, whereas in cells transfected with the empty vector (mCherry alone) the fluorescent signal was constantly restricted to transfected cells (**Figure 16C)**. Although further controls should be generated, this experiment can be considered the first qualitative direct evidence proving the extracellular mobilization of IFI16 upon UVB treatment.

Then, to assess whether acute inflammation involving the epithelial cells, as those observed in some autoimmune conditions (Pisetsky, 2023) or viral infections [(Milora et al., 2014)**;** (Novak et al., 2021)], could be also associated to IFI16 release, HaCaT cells were subjected to TNFa treatment and herpes simplex type 1 (HSV-1) infection.

As shown in **Figure 17A**, 24h of treatment with 100ng/ml of TNF induced a considerable release of IFI16 in the supernatants, paralleled by an important decrease of protein expression in the total extracts. A significant IFI16 release occurred also at 48hpt, whereas these conditions were associated to significant cells death as demonstrated by the increase of LDH release (**Figure 17B**) used as a hallmark of cell distress (Takasu et al., 2016).

Finally, HaCaT cells were also infected with HSV-1 at multiplicity of infection (MOI) of 1. As shown in **Figure 18A**, HSV-1 induced a significant release of IFI16 as soon as 2hpi, with a peak of signal intensity that was three times higher than that observed for mock-infected cells at 4hpi (**Figure 18B**). Since both viability and metabolic rates were unaffected at these early time points, as demonstrated by the LDH and Alamar blue assays (**Figure 18C)**, these data strongly support the idea that an active process is behind the HSV-1-induced IFI16 extracellular release. At later time

point (24hpi), where HSV-1 reached the lytic phase (as demonstrated by the cell morphology shown in **Figure 18D)** these differences between HSV-1- and mock-infected cells were dramatically reduced, probably due to close cell-to-cell contact occurring in mock-infected cells. Consistently, immunofluorescence analysis showed that infected cells displayed a decreased nuclear IFII16 signal at 24hpi compared to uninfected neighboring cells, whereas the nuclear signals remained unaffected in mock-infected cells (**Figure 18E**). As further control, HaCaT cells were infected with UVB-inactivated HSV-1. As expected, in these conditions in which the virus cannot complete its replication cycle (as demonstrated by the absence of ICP0 and ICP27 viral protein expression and cytopathic effect, **Figures 18F and 18G**), we didn't observe extracellular release of IFI16 at early time points, (**Figure 18F).** Our current hypothesis, based on previous demonstrations that IFI16 behaves as a restriction factor for HSV-1 replication, (Johnson et al., 2014), is that the HSV-1-induced IFI16 translocation in the extracellular space works as a viral mechanism of defense. Further experiments have been planned in order to better clarify this hypothesis.

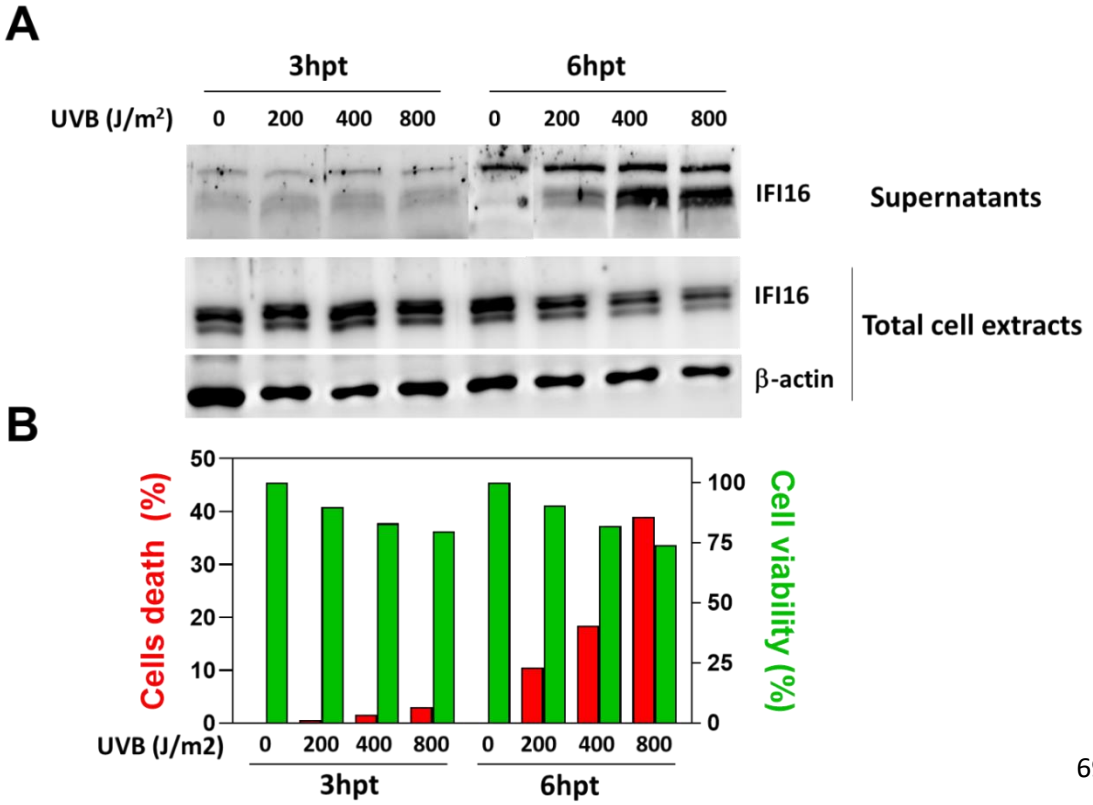

Figure 16. Caption on next page

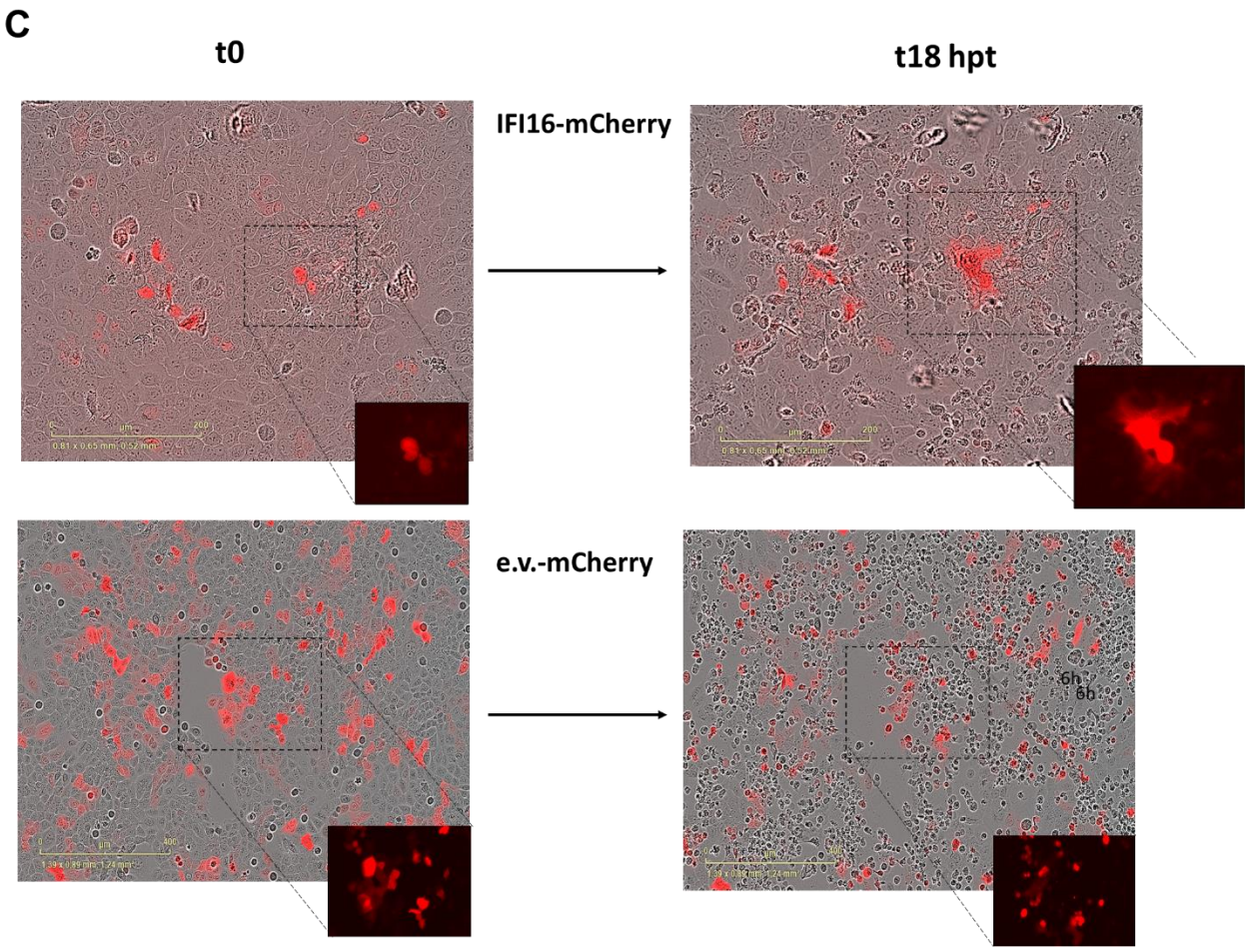

Figure 16. IFI16 release from HaCaT cells upon UVB exposure. (**A, B**) HaCaT cells were irradiated at the indicated doses of UVB (*i.e.* 200, 400, 800 J/m^2), for the indicated period of time (*i.e.* 3 and 6 hpt*)*. Then, **A**) immunoblotting with anti-IFI16 antibody were performed by using 30ul of supernatants and 20ug of total cell extracts (b-actin was used as loading control). **B**) The same supernatants were also used to test LDH release (red bars), and cells were tested for metabolic activity through Alamar blue assay (green bars). (**C**) IFI16KO-HaCaT cells, transfected with the IFI16-mCherry construct or with empty control vector (e.v.-mCherry), were UVB irradiated (400 J/m2) and monitored in an Incucyte system every 30 minute. Representative figures taken at T0 (immediately after the UVB exposure, left panels) and 18 hours after UVB exposure (T18, right panels) with bright-field and a red fluorescent filter (for mCherry) are shown.

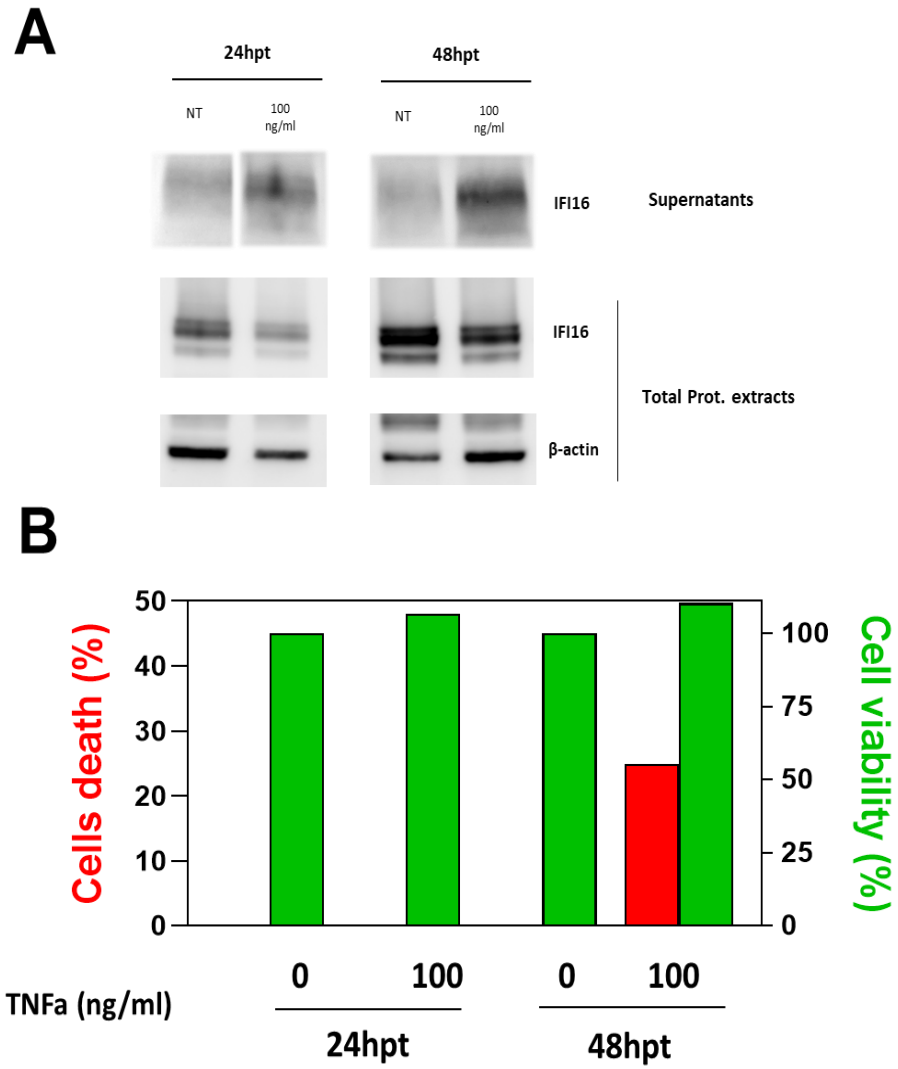

Figure 17. IFI16 release from HaCaT cells upon TNFα treatment. Cells were treated with 100 ng/ml of TNFα, for the indicated period of time (24 and 48hpt). Then, **A**) immunoblotting with anti-IFI16 antibody were performed using 30ul of supernatants and 20ug of total cell extracts (b-actin was used as loading control). **B**) The same supernatants were also used to test the LDH release (red bars) and cells were also tested for metabolic activity through Alamar blue assay (green bars).

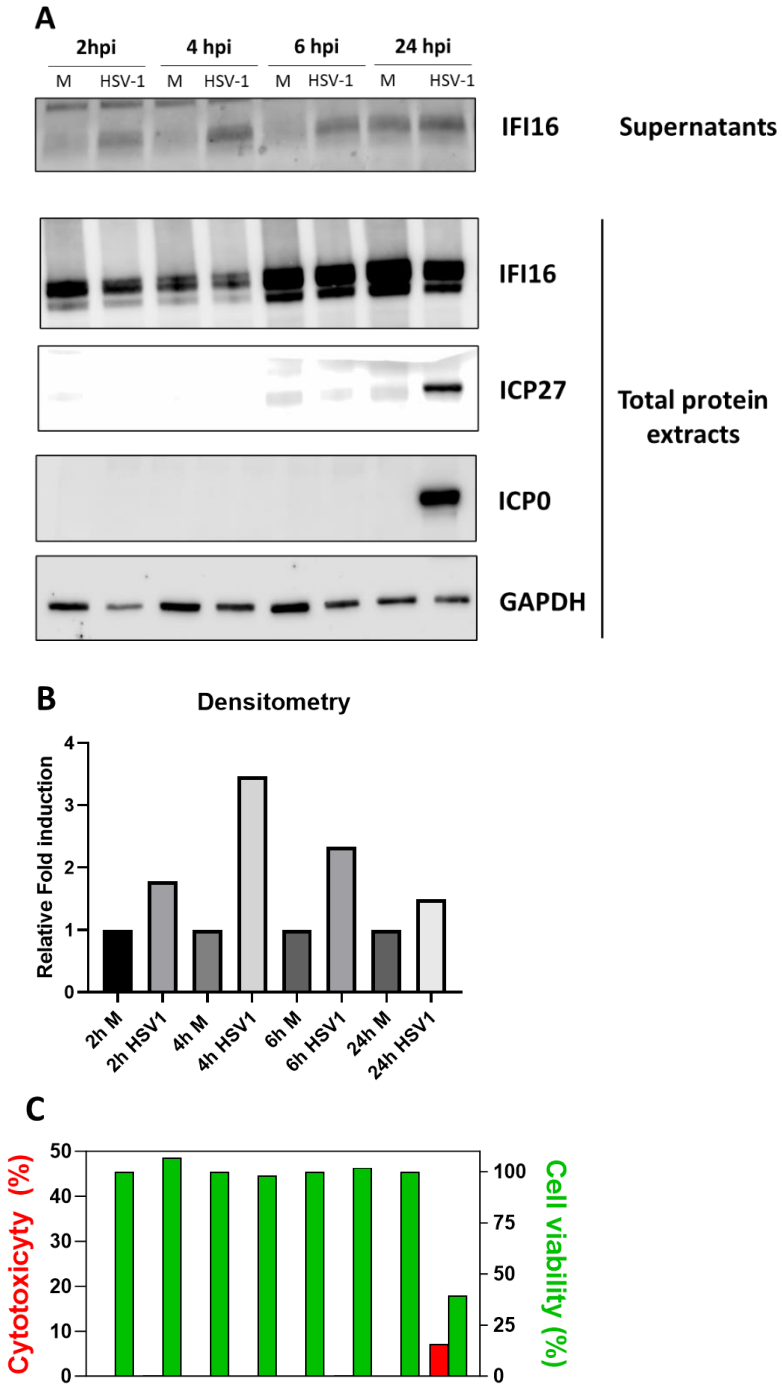

Figure 18. IFI16 release from HaCaT cells upon HSV-1 infection. Cells were infected with HSV-1 (MOI 1) for the indicated time points. Then, **A**) immunoblotting with anti-IFI16 antibody were performed using 30ul of supernatants and 20ug of total cell extracts. Antibodies against ICP0 and ICP27 were used to monitor the infection, while GAPDH was used as loading control. **B**) Densitometric analysis of the bands reported in panel A were performed using Quantity One software (version 4.6.9, Bio-Rad) and the signals of mock-infected cells (M) as reference. **C**) The same supernatants were also used to test the LDH release (red bars) and the cells were also tested for metabolic activity through the Alamar blue assay (green bars). (Continued on next page)

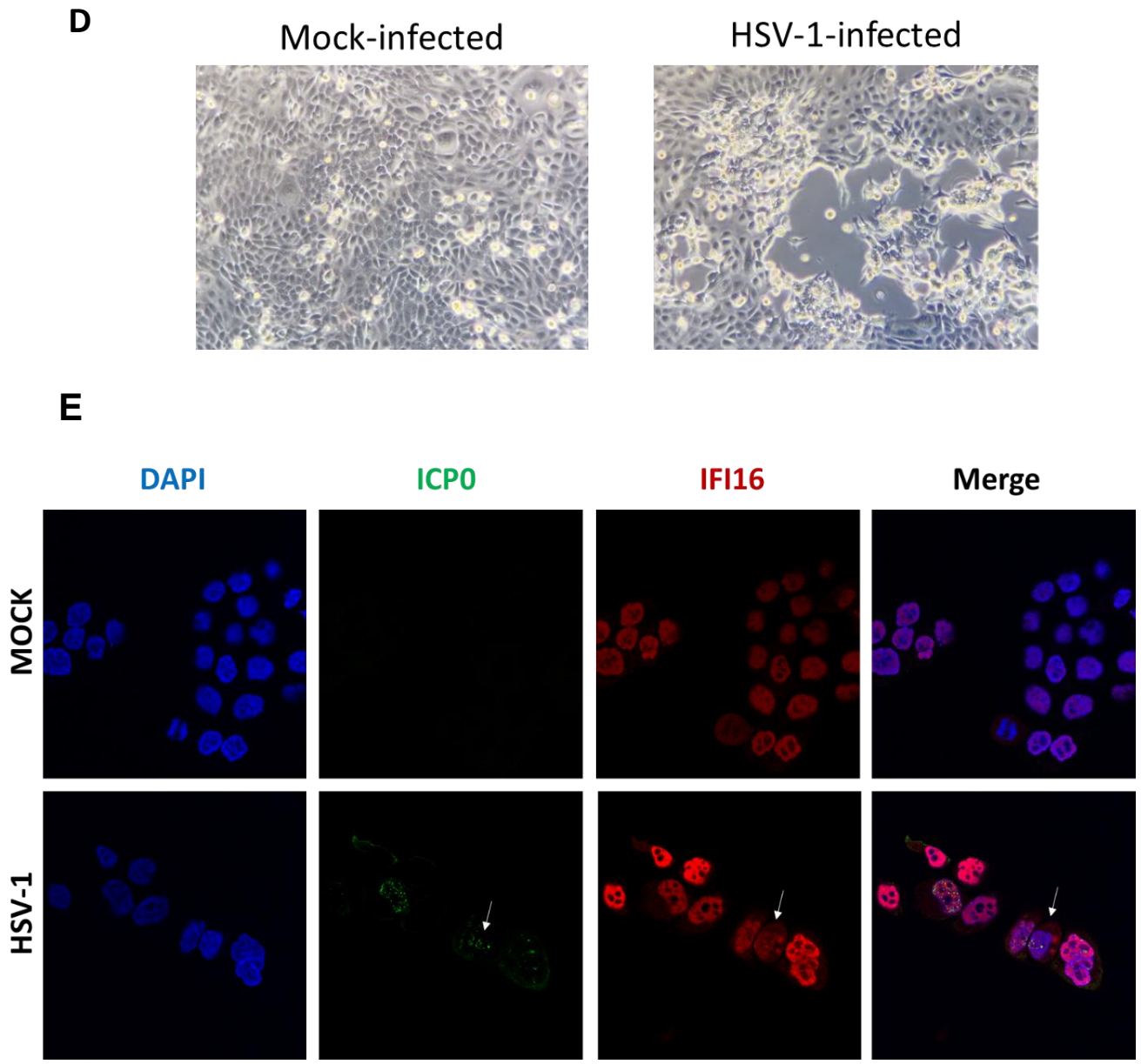

Figure 18 (continued). **D**) Representative bright-field images of mock- and HSV-1-infected cells taken at 24 hpi showing the typical HSV-associated cytopathic effect. **E**) Representative immunofluorescence staining's at ×64 magnification, for the immediate HSV-1 early antigen ICP0 (in green) and human IFI16 (in red) in mock- or HSV-1-infected HaCaT cells at 24hpi. Cell nuclei are visualized by DAPI (blue)**.** (Continued on next page)

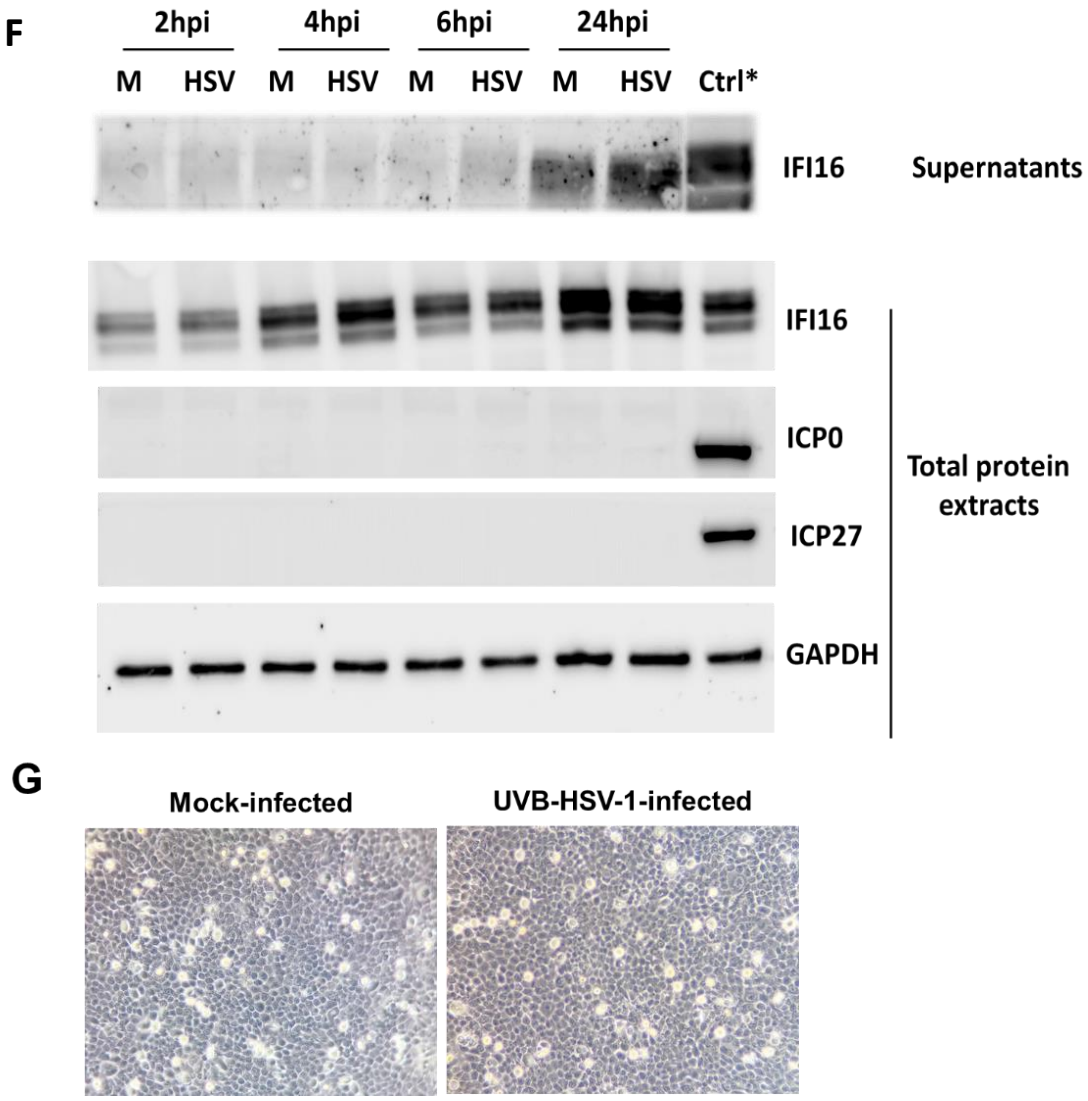

Figure 18 (continued). **E**) Representative immunofluorescence staining's at ×64 magnification, for the immediate HSV-1 early antigen ICP0 (in green) and human IFI16 (in red) in mock- or HSV-1-infected HaCaT cells at 24hpi. Cell nuclei are visualized by DAPI (blue). **F, G**) IFI16 release from HaCaT cells upon infection with UVB-irradiated HSV-1. Cells were infected as described in A with UVB-irradiated (two rounds at 1200J/m2) HSV-1. Then, **F**) immunoblotting with anti-IFI16 antibody were performed using 30ul of supernatants and 20ug of total cell extracts. Antibodies against ICP0 and ICP27 were used to monitor the infection, while GAPDH was used as loading control. Control (Ctrl) refers to an infection done with wt HSV-1 (MOI 1, 24hpi). **G**) Representative bright-field images of mock- and UVB-HSV-1-infected cells taken at 24 hpi showing the lack of the canonical cytopathic effect associated to HSV-1 lytic cycle.

6. Discussion

Besides sensing exogenous microbial components, in recent years TLRs have been shown to be involved in the recognition of endogenous material released during cellular injury, thereby promoting a non-microbial-induced inflammatory state known as sterile inflammation. If not resolved, sterile inflammation can in turn lead to severe acute and chronic inflammatory conditions [(Piccinini and Midwood, 2010); (Rifkin et al., 2005); (Schaefer, 2014)]. Recently, we have demonstrated that IFI16 represents a novel trigger of sterile inflammation acting through the TLR4 signaling pathway (Iannucci et al., 2020). Here, we expanded on those observations by systematically dissecting the IFI16 sequence elements to define the IFI16 and TLR4 interaction and signaling mechanism. For the first time, we showed that the proinflammatory activity of the IFI16 protein specifically lies within its N-terminal region and that the IFI16-PYRIN domain is involved in TLR4/MD2 binding and activation. In relation to this, antibodies against the N-terminal part of IFI16 i) decreased the ability to induce inflammation in human macrophages in a dose-dependent fashion, and ii) decreased the ability to bind the TLR4/MD2 complex in saturation binding experiments. This led us to perform experiments by using specific recombinant subdomain of IFI16. Among all, only the PYRIN domain was able to induce IL-1β, IL-8 and TNF-α transcriptional activation and cytokine release into the supernatants of human macrophages. Moreover, by means of *in vivo* co-immunoprecipitation assay and *in vitro* saturation binding experiments, we have provided the first evidence that the IFI16-PYRIN directly mediates the binding with TLR4/MD2 complex. Interestingly, IFI16 pro-inflammatory activity lies within its PYRIN domain, which is necessary and sufficient to induce overexpression of pro-inflammatory cytokines. The PYRIN domain is commonly composed of six α-helices tightly packed around a hydrophobic core with a highly charged surface like other members of the death domain (DD) superfamily (Jin et al., 2013). Indeed, it is widely spread along

different proteins (Dorfleutner et al., 2015). There are more than 20 PYRIN-containing proteins in the human genome (Kwon et al., 2012), most of which share some residues in their PYRIN domains (Jin et al., 2013), nevertheless no one consensus protein sequence for the PYRIN domain exists across all. Our hypothesis that specific members of PYHIN family could mimic the activity of IFI16-PYRIN domain, paving the way toward the identification of a new class of DAMPs that, once extracellularly released by damaged cells, can trigger sterile inflammation through the engagement of the TLR4/MD2 receptor. In line with this hypothesis, we here provide evidence that the proinflammatory activity of the PYRIN domain is conserved among the PYHIN family members, including both the human and mouse gene families. By producing the recombinant PYRIN domains belonging to different PYHIN proteins we confirmed that sterile inflammation in human and mouse macrophages occurred through the TLR4 pathway, in the same way as for IFI16-PYRIN. The inflammatory signature significantly decreased when we utilized a selective signaling inhibitor of TLR4 (*i.e.*, CLI-095) which hinders both the MyD88- and the TRIF-dependent pathways by binding the cysteine 747 in the intracellular domain of TLR4 (Kawamoto et al., 2008)]. Along with inducing inflammation, we also tested the ability to bind the TLR4/MD2 complex in saturation binding experiments. Consistent with the observation with IFI16-PYRIN, human AIM2-PYRIN and mouse p203-PYRIN (chosen as representative of the PYHIN family) shared the ability to bind TLR4 receptor with high-affinity, while the NLRP3-PYRIN (as paradigm of non-PYHIN protein) did not. All in all, we propose that the PYHIN-PYRINs can be considered as a new class of DAMPs.

Finally, we have also mapped and those specific amino acids located within the IFI16-PYRIN domain and partially conserved across the PHYN family but absent in the PYRIN domain from other gene families, e.g. NRLP3, that are critically involved in their TLR4-mediated proinflammatory activity of the family members.

In this context we chose IFI16 as paradigmatic of the entire PYHIN family to underline the strength interaction with TLR4/MD2 receptor complex to find and inhibit them with new small drugs. Thanks to structural prediction software, we hypothesized either the molecular structure and the interaction mode between IFI16PYRIN and the extracellular domain of TLR4 receptor, revealing three amino acids of IFI16PYRIN involved in the binding with TLR4 and one amino acid with MD2. By site-directed mutagenesis, we generated mutated recombinant domains in the predicted amino acids, and we showed that by mutating them there was a significant decrease in both cytokine release and kinetics of receptor binding. To support this idea, the comparison of quaternary structures between IFI16-PYRIN and NLRP3-PYRIN or ASC-PYRIN, revealed that the amino acids mutated in IFI16 correspond to residues lying in an external loop in both NLRP3 and ASC. This observation suggests a potential explanation for why neither NLRP3 nor ASC can bind to TLR4/MD2. Remarkably, all these information allow to identify a specific region of IFI16 Pyrin responsible for the binding to TLR4/MD2 complex and pave the way for the synthesis new compounds specifically targeting this interaction as future strategy against autoinflammatory/autoimmune disease.

In this regard, abnormal IFI16 expression in otherwise negative cells, or IFI16 delocalization, has been reported in a variety of inflammatory conditions, including SLE (skin, Costa et al., 2011), psoriasis (skin), [Cao et al., 2016; (Chiliveru et al., 2014); Tervaniemi et al., 2016), SSc (skin), (Mondini et al., 2006), IBD (colonic epithelium) [(Caneparo et al., 2016; Vanhove et al., 2015) and SS (salivary epithelial and inflammatory infiltrating cells, [(Alunno et al., 2015); Alunno et al., 2016**;** Antiochos et al., 2019)]. We discovered that high levels of circulating IFI16 (27 ng/ml) were related with overall worse clinical parameters in three RA, SS, and PsA patient cohorts. Interestingly, circulating IFI16 was discovered more often in RA patients with RF/anti-CCP-positive blood and was substantially linked with pulmonary involvement (Alunno et al., 2016).

Furthermore, in SS patients, circulating IFI16 is associated with an increased prevalence of both RF and the degree of glandular infiltration, whereas in PsA patients, it correlates with heightened C-reactive protein (CRP) levels (De Andrea et al., 2020). We discovered that high levels of circulating IFI16 were related with overall worse clinical parameters in three RA, SS, and PsA patient cohorts. Interestingly, circulating IFI16 was discovered more often in RA patients with RF/anti-CCP-positive blood and was substantially linked with pulmonary involvement (Alunno et al., 2016). Furthermore, in SS patients, circulating IFI16 is associated with an increased prevalence of both RF and the degree of glandular infiltration, whereas in PsA patients, it correlates with heightened C-reactive protein (CRP) levels (De Andrea et al., 2020).

The first evidence of IFI16 release in the extracellular milieu in vitro has also been shown by our group in human keratinocytes exposed to UVB radiation (Costa et al., 2011). To confirm that, we treated HaCaT cells with UVB and observed the release in the extracellular milieu after six hours of treatment. In parallel, by measuring the cell viability and metabolic rate, we hypothesized that an active mechanism could be responsible for this release. This is also partially confirmed by using a fluorescent IFI16 chimera that, once overexpressed IFI16-null HaCaT cells, increases its signal towards neighboring cells upon UVB exposure.

Moreover, in the attempt to investigate whether chronic inflammation could induce the release of IFI16 (Jang et al., 2021), we evaluated HaCaT cells response to TNFa treatment. We assessed the presence of IFI16 release in the supernatant at both 24- and 48-hours post-treatment, while cell viability remained high at both time points, with a slight increase in cell death observed only at 48 hpt. These results are consistent with previous studies reporting a correlation between inflammation and circulating IFI16 in various autoimmune diseases.

Finally, we investigate other stress stimuli (*i.e.* viral infection) potentially promoting IFI16 release based on previous evidence [Dell'Oste et al., 2014]. In fact, it's been demonstrated that IFI16 binds

to the HSV-1 genome in a sequence-independent manner and promotes both antiviral cytokine expression and suppresses virus gene expression (Howard et al., 2022). Moreover, HSV1 infects the stratified epithelia of the epidermis, oral or genital mucosa, where the main cell type is the keratinocyte (Kite et al., 2021). For these reasons after infecting HaCaT cells with HSV-1 (which is known for its ability to delocalize IFI16 from nucleus to cytoplasm), we observed the presence of IFI16 in the supernatant only in presence of viable viral particles. These results suggest that HSV-1 may have evolved mechanisms to mislocalize IFI16, serving as an additional strategy to evade IFI16's restrictive activity. The specific mechanism is still unclear and remains to be established.

Although the biological rationale of these findings is far from being completely understood, these observations indicate that the IFI16 protein, whose expression in the natural setting is restricted to the nuclei of a limited number of cell types, such as keratinocytes, can be released upon a broad spectrum of stress stimuli such as strong solar exposure (UVB irradiation), inflammation (TNF-α treatment) and viral infection (HSV-1 infection). In this setting, as largely mentioned above, extracellular IFI16 and other members of the PYHIN family can act as a DAMP in promoting and amplifying sterile inflammation, providing the rational for considering them as new targets for the treatment of autoimmune/autoinflammatory disease.

7. Conclusion and future prospectives

Overall, our findings unveil a central role of the IFI16PYRIN domain in triggering inflammation through its ability to bind the TLR4/MD2 complex. Moreover, we demonstrate that this ability is specifically preserved in all the PYRIN domains of the PYHIN family proteins, introducing a new class of inflammatory molecules with DAMP characteristics. In the near future, we aim to identify novel therapeutic agents (*e.g.*, small molecules, small peptides) that target specific amino acids responsible for TLR4 binding in order to inhibit the IFI16-mediated inflammation. This will be central to dampen the chronic stimulation of the immune system during autoimmune/autoinflammatory diseases. Additionally, we have shown that stress stimuli, *i.e.* UVB irradiation, TNFa treatment and HSV-1 infection, trigger IFI16 release, suggesting pathogenetic mechanisms involved in the generation of circulating IFI16. A more comprehensive analysis is needed to dissect the molecules and compartment implicated in this translocation. Our current hypothesis suggests the participation of Exportin 1 in the relocation from nucleus to the cytoplasm, and of exosomes for the extracellular release, although the latter is likely dependent on stimuli. To advance in this direction, the application of specific inhibitors and tools, such as the fluorescent chimera IFI16-mCherry, the recombinant IFI16 domains and truncated proteins developed in our laboratory, will be pivotal.

8. Bibliography

Aggarwal, A., Miranda-Saksena, M., Boadle, R.A., Kelly, B.J., Diefenbach, R.J., Alam, W., Cunningham, A.L., 2012. Ultrastructural Visualization of Individual Tegument Protein Dissociation during Entry of Herpes Simplex Virus 1 into Human and Rat Dorsal Root Ganglion Neurons. J. Virol. 86, 6123–6137. https://doi.org/10.1128/jvi.07016-11

Aglipay, J.A., Lee, S.W., Okada, S., Fujiuchi, N., Ohtsuka, T., Kwak, J.C., Wang, Y., Johnstone, R.W., Deng, C., Qin, J., Ouchi, T., 2003. A member of the Pyrin family, IFI16, is a novel BRCA1-associated protein involved in the p53-mediated apoptosis pathway. Oncogene 22, 8931–8938. https://doi.org/10.1038/sj.onc.1207057

Ahmad, I., Wilson, D.W., 2020. HSV-1 Cytoplasmic Envelopment and Egress. Int. J. Mol. Sci. 21, 5969. https://doi.org/10.3390/ijms21175969

Akashi, S., Shimazu, R., Ogata, H., Nagai, Y., Takeda, K., Kimoto, M., Miyake, K., 2000. Cutting edge: cell surface expression and lipopolysaccharide signaling via the toll-like receptor 4-MD-2 complex on mouse peritoneal macrophages. J. Immunol. Baltim. Md 1950 164, 3471–3475. https://doi.org/10.4049/jimmunol.164.7.3471

Almine, J.F., O'Hare, C.A.J., Dunphy, G., Haga, I.R., Naik, R.J., Atrih, A., Connolly, D.J., Taylor, J., Kelsall, I.R., Bowie, A.G., Beard, P.M., Unterholzner, L., 2017. IFI16 and cGAS cooperate in the activation of STING during DNA sensing in human keratinocytes. Nat. Commun. 8, 14392. https://doi.org/10.1038/ncomms14392

Alunno, A., Caneparo, V., Bistoni, O., Caterbi, S., Terenzi, R., Gariglio, M., Bartoloni, E., Manzo, A., Landolfo, S., Gerli, R., 2016. Circulating Interferon-Inducible Protein IFI16 Correlates With Clinical and Serological Features in Rheumatoid Arthritis. Arthritis Care Res. 68, 440–445. https://doi.org/10.1002/acr.22695

Alunno, A., Caneparo, V., Carubbi, F., Bistoni, O., Caterbi, S., Bartoloni, E., Giacomelli, R., Gariglio, M., Landolfo, S., Gerli, R., 2015. Interferon gamma-inducible protein 16 in primary Sjögren's syndrome: a novel player in disease pathogenesis? Arthritis Res. Ther. 17, 208. https://doi.org/10.1186/s13075-015-0722-2

Andersson, U., Tracey, K.J., 2003. HMGB1 in sepsis. Scand. J. Infect. Dis. 35, 577–584. https://doi.org/10.1080/00365540310016286

Ansari, M.A., Singh, V.V., Dutta, S., Veettil, M.V., Dutta, D., Chikoti, L., Lu, J., Everly, D., Chandran, B., 2013. Constitutive Interferon-Inducible Protein 16-Inflammasome Activation during Epstein-Barr Virus Latency I, II, and III in B and Epithelial Cells. J. Virol. 87, 8606–8623. https://doi.org/10.1128/jvi.00805-13

Antiochos, B., Matyszewski, M., Sohn, J., Casciola-Rosen, L., Rosen, A., 2019. IFI16 filament formation in salivary epithelial cells shapes the anti-IFI16 immune response in Sjögren's syndrome. JCI Insight 3. https://doi.org/10.1172/jci.insight.120179

Antiochos, B., Trejo-Zambrano, D., Fenaroli, P., Rosenberg, A., Baer, A., Garg, A., Sohn, J., Li, J., Petri, M., Goldman, D.W., Mecoli, C., Casciola-Rosen, L., Rosen, A., 2022. The DNA sensors AIM2 and IFI16 are SLE autoantigens that bind neutrophil extracellular traps. eLife 11, e72103. https://doi.org/10.7554/eLife.72103

Apetoh, L., Ghiringhelli, F., Tesniere, A., Criollo, A., Ortiz, C., Lidereau, R., Mariette, C., Chaput, N., Mira, J.-P., Delaloge, S., André, F., Tursz, T., Kroemer, G., Zitvogel, L., 2007. The interaction between HMGB1 and TLR4 dictates the outcome of anticancer chemotherapy and radiotherapy. Immunol. Rev. 220, 47–59. https://doi.org/10.1111/j.1600-065X.2007.00573.x

Awad, E.A., Mohamed, W.A.I., George, T.M.A., Elshennawy, E.A.M.A., 2023. Anti-IFI16 Antibodies in Inflammatory Bowel Disease and Their Variation with Infliximab Therapy in Comparison to Other Modalities of Treatment. QJM Int. J. Med. 116, hcad069.407. https://doi.org/10.1093/qjmed/hcad069.407

Azzimonti, B., Pagano, M., Mondini, M., De Andrea, M., Valente, G., Monga, G., Tommasino, M., Aluffi, P., Landolfo, S., Gariglio, M., 2004. Altered patterns of the interferon-inducible gene IFI16 expression in head and neck squamous cell carcinoma: immunohistochemical study including correlation with retinoblastoma protein, human papillomavirus infection and proliferation index. Histopathology 45, 560–572. https://doi.org/10.1111/j.1365-2559.2004.02000.x

Baer, A.N., Petri, M., Sohn, J., Rosen, A., Casciola-Rosen, L., 2016. Association of Antibodies to Interferon-Inducible Protein-16 With Markers of More Severe Disease in Primary Sjögren's Syndrome. Arthritis Care Res. 68, 254–260. https://doi.org/10.1002/acr.22632

Baillet, A., Trocmé, C., Berthier, S., Arlotto, M., Grange, L., Chenau, J., Quétant, S., Sève, M., Berger, F., Juvin, R., Morel, F., Gaudin, P., 2010. Synovial fluid proteomic fingerprint: S100A8, S100A9 and S100A12 proteins discriminate rheumatoid arthritis from other inflammatory joint diseases. Rheumatol. Oxf. Engl. 49, 671–682. https://doi.org/10.1093/rheumatology/kep452

Baines, J.D., Ward, P.L., Campadelli-Fiume, G., Roizman, B., 1991. The UL20 gene of herpes simplex virus 1 encodes a function necessary for viral egress. J. Virol. 65, 6414–6424. https://doi.org/10.1128/jvi.65.12.6414-6424.1991

Balka, K.R., De Nardo, D., 2019. Understanding early TLR signaling through the Myddosome. J. Leukoc. Biol. 105, 339–351. https://doi.org/10.1002/JLB.MR0318-096R

Barrat, F.J., Crow, M.K., Ivashkiv, L.B., 2019. Interferon target-gene expression and epigenomic signatures in health and disease. Nat. Immunol. 20, 1574–1583. https://doi.org/10.1038/s41590-019-0466-2

Bawadekar, M., De Andrea, M., Gariglio, M., Landolfo, S., 2015. Mislocalization of the interferon inducible protein IFI16 by environmental insults: Implications in autoimmunity. Cytokine Growth Factor Rev., Interferon Fundamentals: A tribute to the scientific vision of GB Rossi 26, 213–219. https://doi.org/10.1016/j.cytogfr.2014.10.003

Bawadekar, M., De Andrea, M., Lo Cigno, I., Baldanzi, G., Caneparo, V., Graziani, A., Landolfo, S., Gariglio, M., 2015b. The Extracellular IFI16 Protein Propagates Inflammation in Endothelial Cells Via p38 MAPK and NF-κB p65 Activation. J. Interferon Cytokine Res. 35, 441–453. https://doi.org/10.1089/jir.2014.0168

Bhattacharyya, S., Midwood, K.S., Varga, J., 2022. Tenascin-C in fibrosis in multiple organs: Translational implications. Semin. Cell Dev. Biol., Special Issue: Satellite DNA by Yukiko Yamashita / Special Issue: Keratins by Ling-juan Zhang 128, 130–136. https://doi.org/10.1016/j.semcdb.2022.03.019

Bhattacharyya, S., Wang, W., Morales-Nebreda, L., Feng, G., Wu, M., Zhou, X., Lafyatis, R., Lee, J., Hinchcliff, M., Feghali-Bostwick, C., Lakota, K., Budinger, G.R.S., Raparia, K., Tamaki, Z., Varga, J., 2016. Tenascin-C drives persistence of organ fibrosis. Nat. Commun. 7, 11703. https://doi.org/10.1038/ncomms11703

Bonnier, F., Keating, M.E., Wróbel, T.P., Majzner, K., Baranska, M., Garcia-Munoz, A., Blanco, A., Byrne, H.J., 2015. Cell viability assessment using the Alamar blue assay: A comparison of 2D and 3D cell culture models. Toxicol. In Vitro 29, 124–131. https://doi.org/10.1016/j.tiv.2014.09.014

Brandariz-Nuñez, A., Liu, T., Du, T., Evilevitch, A., 2019. Pressure-driven release of viral genome into a host nucleus is a mechanism leading to herpes infection. eLife 8, e47212. https://doi.org/10.7554/eLife.47212

Buch, A., Müller, O., Ivanova, L., Döhner, K., Bialy, D., Bosse, J.B., Pohlmann, A., Binz, A., Hegemann, M., Nagel, C.-H., Koltzenburg, M., Viejo-Borbolla, A., Rosenhahn, B., Bauerfeind, R., Sodeik, B., 2017. Inner tegument proteins of Herpes Simplex Virus are sufficient for intracellular capsid motility in neurons but not for axonal targeting. PLOS Pathog. 13, e1006813. https://doi.org/10.1371/journal.ppat.1006813

Bucks, M.A., O'Regan, K.J., Murphy, M.A., Wills, J.W., Courtney, R.J., 2007. Herpes simplex virus type 1 tegument proteins VP1/2 and UL37 are associated with intranuclear capsids. Virology 361, 316–324. https://doi.org/10.1016/j.virol.2006.11.031

Bürckstümmer, T., Baumann, C., Blüml, S., Dixit, E., Dürnberger, G., Jahn, H., Planyavsky, M., Bilban, M., Colinge, J., Bennett, K.L., Superti-Furga, G., 2009. An orthogonal proteomic-genomic screen identifies AIM2 as a cytoplasmic DNA sensor for the inflammasome. Nat. Immunol. 10, 266–272. https://doi.org/10.1038/ni.1702

Caneparo, V., Cena, T., De Andrea, M., Dell'Oste, V., Stratta, P., Quaglia, M., Tincani, A., Andreoli, L., Ceffa, S., Taraborelli, M., Magnani, C., Landolfo, S., Gariglio, M., 2013. Anti-IFI16 antibodies and their relation to disease characteristics in systemic lupus erythematosus. Lupus 22, 607–613. https://doi.org/10.1177/0961203313484978

Caneparo, V., Landolfo, S., Gariglio, M., De Andrea, M., 2018. The Absent in Melanoma 2-Like Receptor IFN-Inducible Protein 16 as an Inflammasome Regulator in Systemic Lupus Erythematosus: The Dark Side of Sensing Microbes. Front. Immunol. 9.

Caneparo, V., Pastorelli, L., Pisani, L.F., Bruni, B., Prodam, F., Boldorini, R., Roggenbuck, D., Vecchi, M., Landolfo, S., Gariglio, M., De Andrea, M., 2016. Distinct Anti-IFI16 and Anti-GP2 Antibodies in Inflammatory Bowel Disease and Their Variation with Infliximab Therapy. Inflamm. Bowel Dis. 22, 2977–2987. https://doi.org/10.1097/MIB.0000000000000926

Cao, T., Shao, S., Li, B., Jin, L., Lei, J., Qiao, H., Wang, G., 2016. Up-regulation of Interferon-inducible protein 16 contributes to psoriasis by modulating chemokine production in keratinocytes. Sci. Rep. 6, 25381. https://doi.org/10.1038/srep25381

Caposio, P., Gugliesi, F., Zannetti, C., Sponza, S., Mondini, M., Medico, E., Hiscott, J., Young, H.A., Gribaudo, G., Gariglio, M., Landolfo, S., 2007. A Novel Role of the Interferon-inducible Protein IFI16 as Inducer of Proinflammatory Molecules in Endothelial Cells*. J. Biol. Chem. 282, 33515–33529. https://doi.org/10.1074/jbc.M701846200

Chan, Y.K., Gack, M.U., 2016. Viral evasion of intracellular DNA and RNA sensing. Nat. Rev. Microbiol. 14, 360–373. https://doi.org/10.1038/nrmicro.2016.45

Chaplin, D.D., 2010. Overview of the Immune Response. J. Allergy Clin. Immunol. 125, S3-23. https://doi.org/10.1016/j.jaci.2009.12.980

Chen, G.Y., Nuñez, G., 2010. Sterile inflammation: sensing and reacting to damage. Nat. Rev. Immunol. 10, 826–837. https://doi.org/10.1038/nri2873

Chiliveru, S., Rahbek, S.H., Jensen, S.K., Jørgensen, S.E., Nissen, S.K., Christiansen, S.H., Mogensen, T.H., Jakobsen, M.R., Iversen, L., Johansen, C., Paludan, S.R., 2014. Inflammatory Cytokines Break Down Intrinsic Immunological Tolerance of Human Primary Keratinocytes to Cytosolic DNA. J. Immunol. 192, 2395–2404. https://doi.org/10.4049/jimmunol.1302120

Ciesielska, A., Matyjek, M., Kwiatkowska, K., 2021. TLR4 and CD14 trafficking and its influence on LPS-induced pro-inflammatory signaling. Cell. Mol. Life Sci. 78, 1233–1261. https://doi.org/10.1007/s00018-020-03656-y

Costa, S., Borgogna, C., Mondini, M., De Andrea, M., Meroni, P.L., Berti, E., Gariglio, M., Landolfo, S., 2011. Redistribution of the nuclear protein IFI16 into the cytoplasm of ultraviolet B-exposed keratinocytes as a mechanism of autoantigen processing. Br. J. Dermatol. 164, 282–290. https://doi.org/10.1111/j.1365-2133.2010.10097.x

Cridland, J.A., Curley, E.Z., Wykes, M.N., Schroder, K., Sweet, M.J., Roberts, T.L., Ragan, M.A., Kassahn, K.S., Stacey, K.J., 2012. The mammalian PYHIN gene family: Phylogeny, evolution and expression. BMC Evol. Biol. 12, 140. https://doi.org/10.1186/1471-2148-12-140

Cuchet-Lourenço, D., Anderson, G., Sloan, E., Orr, A., Everett, R.D., 2013. The Viral Ubiquitin Ligase ICP0 Is neither Sufficient nor Necessary for Degradation of the Cellular DNA Sensor IFI16 during Herpes Simplex Virus 1 Infection. J. Virol. 87, 13422–13432. https://doi.org/10.1128/jvi.02474-13

Dawson, M.J., Elwood, N.J., Johnstone, R.W., Trapani, J.A., 1998. The IFN-inducible nucleoprotein IFI 16 is expressed in cells of the monocyte lineage, but is rapidly and markedly down-regulated in other myeloid precursor populations. J. Leukoc. Biol. 64, 546–554. https://doi.org/10.1002/jlb.64.4.546

De Andrea, M., De Santis, M., Caneparo, V., Generali, E., Sirotti, S., Isailovic, N., Guidelli, G.M., Ceribelli, A., Fabbroni, M., Simpatico, A., Cantarini, L., Gisondi, P., Idolazzi, L., Gariglio, M., Selmi, C., 2020. Serum IFI16 and anti-IFI16 antibodies in psoriatic arthritis. Clin. Exp. Immunol. 199, 88–96. https://doi.org/10.1111/cei.13376

Dell'Oste, V., Gatti, D., Giorgio, A.G., Gariglio, M., Landolfo, S., De Andrea, M., 2015. The interferon-inducible DNA-sensor protein IFI16: a key player in the antiviral response. New Microbiol. 38, 5–20.

Dell'Oste, V., Gatti, D., Gugliesi, F., De Andrea, M., Bawadekar, M., Lo Cigno, I., Biolatti, M., Vallino, M., Marschall, M., Gariglio, M., Landolfo, S., 2014. Innate Nuclear Sensor IFI16 Translocates into the Cytoplasm during the Early Stage of In Vitro Human Cytomegalovirus Infection and Is Entrapped in the Egressing Virions during the Late Stage. J. Virol. 88, 6970–6982. https://doi.org/10.1128/JVI.00384-14

Dhillon, B., Aleithan, F., Abdul-Sater, Z., Abdul-Sater, A.A., 2019. The Evolving Role of TRAFs in Mediating Inflammatory Responses. Front. Immunol. 10.

Diwaker, D., Wilson, D.W., 2019. Microtubule-Dependent Trafficking of Alphaherpesviruses in the Nervous System: The Ins and Outs. Viruses 11, 1165. https://doi.org/10.3390/v11121165

Döhner, K., Ramos-Nascimento, A., Bialy, D., Anderson, F., Hickford-Martinez, A., Rother, F., Koithan, T., Rudolph, K., Buch, A., Prank, U., Binz, A., Hügel, S., Lebbink, R.J., Hoeben, R.C., Hartmann, E., Bader, M., Bauerfeind, R., Sodeik, B., 2018. Importin α1 is required for nuclear import of herpes simplex virus proteins and capsid assembly in fibroblasts and neurons. PLOS Pathog. 14, e1006823. https://doi.org/10.1371/journal.ppat.1006823

Donnelly, M., Elliott, G., 2001. Nuclear Localization and Shuttling of Herpes Simplex Virus Tegument Protein VP13/14. J. Virol. 75, 2566–2574. https://doi.org/10.1128/jvi.75.6.2566-2574.2001

Dorfleutner, A., Chu, L., Stehlik, C., 2015. Inhibiting the inflammasome: one domain at a time. Immunol. Rev. 265, 205–216. https://doi.org/10.1111/imr.12290

Dunzendorfer, S., Lee, H.-K., Soldau, K., Tobias, P.S., 2004. TLR4 is the signaling but not the lipopolysaccharide uptake receptor. J. Immunol. Baltim. Md 1950 173, 1166–1170. https://doi.org/10.4049/jimmunol.173.2.1166

Fan, X., Jiao, L., Jin, T., 2022. Activation and Immune Regulation Mechanisms of PYHIN Family During Microbial Infection. Front. Microbiol. 12.

Fields, B.N., 2013. Fields virology, 6th ed. ed. Wolters Kluwer Health/Lippincott Williams & Wilkins, Philadelphia.

Fu, Q., He, Q., Dong, Q., Xie, J., Geng, Y., Han, H., Huang, Y., Lu, J., Zeng, Z., Wang, W., Chen, K., Zhan, X., 2022. The role of cyclic GMP-AMP synthase and Interferon-I-inducible protein 16 as candidatebiomarkers of systemic lupus erythematosus. Clin. Chim. Acta 524, 69–77. https://doi.org/10.1016/j.cca.2021.11.003

Fujiuchi, N., Aglipay, J.A., Ohtsuka, T., Maehara, N., Sahin, F., Su, G.H., Lee, S.W., Ouchi, T., 2004. Requirement of IFI16 for the Maximal Activation of p53 Induced by Ionizing Radiation*. J. Biol. Chem. 279, 20339–20344. https://doi.org/10.1074/jbc.M400344200

Garcia, M.M., Goicoechea, C., Molina-Álvarez, M., Pascual, D., 2020. Toll-like receptor 4: A promising crossroads in the diagnosis and treatment of several pathologies. Eur. J. Pharmacol. 874, 172975. https://doi.org/10.1016/j.ejphar.2020.172975

Gariano, G.R., Dell'Oste, V., Bronzini, M., Gatti, D., Luganini, A., Andrea, M.D., Gribaudo, G., Gariglio, M., Landolfo, S., 2012. The Intracellular DNA Sensor IFI16 Gene Acts as Restriction Factor for Human Cytomegalovirus Replication. PLOS Pathog. 8, e1002498. https://doi.org/10.1371/journal.ppat.1002498

Gariglio, M., Azzimonti, B., Pagano, M., Palestro, G., De Andrea, M., Valente, G., Voglino, G., Navino, L., Landolfo, S., 2002. Immunohistochemical expression analysis of the human interferon-inducible gene IFI16, a member of the HIN200 family, not restricted to hematopoietic cells. J. Interferon Cytokine Res. Off. J. Int. Soc. Interferon Cytokine Res. 22, 815–821. https://doi.org/10.1089/107999002320271413

Gay, N.J., Gangloff, M., O'Neill, L.A.J., 2011. What the Myddosome structure tells us about the initiation of innate immunity. Trends Immunol. 32, 104–109. https://doi.org/10.1016/j.it.2010.12.005

Gioannini, T.L., Teghanemt, A., Zhang, D., Coussens, N.P., Dockstader, W., Ramaswamy, S., Weiss, J.P., 2004. Isolation of an endotoxin–MD-2 complex that produces Toll-like receptor 4-dependent cell activation at picomolar concentrations. Proc. Natl. Acad. Sci. 101, 4186–4191. https://doi.org/10.1073/pnas.0306906101

Goldstein, R.S., Bruchfeld, A., Yang, L., Qureshi, A.R., Gallowitsch-Puerta, M., Patel, N.B., Huston, B.J., Chavan, S., Rosas-Ballina, M., Gregersen, P.K., Czura, C.J., Sloan, R.P., Sama, A.E., Tracey, K.J., 2007. Cholinergic anti-inflammatory pathway activity and High Mobility Group Box-1 (HMGB1) serum levels in patients with rheumatoid arthritis. Mol. Med. Camb. Mass 13, 210–215. https://doi.org/10.2119/2006–00108.goldstein

Gondokaryono, S.P., Ushio, H., Niyonsaba, F., Hara, M., Takenaka, H., Jayawardana, S.T.M., Ikeda, S., Okumura, K., Ogawa, H., 2007. The extra domain A of fibronectin stimulates murine mast cells via Toll-like receptor 4. J. Leukoc. Biol. 82, 657–665. https://doi.org/10.1189/jlb.1206730

Gong, T., Liu, L., Jiang, W., Zhou, R., 2020. DAMP-sensing receptors in sterile inflammation and inflammatory diseases. Nat. Rev. Immunol. 20, 95–112. https://doi.org/10.1038/s41577-019-0215-7

Goodwin, G.H., Johns, E.W., 1973. Isolation and Characterisation of Two Calf-Thymus Chromatin Non-Histone Proteins with High Contents of Acidic and Basic Amino Acids. Eur. J. Biochem. 40, 215–219. https://doi.org/10.1111/j.1432-1033.1973.tb03188.x

Gopinath, D., Koe, K.H., Maharajan, M.K., Panda, S., 2023. A Comprehensive Overview of Epidemiology, Pathogenesis and the Management of Herpes Labialis. Viruses 15, 225. https://doi.org/10.3390/v15010225

Gray, E.E., Winship, D., Snyder, J.M., Child, S.J., Geballe, A.P., Stetson, D.B., 2016. The AIM2-like receptors are dispensable for the interferon response to intracellular DNA. Immunity 45, 255–266. https://doi.org/10.1016/j.immuni.2016.06.015

Gugliesi, F., Bawadekar, M., Andrea, M.D., Dell'Oste, V., Caneparo, V., Tincani, A., Gariglio, M., Landolfo, S., 2013. Nuclear DNA Sensor IFI16 as Circulating Protein in Autoimmune Diseases Is a Signal of Damage that Impairs Endothelial Cells through High-Affinity Membrane Binding. PLOS ONE 8, e63045. https://doi.org/10.1371/journal.pone.0063045

He, M., Bianchi, M.E., Coleman, T.R., Tracey, K.J., Al-Abed, Y., 2018. Exploring the biological functional mechanism of the HMGB1/TLR4/MD-2 complex by surface plasmon resonance. Mol. Med. 24, 21. https://doi.org/10.1186/s10020-018-0023-8

Hillion, S., Arleevskaya, M.I., Blanco, P., Bordron, A., Brooks, W.H., Cesbron, J.Y., Kaveri, S., Vivier, E., Renaudineau, Y., 2020. The Innate Part of the Adaptive Immune System. Clin. Rev. Allergy Immunol. 58, 151–154. https://doi.org/10.1007/s12016-019-08740-1

Hilterbrand, A.T., Heldwein, E.E., 2019. Go go gadget glycoprotein!: HSV-1 draws on its sizeable glycoprotein tool kit to customize its diverse entry routes. PLOS Pathog. 15, e1007660. https://doi.org/10.1371/journal.ppat.1007660

Horng, T., Barton, G.M., Medzhitov, R., 2001. TIRAP: an adapter molecule in the Toll signaling pathway. Nat. Immunol. 2, 835–841. https://doi.org/10.1038/ni0901-835

Howard, T.R., Lum, K.K., Kennedy, M.A., Cristea, I.M., 2022. The Nuclear DNA Sensor IFI16 Indiscriminately Binds to and Diminishes Accessibility of the HSV-1 Genome to Suppress Infection. mSystems 7, e00198-22. https://doi.org/10.1128/msystems.00198-22

Hughes, C., Choi, M.L., Yi, J.-H., Kim, S.-C., Drews, A., George-Hyslop, P.S., Bryant, C., Gandhi, S., Cho, K., Klenerman, D., 2020. Beta amyloid aggregates induce sensitised TLR4 signalling causing long-term potentiation deficit and rat neuronal cell death. Commun. Biol. 3, 1–7. https://doi.org/10.1038/s42003-020-0792-9

Iannucci, A., Caneparo, V., Raviola, S., Debernardi, I., Colangelo, D., Miggiano, R., Griffante, G., Landolfo, S., Gariglio, M., Andrea, M.D., 2020. Toll-like receptor 4-mediated inflammation triggered by extracellular IFI16 is enhanced by lipopolysaccharide binding. PLOS Pathog. 16, e1008811. https://doi.org/10.1371/journal.ppat.1008811

Iqbal, J., Ansari, M.A., Kumar, B., Dutta, D., Roy, A., Chikoti, L., Pisano, G., Dutta, S., Vahedi, S., Veettil, M.V., Chandran, B., 2016. Histone H2B-IFI16 Recognition of Nuclear Herpesviral Genome Induces Cytoplasmic Interferon-β Responses. PLOS Pathog. 12, e1005967. https://doi.org/10.1371/journal.ppat.1005967

Ivanova, L., Buch, A., Döhner, K., Pohlmann, A., Binz, A., Prank, U., Sandbaumhüter, M., Bauerfeind, R., Sodeik, B., 2016. Conserved Tryptophan Motifs in the Large Tegument Protein pUL36 Are Required for Efficient Secondary Envelopment of Herpes Simplex Virus Capsids. J. Virol. 90, 5368–5383. https://doi.org/10.1128/jvi.03167-15

Ivashkiv, L.B., Donlin, L.T., 2014. Regulation of type I interferon responses. Nat. Rev. Immunol. 14, 36–49. https://doi.org/10.1038/nri3581

Jakobsen, M.R., Paludan, S.R., 2014. IFI16: At the interphase between innate DNA sensing and genome regulation. Cytokine Growth Factor Rev., Special issue: Innate Sensing and Response to Pathogens 25, 649–655. https://doi.org/10.1016/j.cytogfr.2014.06.004

Jang, D., Lee, A.-H., Shin, H.-Y., Song, H.-R., Park, J.-H., Kang, T.-B., Lee, S.-R., Yang, S.-H., 2021. The Role of Tumor Necrosis Factor Alpha (TNF-α) in Autoimmune Disease and Current TNF-α Inhibitors in Therapeutics. Int. J. Mol. Sci. 22, 2719. https://doi.org/10.3390/ijms22052719

Jayachandra, S., Baghian, A., Kousoulas, K.G., 1997. Herpes simplex virus type 1 glycoprotein K is not essential for infectious virus production in actively replicating cells but is required for efficient envelopment and translocation of infectious virions from the cytoplasm to the extracellular space. J. Virol. 71, 5012–5024. https://doi.org/10.1128/jvi.71.7.5012-5024.1997

Jiang, J., Zhao, M., Chang, C., Wu, H., Lu, Q., 2020. Type I Interferons in the Pathogenesis and Treatment of Autoimmune Diseases. Clin. Rev. Allergy Immunol. 59, 248–272. https://doi.org/10.1007/s12016-020-08798-2

Jin, T., Perry, A., Smith, P., Jiang, J., Xiao, T.S., 2013. Structure of the Absent in Melanoma 2 (AIM2) Pyrin Domain Provides Insights into the Mechanisms of AIM2 Autoinhibition and Inflammasome Assembly*. J. Biol. Chem. 288, 13225–13235. https://doi.org/10.1074/jbc.M113.468033

Johnson, D.C., Baines, J.D., 2011. Herpesviruses remodel host membranes for virus egress. Nat. Rev. Microbiol. 9, 382–394. https://doi.org/10.1038/nrmicro2559

Johnson, K.E., Bottero, V., Flaherty, S., Dutta, S., Singh, V.V., Chandran, B., 2014. IFI16 Restricts HSV-1 Replication by Accumulating on the HSV-1 Genome, Repressing HSV-1 Gene Expression, and Directly or Indirectly Modulating Histone Modifications. PLOS Pathog. 10, e1004503. https://doi.org/10.1371/journal.ppat.1004503

Kagan, J.C., Magupalli, V.G., Wu, H., 2014. SMOCs: supramolecular organizing centres that control innate immunity. Nat. Rev. Immunol. 14, 821–826. https://doi.org/10.1038/nri3757

Kagan, J.C., Medzhitov, R., 2006. Phosphoinositide-Mediated Adaptor Recruitment Controls Toll-like Receptor Signaling. Cell 125, 943–955. https://doi.org/10.1016/j.cell.2006.03.047

Katze, M.G., He, Y., Gale, M., 2002. Viruses and interferon: a fight for supremacy. Nat. Rev. Immunol. 2, 675–687. https://doi.org/10.1038/nri888

Kawai, T., Akira, S., 2010. The role of pattern-recognition receptors in innate immunity: update on Toll-like receptors. Nat. Immunol. 11, 373–384. https://doi.org/10.1038/ni.1863

Kawai, T., Akira, S., 2009. The roles of TLRs, RLRs and NLRs in pathogen recognition. Int. Immunol. 21, 317–337. https://doi.org/10.1093/intimm/dxp017

Kawamoto, T., Ii, M., Kitazaki, T., Iizawa, Y., Kimura, H., 2008. TAK-242 selectively suppresses Toll-like receptor 4-signaling mediated by the intracellular domain. Eur. J. Pharmacol. 584, 40–48. https://doi.org/10.1016/j.ejphar.2008.01.026

Kelly, B.J., Bauerfeind, R., Binz, A., Sodeik, B., Laimbacher, A.S., Fraefel, C., Diefenbach, R.J., 2014. The interaction of the HSV-1 tegument proteins pUL36 and pUL37 is essential for secondary envelopment during viral egress. Virology 454–455, 67–77. https://doi.org/10.1016/j.virol.2014.02.003

Kerur, N., Veettil, M.V., Sharma-Walia, N., Bottero, V., Sadagopan, S., Otageri, P., Chandran, B., 2011. IFI16 Acts as a Nuclear Pathogen Sensor to Induce the Inflammasome in Response to Kaposi Sarcoma-Associated Herpesvirus Infection. Cell Host Microbe 9, 363–375. https://doi.org/10.1016/j.chom.2011.04.008

Khare, S., Ratsimandresey, R.A., de Almeida, L., Cuda, C.M., Rellick, S.L., Misharin, A.V., Wallin, M.C., Gangopadhyay, A., Forte, E., Gottwein, E., Perlman, H., Reed, J.C., Greaves, D.R., Dorfleutner, A., Stehlik, C., 2014. The PYRIN domain–only protein POP3 inhibits ALR inflammasomes and regulates responses to infection with DNA viruses. Nat. Immunol. 15, 343–353. https://doi.org/10.1038/ni.2829

Kim, D.E., Chivian, D., Baker, D., 2004. Protein structure prediction and analysis using the Robetta server. Nucleic Acids Res. 32, W526–W531. https://doi.org/10.1093/nar/gkh468

Kim, E.-J., Park, J.-I., Nelkin, B.D., 2005. IFI16 Is an Essential Mediator of Growth Inhibition, but Not Differentiation, Induced by the Leukemia Inhibitory Factor/JAK/STAT Pathway in Medullary Thyroid Carcinoma Cells*. J. Biol. Chem. 280, 4913–4920. https://doi.org/10.1074/jbc.M410542200

Kite, J., Russell, T., Jones, J., Elliott, G., 2021. Cell-to-cell transmission of HSV1 in human keratinocytes in the absence of the major entry receptor, nectin1. PLoS Pathog. 17, e1009631. https://doi.org/10.1371/journal.ppat.1009631

Kratchmarov, R., Taylor, M.P., Enquist, L.W., 2012. Making the case: Married versus Separate models of alphaherpes virus anterograde transport in axons. Rev. Med. Virol. 22, 378–391. https://doi.org/10.1002/rmv.1724

Kwon, D., Yoon, J.H., Shin, S.-Y., Jang, T.-H., Kim, H.-G., So, I., Jeon, J.-H., Park, H.H., 2012. A comprehensive manually curated protein–protein interaction database for the Death Domain superfamily. Nucleic Acids Res. 40, D331–D336. https://doi.org/10.1093/nar/gkr1149

Laine, R.F., Albecka, A., van de Linde, S., Rees, E.J., Crump, C.M., Kaminski, C.F., 2015. Structural analysis of herpes simplex virus by optical super-resolution imaging. Nat. Commun. 6, 5980. https://doi.org/10.1038/ncomms6980

Land, W., 2003. Allograft injury mediated by reactive oxygen species: from conserved proteins of Drosophila to acute and chronic rejection of human transplants. Part III: interaction of (oxidative) stress-induced heat shock proteins with toll-like receptor-bearing cells of innate immunity and its consequences for the development of acute and chronic allograft rejection. Transplant. Rev. 2, 67–86. https://doi.org/10.1016/S0955-470X(02)00009-5

Landolfo, S., Gariglio, M., Gribaudo, G., Lembo, D., 1998. The Ifi 200 genes: An emerging family of IFN-inducible genes. Biochimie 80, 721–728. https://doi.org/10.1016/S0300-9084(99)80025-X

Leavy, O., 2013. A fibrinogen root to airway inflammation. Nat. Rev. Immunol. 13, 704–704. https://doi.org/10.1038/nri3538

Lee, G.E., Murray, J.W., Wolkoff, A.W., Wilson, D.W., 2006. Reconstitution of Herpes Simplex Virus Microtubule-Dependent Trafficking In Vitro. J. Virol. 80, 4264–4275. https://doi.org/10.1128/jvi.80.9.4264-4275.2006

Legrand, C., Bour, J.M., Jacob, C., Capiaumont, J., Martial, A., Marc, A., Wudtke, M., Kretzmer, G., Demangel, C., Duval, D., Hache, J., 1992. Lactate dehydrogenase (LDH) activity of the number of dead cells in the medium of cultured eukaryotic cells as marker. J. Biotechnol. 25, 231–243. https://doi.org/10.1016/0168-1656(92)90158-6

Li, D., Wu, R., Guo, W., Xie, L., Qiao, Z., Chen, S., Zhu, J., Huang, C., Huang, J., Chen, B., Qin, Y., Xu, F., Ma, F., 2019. STING-Mediated IFI16 Degradation Negatively Controls Type I Interferon Production. Cell Rep. 29, 1249-1260.e4. https://doi.org/10.1016/j.celrep.2019.09.069

Li, D., Xie, L., Qiao, Z., Mai, S., Zhu, J., Zhang, F., Chen, S., Li, L., Shen, F., Qin, Y., Yao, H., He, S., Ma, F., 2021. STING-mediated degradation of IFI16 negatively regulates apoptosis by inhibiting p53 phosphorylation at serine 392. J. Biol. Chem. 297, 100930. https://doi.org/10.1016/j.jbc.2021.100930

Li, L., Lu, Y.-Q., 2021. The Regulatory Role of High-Mobility Group Protein 1 in Sepsis-Related Immunity. Front. Immunol. 11, 601815. https://doi.org/10.3389/fimmu.2020.601815

Li, T., Chen, J., Cristea, I.M., 2013. Human Cytomegalovirus Tegument Protein pUL83 Inhibits IFI16-Mediated DNA Sensing for Immune Evasion. Cell Host Microbe 14, 591–599. https://doi.org/10.1016/j.chom.2013.10.007

Li, T., Diner, B.A., Chen, J., Cristea, I.M., 2012. Acetylation modulates cellular distribution and DNA sensing ability of interferon-inducible protein IFI16. Proc. Natl. Acad. Sci. 109, 10558–10563. https://doi.org/10.1073/pnas.1203447109

Liao, J.C.C., Lam, R., Brazda, V., Duan, S., Ravichandran, M., Ma, J., Xiao, T., Tempel, W., Zuo, X., Wang, Y.-X., Chirgadze, N.Y., Arrowsmith, C.H., 2011. Interferon-Inducible Protein 16: Insight into the Interaction with Tumor Suppressor p53. Struct. Lond. Engl. 1993 19, 418–429. https://doi.org/10.1016/j.str.2010.12.015

Liepinsh, E., Barbals, R., Dahl, E., Sharipo, A., Staub, E., Otting, G., 2003. The Death-domain Fold of the ASC PYRIN Domain, Presenting a Basis for PYRIN/PYRIN Recognition. J. Mol. Biol. 332, 1155–1163. https://doi.org/10.1016/j.jmb.2003.07.007

Liu, T., Rojas, A., Ye, Y., Godzik, A., 2003. Homology modeling provides insights into the binding mode of the PAAD/DAPIN/pyrin domain, a fourth member of the CARD/DD/DED domain family. Protein Sci. Publ. Protein Soc. 12, 1872–1881. https://doi.org/10.1110/ps.0359603

Liu, Z., Kato, A., Oyama, M., Kozuka-Hata, H., Arii, J., Kawaguchi, Y., 2015. Role of Host Cell p32 in Herpes Simplex Virus 1 De-Envelopment during Viral Nuclear Egress. J. Virol. 89, 8982–8998. https://doi.org/10.1128/jvi.01220-15

Liu, Z., Kato, A., Shindo, K., Noda, T., Sagara, H., Kawaoka, Y., Arii, J., Kawaguchi, Y., 2014. Herpes Simplex Virus 1 UL47 Interacts with Viral Nuclear Egress Factors UL31, UL34, and Us3 and Regulates Viral Nuclear Egress. J. Virol. 88, 4657–4667. https://doi.org/10.1128/jvi.00137-14

Lo Cigno, I., De Andrea, M., Borgogna, C., Albertini, S., Landini, M.M., Peretti, A., Johnson, K.E., Chandran, B., Landolfo, S., Gariglio, M., 2015. The Nuclear DNA Sensor IFI16 Acts as a Restriction Factor for Human Papillomavirus Replication through Epigenetic Modifications of the Viral Promoters. J. Virol. 89, 7506–7520. https://doi.org/10.1128/jvi.00013-15

Long, H., Zhang, S., Zeng, S., Tong, Y., Liu, J., Liu, C., Li, D., 2022. Interaction of RAGE with α-synuclein fibrils mediates inflammatory response of microglia. Cell Rep. 40, 111401. https://doi.org/10.1016/j.celrep.2022.111401

Ludlow, L.E.A., Johnstone, R.W., Clarke, C.J.P., 2005. The HIN-200 family: More than interferon-inducible genes? Exp. Cell Res. 308, 1–17. https://doi.org/10.1016/j.yexcr.2005.03.032

Lum, K.K., Howard, T.R., Pan, C., Cristea, I.M., 2019. Charge-Mediated Pyrin Oligomerization Nucleates Antiviral IFI16 Sensing of Herpesvirus DNA. mBio 10, e01428-19. https://doi.org/10.1128/mBio.01428-19

Macdonald, S.J., Mostafa, H.H., Morrison, L.A., Davido, D.J., 2012. Genome Sequence of Herpes Simplex Virus 1 Strain KOS. J. Virol. 86, 6371–6372. https://doi.org/10.1128/jvi.00646-12

Marcocci, M.E., Napoletani, G., Protto, V., Kolesova, O., Piacentini, R., Puma, D.D.L., Lomonte, P., Grassi, C., Palamara, A.T., Chiara, G.D., 2020. Herpes Simplex Virus-1 in the Brain: The Dark Side of a Sneaky Infection. Trends Microbiol. 28, 808–820. https://doi.org/10.1016/j.tim.2020.03.003

Matzinger, P., 1994. Tolerance, Danger, and the Extended Family. Annu. Rev. Immunol. 12, 991–1045. https://doi.org/10.1146/annurev.iy.12.040194.005015

McMahan, Z.H., Shah, A.A., Vaidya, D., Wigley, F.M., Rosen, A., Casciola-Rosen, L., 2016. Anti–Interferon-Inducible Protein 16 Antibodies Associate With Digital Gangrene in Patients With Scleroderma. Arthritis Rheumatol. 68, 1262–1271. https://doi.org/10.1002/art.39558

Midwood, K., Sacre, S., Piccinini, A.M., Inglis, J., Trebaul, A., Chan, E., Drexler, S., Sofat, N., Kashiwagi, M., Orend, G., Brennan, F., Foxwell, B., 2009. Tenascin-C is an endogenous activator of Toll-like receptor 4 that is essential for maintaining inflammation in arthritic joint disease. Nat. Med. 15, 774–780. https://doi.org/10.1038/nm.1987

Milora, K.A., Miller, S.L., Sanmiguel, J.C., Jensen, L.E., 2014. Interleukin-1α released from HSV-1-infected keratinocytes acts as a functional alarmin in the skin. Nat. Commun. 5, 5230. https://doi.org/10.1038/ncomms6230

Mondini, M., Vidali, M., Airò, P., De Andrea, M., Riboldi, P., Meroni, P.L., Gariglio, M., Landolfo, S., 2007. Role of the Interferon-Inducible Gene IFI16 in the Etiopathogenesis of Systemic Autoimmune Disorders. Ann. N. Y. Acad. Sci. 1110, 47–56. https://doi.org/10.1196/annals.1423.006

Mondini, M., Vidali, M., Andrea, M.D., Azzimonti, B., Airò, P., D'Ambrosio, R., Riboldi, P., Meroni, P.L., Albano, E., Shoenfeld, Y., Gariglio, M., Landolfo, S., 2006. A novel autoantigen to differentiate limited cutaneous systemic sclerosis from diffuse cutaneous systemic sclerosis: The interferon-inducible gene IFI16. Arthritis Rheum. 54, 3939–3944. https://doi.org/10.1002/art.22266

Monroe, K.M., Yang, Z., Johnson, J.R., Geng, X., Doitsh, G., Krogan, N.J., Greene, W.C., 2014. IFI16 DNA Sensor Is Required for Death of Lymphoid CD4 T Cells Abortively Infected with HIV. Science 343, 428–432. https://doi.org/10.1126/science.1243640

Musarrat, F., Chouljenko, V., Kousoulas, K.G., 2021. Cellular and Viral Determinants of Herpes Simplex Virus 1 Entry and Intracellular Transport toward the Nuclei of Infected Cells. J. Virol. 95, 10.1128/jvi.02434-20. https://doi.org/10.1128/jvi.02434-20

Novak, N., Weighardt, H., Valdelvira, R., Izquierdo, E., Förster, I., Cabanillas, B., 2021. Herpes simplex virus 1 proteins can induce skin inflammation in an atopic dermatitis-like mouse model. Exp. Dermatol. 30, 1699–1704. https://doi.org/10.1111/exd.14327

Ohnishi, H., Tochio, H., Kato, Z., Orii, K.E., Li, A., Kimura, T., Hiroaki, H., Kondo, N., Shirakawa, M., 2009. Structural basis for the multiple interactions of the MyD88 TIR domain in TLR4 signaling. Proc. Natl. Acad. Sci. 106, 10260–10265. https://doi.org/10.1073/pnas.0812956106

Orvain, C., Lin, Y.-L., Jean-Louis, F., Hocini, H., Hersant, B., Bennasser, Y., Ortonne, N., Hotz, C., Wolkenstein, P., Boniotto, M., Tisserand, P., Lefebvre, C., Lelièvre, J.-D., Benkirane, M., Pasero, P., Lévy, Y., Hüe, S., 2020. Hair follicle stem cell replication stress drives IFI16/STING-dependent inflammation in hidradenitis suppurativa. J. Clin. Invest. 130, 3777–3790. https://doi.org/10.1172/JCI131180

Orzalli, M.H., Conwell, S.E., Berrios, C., DeCaprio, J.A., Knipe, D.M., 2013. Nuclear interferon-inducible protein 16 promotes silencing of herpesviral and transfected DNA. Proc. Natl. Acad. Sci. 110, E4492–E4501. https://doi.org/10.1073/pnas.1316194110

Orzalli, M.H., DeLuca, N.A., Knipe, D.M., 2012. Nuclear IFI16 induction of IRF-3 signaling during herpesviral infection and degradation of IFI16 by the viral ICP0 protein. Proc. Natl. Acad. Sci. 109, E3008–E3017. https://doi.org/10.1073/pnas.1211302109

Owen, D.J., Crump, C.M., Graham, S.C., 2015. Tegument Assembly and Secondary Envelopment of Alphaherpesviruses. Viruses 7, 5084–5114. https://doi.org/10.3390/v7092861

Paludan, S.R., Pradeu, T., Masters, S.L., Mogensen, T.H., 2021. Constitutive immune mechanisms: mediators of host defence and immune regulation. Nat. Rev. Immunol. 21, 137–150. https://doi.org/10.1038/s41577-020-0391-5

Pandolfi, F., Altamura, S., Frosali, S., Conti, P., 2016. Key Role of DAMP in Inflammation, Cancer, and Tissue Repair. Clin. Ther. 38, 1017–1028. https://doi.org/10.1016/j.clinthera.2016.02.028

Piao, H., Choi, Y.H., Li, H., Wang, C., Xian, Z., Ogasawara, M., Jiang, J., Li, L., Yamauchi, K., Yan, G., 2019. Recombinant pyrin domain protein attenuates allergic inflammation by suppressing NF-κB pathway in asthmatic mice. Scand. J. Immunol. 89, e12720. https://doi.org/10.1111/sji.12720

Piccinini, A.M., Midwood, K.S., 2010. DAMPening Inflammation by Modulating TLR Signalling. Mediators Inflamm. 2010, 672395. https://doi.org/10.1155/2010/672395

Pisetsky, D.S., 2023. Pathogenesis of autoimmune disease. Nat. Rev. Nephrol. 19, 509–524. https://doi.org/10.1038/s41581-023-00720-1

Platanias, L.C., 2005. Mechanisms of type-I- and type-II-interferon-mediated signalling. Nat. Rev. Immunol. 5, 375–386. https://doi.org/10.1038/nri1604

Radtke, K., Kieneke, D., Wolfstein, A., Michael, K., Steffen, W., Scholz, T., Karger, A., Sodeik, B., 2010. Plus- and Minus-End Directed Microtubule Motors Bind Simultaneously to Herpes Simplex Virus Capsids Using Different Inner Tegument Structures. PLOS Pathog. 6, e1000991. https://doi.org/10.1371/journal.ppat.1000991

Raffaella, R., Gioia, D., De Andrea, M., Cappello, P., Giovarelli, M., Marconi, P., Manservigi, R., Gariglio, M., Landolfo, S., 2004. The interferon-inducible IFI16 gene inhibits tube morphogenesis and proliferation of primary, but not HPV16 E6/E7-immortalized human endothelial cells. Exp. Cell Res. 293, 331–345. https://doi.org/10.1016/j.yexcr.2003.10.014

Rajpoot, S., Wary, K.K., Ibbott, R., Liu, D., Saqib, U., Thurston, T.L.M., Baig, M.S., 2021. TIRAP in the Mechanism of Inflammation. Front. Immunol. 12.

Richards, A.L., Sollars, P.J., Pitts, J.D., Stults, A.M., Heldwein, E.E., Pickard, G.E., Smith, G.A., 2017. The pUL37 tegument protein guides alpha-herpesvirus retrograde axonal transport to promote neuroinvasion. PLOS Pathog. 13, e1006741. https://doi.org/10.1371/journal.ppat.1006741

Rifkin, I.R., Leadbetter, E.A., Busconi, L., Viglianti, G., Marshak-Rothstein, A., 2005. Toll-like receptors, endogenous ligands, and systemic autoimmune disease. Immunol. Rev. 204, 27–42. https://doi.org/10.1111/j.0105-2896.2005.00239.x

Roh, J.S., Sohn, D.H., 2018. Damage-Associated Molecular Patterns in Inflammatory Diseases. Immune Netw. 18. https://doi.org/10.4110/in.2018.18.e27

Romerio, A., Peri, F., 2020. Increasing the Chemical Variety of Small-Molecule-Based TLR4 Modulators: An Overview. Front. Immunol. 11. https://doi.org/10.3389/fimmu.2020.01210

Roy, A., Ghosh, A., Kumar, B., Chandran, B., 2019. IFI16, a nuclear innate immune DNA sensor, mediates epigenetic silencing of herpesvirus genomes by its association with H3K9 methyltransferases SUV39H1 and GLP. eLife 8, e49500. https://doi.org/10.7554/eLife.49500

Samanta, H., DOUGHERTY, J.P., BRAWNER, M.E., SCHMIDT, H., LENGYEL, P., 1982. Interferon action: Cloning of cDNA segments complementary to messenger RNAs induced by interferons. UCLA Symposia on Molecular and Cellular Biology" (T. C. Merigan and R. M. Friedman, eds.), Vol. 25, 59-72.

Sandbaumhüter, M., Döhner, K., Schipke, J., Binz, A., Pohlmann, A., Sodeik, B., Bauerfeind, R., 2013. Cytosolic herpes simplex virus capsids not only require binding inner tegument protein pUL36 but also pUL37 for active transport prior to secondary envelopment. Cell. Microbiol. 15, 248–269. https://doi.org/10.1111/cmi.12075

Satoh, T., Arii, J., Suenaga, T., Wang, J., Kogure, A., Uehori, J., Arase, N., Shiratori, I., Tanaka, S., Kawaguchi, Y., Spear, P.G., Lanier, L.L., Arase, H., 2008. PILRα Is a Herpes Simplex Virus-1 Entry Coreceptor That Associates with Glycoprotein B. Cell 132, 935–944. https://doi.org/10.1016/j.cell.2008.01.043

Schaefer, L., 2014. Complexity of Danger: The Diverse Nature of Damage-associated Molecular Patterns*. J. Biol. Chem. 289, 35237–35245. https://doi.org/10.1074/jbc.R114.619304

Schattgen, S.A., Fitzgerald, K.A., 2011. The PYHIN protein family as mediators of host defenses. Immunol. Rev. 243, 109–118. https://doi.org/10.1111/j.1600-065X.2011.01053.x

Schnappauf, O., Chae, J.J., Kastner, D.L., Aksentijevich, I., 2019. The Pyrin Inflammasome in Health and Disease. Front. Immunol. 10.

Schoggins, J.W., 2019. Interferon-Stimulated Genes: What Do They All Do? Annu. Rev. Virol. 6, 567–584. https://doi.org/10.1146/annurev-virology-092818-015756

Schumann, R.R., Leong, S.R., Flaggs, G.W., Gray, P.W., Wright, S.D., Mathison, J.C., Tobias, P.S., Ulevitch, R.J., 1990. Structure and function of lipopolysaccharide binding protein. Science 249, 1429–1431. https://doi.org/10.1126/science.2402637

Seelig, H.P., Ehrfeld, H., Renz, M., 1994. Interferon-γ–inducible protein p16. a new target of antinuclear antibodies in patients with systemic lupus erythematosus. Arthritis Rheum. 37, 1672–1683. https://doi.org/10.1002/art.1780371117

Shaw, N., Liu, Z.-J., 2014. Role of the HIN Domain in Regulation of Innate Immune Responses. Mol. Cell. Biol. 34, 2–15. https://doi.org/10.1128/MCB.00857-13

Singh, Vivek Vikram, Kerur, N., Bottero, V., Dutta, S., Chakraborty, S., Ansari, M.A., Paudel, N., Chikoti, L., Chandran, B., 2013. Kaposi's Sarcoma-Associated Herpesvirus Latency in Endothelial and B Cells Activates Gamma Interferon-Inducible Protein 16-Mediated Inflammasomes. J. Virol. 87, 4417–4431. https://doi.org/10.1128/jvi.03282-12

Smiley, S.T., King, J.A., Hancock, W.W., 2001. Fibrinogen stimulates macrophage chemokine secretion through toll-like receptor 4. J. Immunol. Baltim. Md 1950 167, 2887–2894. https://doi.org/10.4049/jimmunol.167.5.2887

Sodroski, C.N., Knipe, D.M., 2023. Nuclear interferon-stimulated gene product maintains heterochromatin on the herpes simplex viral genome to limit lytic infection. Proc. Natl. Acad. Sci. 120, e2310996120. https://doi.org/10.1073/pnas.2310996120

Sohn, D.H., Sokolove, J., Sharpe, O., Erhart, J.C., Chandra, P.E., Lahey, L.J., Lindstrom, T.M., Hwang, I., Boyer, K.A., Andriacchi, T.P., Robinson, W.H., 2012. Plasma proteins present in osteoarthritic synovial fluid can stimulate cytokine production via Toll-like receptor 4. Arthritis Res. Ther. 14, R7. https://doi.org/10.1186/ar3555

Sokolove, J., Zhao, X., Chandra, P.E., Robinson, W.H., 2010. Immune complexes containing citrullinated fibrinogen costimulate macrophages via Toll-like receptor 4 and Fcγ receptor. Arthritis Rheum. 63, 53–62. https://doi.org/10.1002/art.30081

Stehlik, C., 2007. The PYRIN domain in signal transduction. Curr. Protein Pept. Sci. 8, 293–310.

Steward, A., McDowell, G.S., Clarke, J., 2009. Topology is the Principal Determinant in the Folding of a Complex All-alpha Greek Key Death Domain from Human FADD. J. Mol. Biol. 389, 425–437. https://doi.org/10.1016/j.jmb.2009.04.004

Suenaga, T., Satoh, T., Somboonthum, P., Kawaguchi, Y., Mori, Y., Arase, H., 2010. Myelin-associated glycoprotein mediates membrane fusion and entry of neurotropic herpesviruses. Proc. Natl. Acad. Sci. 107, 866–871. https://doi.org/10.1073/pnas.0913351107

Taguchi, T., Mukai, K., 2019. Innate immunity signalling and membrane trafficking. Curr. Opin. Cell Biol., Membrane Trafficking 59, 1–7. https://doi.org/10.1016/j.ceb.2019.02.002

Takasu, A., Masui, A., Hamada, M., Imai, T., Iwai, S., Yura, Y., 2016. Immunogenic cell death by oncolytic herpes simplex virus type 1 in squamous cell carcinoma cells. Cancer Gene Ther. 23, 107–113. https://doi.org/10.1038/cgt.2016.8

Tan, Y., Zanoni, I., Cullen, T.W., Goodman, A.L., Kagan, J.C., 2015. Mechanisms of Toll-like Receptor 4 Endocytosis Reveal a Common Immune-Evasion Strategy Used by Pathogenic and Commensal Bacteria. Immunity 43, 909–922. https://doi.org/10.1016/j.immuni.2015.10.008

Tervaniemi, M.H., Katayama, S., Skoog, T., Siitonen, H.A., Vuola, J., Nuutila, K., Sormunen, R., Johnsson, A., Linnarsson, S., Suomela, S., Kankuri, E., Kere, J., Elomaa, O., 2016. NOD-like receptor signaling and inflammasome-related pathways are highlighted in psoriatic epidermis. Sci. Rep. 6, 22745. https://doi.org/10.1038/srep22745

Theobald, D.L., Mitton-Fry, R.M., Wuttke, D.S., 2003. NUCLEIC ACID RECOGNITION BY OB-FOLD PROTEINS. Annu. Rev. Biophys. Biomol. Struct. 32, 115–133. https://doi.org/10.1146/annurev.biophys.32.110601.142506

Tian, J., Avalos, A.M., Mao, S.-Y., Chen, B., Senthil, K., Wu, H., Parroche, P., Drabic, S., Golenbock, D., Sirois, C., Hua, J., An, L.L., Audoly, L., La Rosa, G., Bierhaus, A., Naworth, P., Marshak-Rothstein, A., Crow, M.K., Fitzgerald, K.A., Latz, E., Kiener, P.A., Coyle, A.J., 2007. Toll-like receptor 9–dependent activation by DNA-containing immune complexes is mediated by HMGB1 and RAGE. Nat. Immunol. 8, 487–496. https://doi.org/10.1038/ni1457

Tian, J., Guo, X., Liu, X.-M., Liu, L., Weng, Q.-F., Dong, S.-J., Knowlton, A.A., Yuan, W.-J., Lin, L., 2013. Extracellular HSP60 induces inflammation through activating and up-regulating TLRs in cardiomyocytes. Cardiovasc. Res. 98, 391–401. https://doi.org/10.1093/cvr/cvt047

Tobias, P.S., Soldaau, K., Ulevitch, R.J., 1986. Isolation of a lipopolysaccharide-binding acute phase reactant from rabbit serum. J. Exp. Med. 164, 777–793.

Toshchakov, V., Jones, B.W., Perera, P.-Y., Thomas, K., Cody, M.J., Zhang, S., Williams, B.R.G., Major, J., Hamilton, T.A., Fenton, M.J., Vogel, S.N., 2002. TLR4, but not TLR2, mediates IFN-β–induced STAT1α/β-dependent gene expression in macrophages. Nat. Immunol. 3, 392–398. https://doi.org/10.1038/ni774

Trapani, J.A., Dawson, M., Apostolidis, V.A., Browne, K.A., 1994. Genomic organization of IFI16, an interferon-inducible gene whose expression is associated with human myeloid cell differentiation: correlation of predicted protein domains with exon organization. Immunogenetics 40, 415–424. https://doi.org/10.1007/BF00177824

Trus, B.L., Newcomb, W.W., Cheng, N., Cardone, G., Marekov, L., Homa, F.L., Brown, J.C., Steven, A.C., 2007. Allosteric Signaling and a Nuclear Exit Strategy: Binding of UL25/UL17 Heterodimers to DNA-Filled HSV-1 Capsids. Mol. Cell 26, 479–489. https://doi.org/10.1016/j.molcel.2007.04.010

Tsung, A., Sahai, R., Tanaka, H., Nakao, A., Fink, M.P., Lotze, M.T., Yang, H., Li, J., Tracey, K.J., Geller, D.A., Billiar, T.R., 2005. The nuclear factor HMGB1 mediates hepatic injury after murine liver ischemia-reperfusion. J. Exp. Med. 201, 1135–1143. https://doi.org/10.1084/jem.20042614

Turcotte, S., Letellier, J., Lippé, R., 2005. Herpes Simplex Virus Type 1 Capsids Transit by the trans-Golgi Network, Where Viral Glycoproteins Accumulate Independently of Capsid Egress. J. Virol. 79, 8847–8860. https://doi.org/10.1128/jvi.79.14.8847-8860.2005

Uchida, K., Akita, Y., Matsuo, K., Fujiwara, S., Nakagawa, A., Kazaoka, Y., Hachiya, H., Naganawa, Y., Oh-iwa, I., Ohura, K., Saga, S., Kawai, T., Matsumoto, Y., Shimozato, K., Kozaki, K., 2005. Identification of specific autoantigens in Sjögren's syndrome by SEREX. Immunology 116, 53–63. https://doi.org/10.1111/j.1365-2567.2005.02197.x

Ummarino, D., 2016. Tenascin C perpetuates tissue fibrosis. Nat. Rev. Rheumatol. 12, 375–375. https://doi.org/10.1038/nrrheum.2016.99

Unterholzner, L., Keating, S.E., Baran, M., Horan, K.A., Jensen, S.B., Sharma, S., Sirois, C.M., Jin, T., Latz, E., Xiao, T.S., Fitzgerald, K.A., Paludan, S.R., Bowie, A.G., 2010. IFI16 is an innate immune sensor for intracellular DNA. Nat. Immunol. 11, 997–1004. https://doi.org/10.1038/ni.1932

Valkov, E., Stamp, A., DiMaio, F., Baker, D., Verstak, B., Roversi, P., Kellie, S., Sweet, M.J., Mansell, A., Gay, N.J., Martin, J.L., Kobe, B., 2011. Crystal structure of Toll-like receptor adaptor MAL/TIRAP reveals the molecular basis for signal transduction and disease protection. Proc. Natl. Acad. Sci. U. S. A. 108, 14879–14884. https://doi.org/10.1073/pnas.1104780108

van Zundert, G.C.P., Rodrigues, J.P.G.L.M., Trellet, M., Schmitz, C., Kastritis, P.L., Karaca, E., Melquiond, A.S.J., van Dijk, M., de Vries, S.J., Bonvin, A.M.J.J., 2016. The HADDOCK2.2 Web Server: User-Friendly

Integrative Modeling of Biomolecular Complexes. J. Mol. Biol., Computation Resources for Molecular Biology 428, 720–725. https://doi.org/10.1016/j.jmb.2015.09.014

Vanhove, W., Peeters, P.M., Staelens, D., Schraenen, A., Van der Goten, J., Cleynen, I., De Schepper, S., Van Lommel, L., Reynaert, N.L., Schuit, F., Van Assche, G., Ferrante, M., De Hertogh, G., Wouters, E.F.M., Rutgeerts, P., Vermeire, S., Nys, K., Arijs, I., 2015. Strong Upregulation of AIM2 and IFI16 Inflammasomes in the Mucosa of Patients with Active Inflammatory Bowel Disease. Inflamm. Bowel Dis. 21, 2673–2682. https://doi.org/10.1097/MIB.0000000000000535

Veeranki, S., Choubey, D., 2012. Interferon-inducible p200-family protein IFI16, an innate immune sensor for cytosolic and nuclear double-stranded DNA: Regulation of subcellular localization. Mol. Immunol. 49, 567–571. https://doi.org/10.1016/j.molimm.2011.11.004

Vénéreau, E., Ceriotti, C., Bianchi, M.E., 2015. DAMPs from Cell Death to New Life. Front. Immunol. 6.

Wang, Jialing, Yuan, S., Zhu, D., Tang, H., Wang, N., Chen, W., Gao, Q., Li, Y., Wang, Junzhi, Liu, H., Zhang, X., Rao, Z., Wang, X., 2018. Structure of the herpes simplex virus type 2 C-capsid with capsid-vertex-specific component. Nat. Commun. 9, 3668. https://doi.org/10.1038/s41467-018-06078-4

Wei, W., Clarke, C.J.P., Somers, G.R., Cresswell, K.S., Loveland, K.A., Trapani, J.A., Johnstone, R.W., 2003. Expression of IFI 16 in epithelial cells and lymphoid tissues. Histochem. Cell Biol. 119, 45–54. https://doi.org/10.1007/s00418-002-0485-0

Wolfstein, A., Nagel, C.-H., Radtke, K., Döhner, K., Allan, V.J., Sodeik, B., 2005. The Inner Tegument Promotes Herpes Simplex Virus Capsid Motility Along Microtubules in vitro. Traffic 7, 227–237. https://doi.org/10.1111/j.1600-0854.2005.00379.x

Wu, S., Pan, S., Zhang, L., Baines, J., Roller, R., Ames, J., Yang, M., Wang, J., Chen, D., Liu, Y., Zhang, C., Cao, Y., He, B., 2016. Herpes Simplex Virus 1 Induces Phosphorylation and Reorganization of Lamin A/C through the γ134.5 Protein That Facilitates Nuclear Egress. J. Virol. 90, 10414–10422. https://doi.org/10.1128/jvi.01392-16

Wysocka, J., Herr, W., 2003. The herpes simplex virus VP16-induced complex: the makings of a regulatory switch. Trends Biochem. Sci. 28, 294–304. https://doi.org/10.1016/S0968-0004(03)00088-4

Xin, H., Curry, J., Johnstone, R.W., Nickoloff, B.J., Choubey, D., 2003. Role of IFI 16, a member of the interferon-inducible p200-protein family, in prostate epithelial cellular senescence. Oncogene 22, 4831–4840. https://doi.org/10.1038/sj.onc.1206754

Yamamoto, M., Sato, S., Hemmi, H., Hoshino, K., Kaisho, T., Sanjo, H., Takeuchi, O., Sugiyama, M., Okabe, M., Takeda, K., Akira, S., 2003. Role of adaptor TRIF in the MyD88-independent toll-like receptor signaling pathway. Science 301, 640–643. https://doi.org/10.1126/science.1087262

Yan, H., Dalal, K., Hon, B.K., Youkharibache, P., Lau, D., Pio, F., 2008. RPA nucleic acid-binding properties of IFI16-HIN200. Biochim. Biophys. Acta BBA - Proteins Proteomics 1784, 1087–1097. https://doi.org/10.1016/j.bbapap.2008.04.004

Yang, H., Hreggvidsdottir, H.S., Palmblad, K., Wang, H., Ochani, M., Li, J., Lu, B., Chavan, S., Rosas-Ballina, M., Al-Abed, Y., Akira, S., Bierhaus, A., Erlandsson-Harris, H., Andersson, U., Tracey, K.J., 2010. A critical cysteine is required for HMGB1 binding to Toll-like receptor 4 and activation of macrophage cytokine release. Proc. Natl. Acad. Sci. U. S. A. 107, 11942–11947. https://doi.org/10.1073/pnas.1003893107

Yang, H., Wang, H., Andersson, U., 2020. Targeting Inflammation Driven by HMGB1. Front. Immunol. 11.

Ye, R.D., Sun, L., 2015. Emerging functions of serum amyloid A in inflammation. J. Leukoc. Biol. 98, 923–929. https://doi.org/10.1189/jlb.3VMR0315-080R

Yi, Y.-S., 2017. Caspase-11 non-canonical inflammasome: a critical sensor of intracellular lipopolysaccharide in macrophage-mediated inflammatory responses. Immunology 152, 207–217. https://doi.org/10.1111/imm.12787

Zanoni, I., Ostuni, R., Marek, L.R., Barresi, S., Barbalat, R., Barton, G.M., Granucci, F., Kagan, J.C., 2011. CD14 controls the LPS-induced endocytosis of Toll-like receptor 4. Cell 147, 868–880. https://doi.org/10.1016/j.cell.2011.09.051

Zanoni, I., Tan, Y., Di Gioia, M., Springstead, J.R., Kagan, J.C., 2017. By Capturing Inflammatory Lipids Released from Dying Cells, the Receptor CD14 Induces Inflammasome-Dependent Phagocyte Hyperactivation. Immunity 47, 697-709.e3. https://doi.org/10.1016/j.immuni.2017.09.010

Zhang, P., Yang, M., Chen, C., Liu, L., Wei, X., Zeng, S., 2020. Toll-Like Receptor 4 (TLR4)/Opioid Receptor Pathway Crosstalk and Impact on Opioid Analgesia, Immune Function, and Gastrointestinal Motility. Front. Immunol. 11.

Zhou, Y.J., Binder, R.J., 2014. The heat shock protein-CD91 pathway mediates tumor immunosurveillance. OncoImmunology 3, e28222. https://doi.org/10.4161/onci.28222

Zhu, S., Viejo-Borbolla, A., 2021. Pathogenesis and virulence of herpes simplex virus. Virulence 12, 2670–2702. https://doi.org/10.1080/21505594.2021.1982373

Zuliani-Alvarez, L., Marzeda, A.M., Deligne, C., Schwenzer, A., McCann, F.E., Marsden, B.D., Piccinini, A.M., Midwood, K.S., 2017. Mapping tenascin-C interaction with toll-like receptor 4 reveals a new subset of endogenous inflammatory triggers. Nat. Commun. 8, 1595. https://doi.org/10.1038/s41467-017-01718-7

9. Publications

- Pasquero S, Gugliesi F, Biolatti M, Dell'Oste V, Albano C, Bajetto G, Griffante G, Trifirò L, Brugo B, Raviola S, **Lacarbonara D**, Yang Q, Sudeshna S, Barasa L, Haniff H, Thompson PR, Landolfo S, De Andrea M. Citrullination profile analysis reveals peptidylarginine deaminase 3 as an HSV-1 target to dampen the activity of candidate antiviral restriction factors. **PLoS Pathog. 2023 Dec 6**;19(12):e1011849. doi: 10.1371/journal.ppat.1011849. PMID: 38055760; PMCID: PMC10727434

- Raviola S, Griffante G, Iannucci A, Chandel S, Lo Cigno I, **Lacarbonara D**, Caneparo V, Favero F, Corà D, Trisolini E, Boldorini E, Cantaluppi V,Landolfo S, Gariglio M, De Andrea M. Human cytomegalovirus infection triggers a paracrine senescence loop in renal epithelial cells. **Communications Biology (Accepted).**

- **Lacarbonara D.***, Iannucci A.*, Caneparo V., Raviola S., Miggiano R., Gariglio M., and De Andrea M. The PYRIN domain of the PYHIN family members specifically drives TLR4-mediated proinflammatory action via TLR4/MD2 inflammation. **Manuscript in Preparation**

PLOS PATHOGENS

RESEARCH ARTICLE

Citrullination profile analysis reveals peptidylarginine deaminase 3 as an HSV-1 target to dampen the activity of candidate antiviral restriction factors

Selina Pasquero[1☯], Francesca Gugliesi[1☯], Matteo Biolatti[1], Valentina Dell'Oste[1], Camilla Albano[1], Greta Bajetto[1,2], Gloria Griffante[3], Linda Trifirò[1], Bianca Brugo[1], Stefano Raviola[2,3], Davide Lacarbonara[2,3], Qiao Yang[1,4], Sen Sudeshna[5], Leonard Barasa[5], Hafeez Haniff[5], Paul R. Thompson[5], Santo Landolfo[1], Marco De Andrea[1,2*]

1 Department of Public Health and Pediatric Sciences, University of Turin – Medical School, Turin, Italy, **2** CAAD Center for Translational Research on Autoimmune and Allergic Disease, University of Piemonte Orientale, Novara Medical School, Novara, Italy, **3** Department of Translational Medicine, University of Piemonte Orientale, Novara, Italy, **4** Avian Disease Research Center, College of Veterinary Medicine, Sichuan Agricultural University, Wenjiang, Chengdu City, P.R. China, **5** Department of Biochemistry and Molecular Pharmacology, UMass Medical School, Worcester, Massachusetts, United States of America

☯ These authors contributed equally to this work.
* marco.deandrea@unito.it

OPEN ACCESS

Citation: Pasquero S, Gugliesi F, Biolatti M, Dell'Oste V, Albano C, Bajetto G, et al. (2023) Citrullination profile analysis reveals peptidylarginine deaminase 3 as an HSV-1 target to dampen the activity of candidate antiviral restriction factors. PLoS Pathog 19(12): e1011849. https://doi.org/10.1371/journal.ppat.1011849

Editor: Donna M Neumann, University of Wisconsin-Madison, UNITED STATES

Received: July 14, 2023

Accepted: November 20, 2023

Published: December 6, 2023

Peer Review History: PLOS recognizes the benefits of transparency in the peer review process; therefore, we enable the publication of all of the content of peer review and author responses alongside final, published articles. The editorial history of this article is available here: https://doi.org/10.1371/journal.ppat.1011849

Data Availability Statement: All relevant data are within the manuscript and its Supporting information files.

Abstract

Herpes simplex virus 1 (HSV-1) is a neurotropic virus that remains latent in neuronal cell bodies but reactivates throughout an individual's life, causing severe adverse reactions, such as herpes simplex encephalitis (HSE). Recently, it has also been implicated in the etiology of Alzheimer's disease (AD). The absence of an effective vaccine and the emergence of numerous drug-resistant variants have called for the development of new antiviral agents that can tackle HSV-1 infection. Host-targeting antivirals (HTAs) have recently emerged as promising antiviral compounds that act on host-cell factors essential for viral replication. Here we show that a new class of HTAs targeting peptidylarginine deiminases (PADs), a family of calcium-dependent enzymes catalyzing protein citrullination, exhibits a marked inhibitory activity against HSV-1. Furthermore, we show that HSV-1 infection leads to enhanced protein citrullination through transcriptional activation of three PAD isoforms: PAD2, PAD3, and PAD4. Interestingly, PAD3-depletion by specific drugs or siRNAs dramatically inhibits HSV-1 replication. Finally, an analysis of the citrullinome reveals significant changes in the deimination levels of both cellular and viral proteins, with the interferon (IFN)-inducible proteins IFIT1 and IFIT2 being among the most heavily deiminated ones. As genetic depletion of IFIT1 and IFIT2 strongly enhances HSV-1 growth, we propose that viral-induced citrullination of IFIT1 and 2 is a highly efficient HSV-1 evasion mechanism from host antiviral resistance. Overall, our findings point to a crucial role of citrullination in subverting cellular responses to viral infection and demonstrate that PAD inhibitors efficiently suppress HSV-1 infection *in vitro*, which may provide the rationale for their repurposing as HSV-1 antiviral drugs.

Funding: This research was supported by the University of Turin (RILO2021 and RILO2022 to M. D.A., F.G., V.D.O. and M.B.), by the Ministry of Education, University and Research – MUR (PRIN Project 2017ALPCM to V.D.O.), by Cassa di Risparmio of Turin Foundation (RF=2021.1745 to M.B.), and by EU funding within the MUR PNRR Extended Partnership initiative on Emerging Infectious Diseases (Project no. PE00000007, INF-ACT to M.D.A). The funders had no role in study design, data collection and analysis, decision to publish, or preparation of the manuscript.

Competing interests: The authors have declared that no competing interests exist.

Author summary

HSV-1 is a common human pathogen that infects approximately 70% of the population for life. After infection, the virus remains dormant in sensory neurons but reactivates periodically, releasing virus particles that move down the axon to infect skin epithelial cells, where it can be spread to other individuals. Depending on the recipient's immune condition, primary infection or reactivation can cause a wide range of symptoms. However, accessible HSV-1 antivirals are currently limited, and most of them target viral DNA polymerase, thus leading to the emergence of drug-resistant viral infections. Citrullination, an irreversible protein alteration driven by peptidylarginine deiminases (PADs), has been linked to various inflammation-related events, including viral infections. In our study, we provide evidence that HSV-1 triggers citrullination of multiple proteins, some of which possess anti-viral properties, thereby promoting viral fitness. Notably, we show that specifically targeting the PAD3 isoform dramatically reduces viral replication. Overall, our study sheds light on the potential of using host PAD inhibitors for developing antiviral agents against HSV-1.

Introduction

Herpes simplex virus 1 (HSV-1) is a widespread and highly infectious alpha-herpesvirus, with seroprevalence reaching up to 75% in the adult population [1]. Primarily transmitted by oral-oral contact and often causing orolabial herpes, commonly known as "cold sores", HSV-1 can persist latently and lifelong in the local ganglia of its host. In response to a variety of diverse stimuli, the virus can reactivate to produce new virus progeny. Reactivation results in clinical signs and symptoms ranging from painful, but self-limited, infections of the oral or genital mucosa to severe infections of the eye or life-threatening infections in immunocompromised hosts or newborns [2]. Additionally, recent evidence suggests that HSV-1 may be involved in the etiology of Alzheimer's disease (AD) [3,4]. Although numerous vaccine candidates have been investigated in clinical trials, no licensed vaccine is available to prevent HSV infections [5].

Acute HSV infections can be treated with antiviral drugs that inhibit its DNA-polymerase. Even though these drugs have been approved and used for decades, their effectiveness has been hampered by the emergence of drug resistant HSV strains [6]. A new strategy to develop antiviral drugs that can overcome these obstacles is to target the host cell factors that participate in viral replication. These drugs are known as host-targeting antivirals (HATs) [7,8].

An example of a host cell factor that can be targeted by HATs is peptidylarginine deiminases (PADs). PADs are a family of enzymes that need calcium to work and can change the structure of proteins by a process called citrullination. This post-translational modification (PTM), also called deimination, is a process in which the guanidinium group of a peptidyl-arginine is hydrolyzed to form peptidyl-citrulline, a non-genetically coded amino acid [9,10]. Five PAD isozymes (PADs 1–4 and 6) are expressed in humans, with a unique distribution in various tissues [9,11,12], and their dysregulation has been associated with various inflammatory conditions and neurodegenerative disorders, such as multiple sclerosis (MS) and AD [13–18]. Given the involvement of PADs in several pathological settings, several PAD inhibitors have been synthesized in recent years. Some of these compounds, such as Cl-amidine (Cl-A) and its derivative BB-Cl-amidine (BB-Cl) [19–21], can inhibit the activity of all the different isoforms and, as such, are called pan-PAD inhibitors [19,22]. Other available inhibitors are

highly specific for the different PAD-isozymes, like AFM-30 for PAD2, CAY10727, and HF4 for PAD3, and GSK199 for PAD4 [23,24].

There is growing evidence of a link between PAD dysregulation and viral infections. Specifically, Arisan and colleagues [25] have recently shown that SARS-CoV-2 infection can modulate PADI gene expression, especially in lung tissues. In addition, we have recently demonstrated an *in vitro* antiviral activity of PAD inhibitors against betacoronaviruses [26]. It has also been found that the antiviral activity of the LL37 protein is weakened by human rhinovirus-induced citrullination [27], and that sera from rheumatoid arthritis (RA) patients specifically recognize artificially citrullinated Epstein-Barr virus proteins [28,29]. Finally, we have demonstrated that another member of the *Herpesviridae* family, human cytomegalovirus (HCMV), upregulates two members of the PAD family (*i.e.*, PAD2 and PAD4) to promote viral fitness, while PAD-inhibitors significantly dampen HCMV replication *in vitro* [30].

Here we report that HSV-1 can alter the protein citrullination profile in different cell lines upon infection, and that this function is mediated by the specific activation of PAD3. Furthermore, by analyzing the citrullinome profile, we also identify IFIT1 and IFIT2 as potential restriction factors for HSV-1 replication. Our findings suggest that: i) HSV-1 replication can be blocked by a new type of HTAs, namely PAD inhibitors, with PAD3 and its specific inhibitor being key players, and ii) HSV-1 manipulates IFIT1/2 to enhance its replication rate.

The potential impact of peptidylarginine deiminases as novel targets for antiviral therapy against HSV-1 are further discussed below.

Results

Pan-PAD inhibitors block HSV-1 replication

We have previously shown that HCMV triggers PAD-mediated citrullination to enhance its replication [30]. To test whether this feature would apply to other herpesviruses, we first measured total protein citrullination in human foreskin fibroblasts (HFFs) upon HSV-1 infection (MOI 1) at different time points. We used electrophoresis to analyze the protein lysates incubated with the citrulline-specific probe Rh-PG. HSV-1-infection increased and altered the pattern of total protein citrullination in lysates from infected *vs* uninfected mock cells, starting from 16 h post-infection (hpi) (Fig 1A, left panel). In particular, we observed a specific enrichment of bands corresponding to proteins with molecular weights higher than 75 kDa, whereas the total amount of proteins remained unchanged, as shown by the similar blue Coomassie staining at different time points (Fig 1A, right panel).

Since citrullination is catalyzed by the PAD family of enzymes [31], we tested whether the cell-permeable pan-PAD inhibitors Cl-amidine (Cl-A) and BB-Cl-amidine (BB-Cl) would affect HSV-1 replication. For this purpose, we assessed viral plaque formation in HSV-1-infected HFFs (MOI 1) treated for 1 h before infection with increasing concentrations of Cl-A (25–200 μM; Fig 1B) or BB-Cl (0.6–5 μM; Fig 1C). After 24 h of continuous exposure to the inhibitors, we observed a dose-dependent decrease in the number of viral particles in all treated cells. The IC50 values of Cl-A and BB-Cl were ~61 μM and ~0.7 μM, respectively, which is consistent with our previous results [30]. Notably, 100 μM Cl-A and 2.5 μM BB-Cl were able to significantly reduce the virus yield by approximately 1 log. We also assessed cell viability using the 3-(4,5-dimethylthiazol-2-yl)-2,5-diphenyl tetrazolium bromide (MTT) assay in cells treated under the same conditions and found that the drugs were not cytotoxic at these concentrations (S1A and S1B Fig). To confirm these results in other cell types, we repeated the experiments in adult retinal pigment epithelial (ARPE-19) and neuroblastoma (SH-SY5Y) cells. We observed similar antiviral effects of Cl-A in both cell lines (S1C and S1D Fig), with only a slight cytotoxic effect in SH-SY5Y cells at higher concentrations (S1A Fig). These

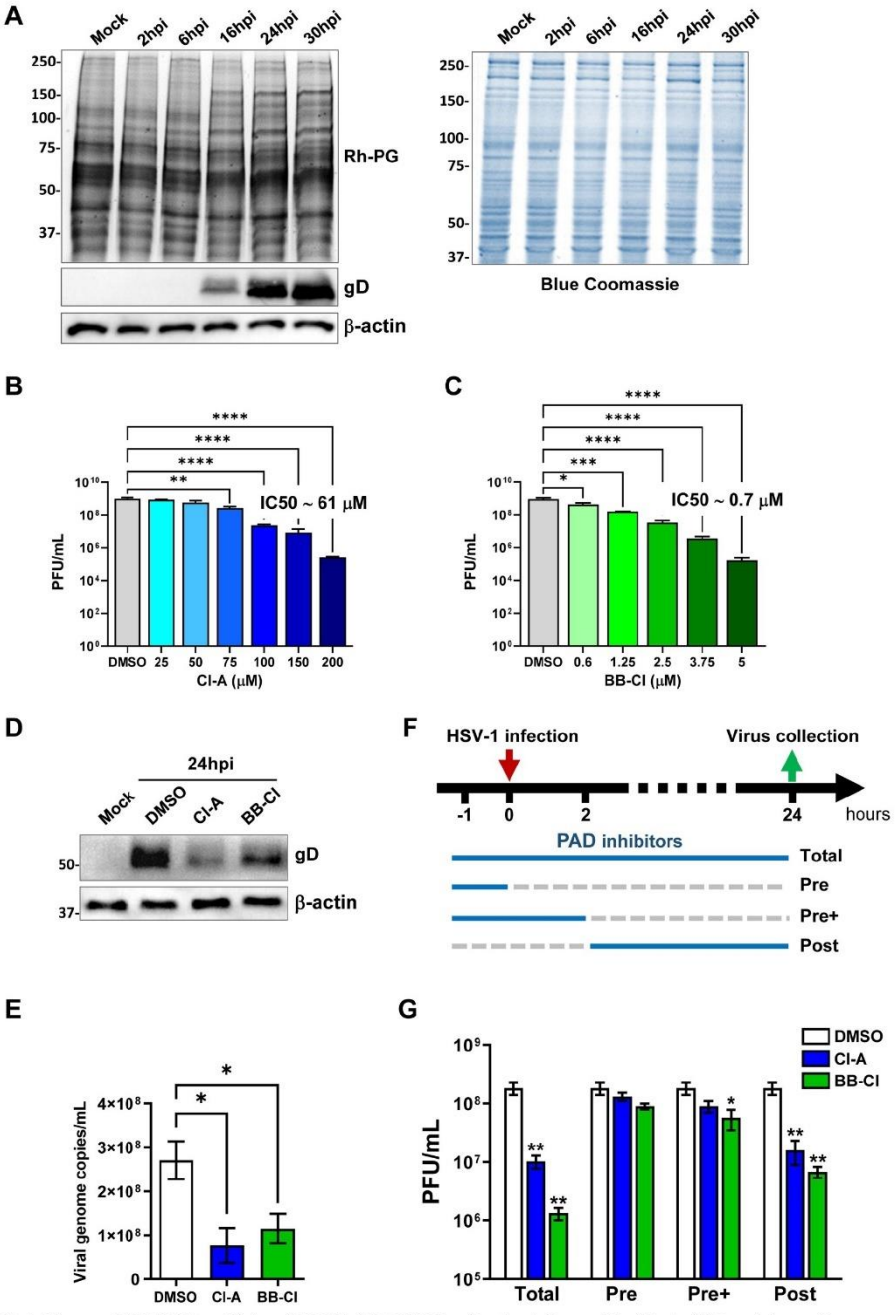

Fig 1. The pan-PAD inhibitors Cl-A and BB-Cl inhibit HSV-1 replication in human fibroblasts. (A) Protein lysates from HFFs infected with HSV-1 (MOI 1 PFU/cell) at different hours post-infection (hpi) or from uninfected HFFs (Mock) were exposed to an Rh-PG citrulline-specific probe (left panel) and subjected to gel electrophoresis to detect citrullinated proteins. An

anti-gD antibody was used to assess HSV-1 infection, while β-actin cellular expression was used for protein loading control. Equal loading was also assessed by Coomassie blue staining (right panel). One representative gel of three independent experiments is shown. **(B, C)** Dose-response curves of the cell-permeable pan-PAD inhibitors Cl-A (B) and BB-Cl (C) in HFFs infected with HSV-1 (MOI 1). Inhibitors were given 1 h prior to virus adsorption and kept throughout the whole experiment. 24 hpi viral plaques were microscopically counted and the number of plaques was plotted as a function of inhibitor concentration. Values are expressed as mean ± SEM of three independent experiments, $^{*}P < 0.05$, $^{**}P < 0.01$, $^{***}P < 0.001$; one-way ANOVA followed by Bonferroni's post test. **(D)** Protein lysates from uninfected (mock) or infected HFFs (24 hpi) at an MOI of 1 PFU/cell treated with Cl-A (100 μM), BB-Cl (2.5 μM), or vehicle (DMSO) were analyzed by immunoblotting for viral expression (gD) and normalized to β-actin. (**E**) To determine the number of viral DNA genomes in HSV-1-infected HFFs, viral DNA was isolated at 24 hpi and analyzed by qPCR using primers amplifying a region of the gE gene. GAPDH was used to normalize HSV-1 genome counts. Values are expressed as mean ± SEM of three independent experiments. HFFs were infected with HSV-1 (MOI 1 PFU/cell) and then treated with Cl-A (100 μM), BB-Cl (2.5 μM), or vehicle (DMSO), which were given at four different time points as indicated (**F**). At 24 hpi, viral plaques were microscopically counted and expressed as PFU/mL (**G**). Values are expressed as mean ± SEM of three independent experiments, $^{*}P < 0.05$, $^{**}P < 0.01$; one-way ANOVA followed by Bonferroni's post test.

https://doi.org/10.1371/journal.ppat.1011849.g001

findings suggest that citrullination is a common and important event for HSV-1 replication in different cell models.

We next examined the effect of Cl-A and BB-Cl on HSV-1 protein expression and citrullination in HFFs. We treated HSV-infected cells with the same concentrations of the drugs as before and collected them at 24 hpi. We found that both drugs significantly reduced the expression of gD, a late viral protein, compared to the vehicle control (Fig 1D). We also observed that the drugs restored the normal citrullination profile of the cells, which was altered by the infection (S1E Fig). Moreover, the drugs prevented the cytopathic effect caused by the virus (S1F Fig).

To measure viral DNA replication, we performed qPCR analysis on the same cell samples. We detected a slight decrease in viral DNA copies in the drug-treated cells, albeit not as pronounced as that observed in the plaque assay (Fig 1E), suggesting that PAD inhibitors may target multiple stages of the HSV-1 life cycle.

To further investigate this possibility, we tested tree different treatment schedules using Cl-A and BB-Cl (Fig 1F). We either added the drugs before infection and washed them away prior to viral addition (pre-treatment, Pre) or removed them at 2 hpi (pre-treatment + infection, Pre+). We observed only a slight difference in the number of viral particles counted by plaque assay between Pre and Pre+ cells, with neither group achieving a notable reduction in the number of viral particles when compared to Post cells (Fig 1G).

These data suggest that PAD activity plays a less important role in the early phases of infection, such as binding and entry, but becomes essential during the later stages of viral replication.

HSV-1 infection upregulates PAD expression

To determine whether HSV-1-enhanced citrullination was modulated by any of the five known PAD isoforms (*i.e.*, PADs 1–4 and PAD6) and if they played a role in this process, we conducted RT-qPCR analysis in infected HFFs. The results revealed that the *PADI2*, *3*, and *4* genes were all expressed at significantly higher levels in HSV-1-infected HFFs at 16 hpi compared to mock-infected controls (Fig 2A). By contrast, the other PAD isoforms (*PADI1* and *6*) were expressed at very low levels and did not significantly change following HSV-1 infection (S2A Fig). Consistent with their mRNA expression, PAD2, 3, and 4 protein levels were increased upon HSV-1 infection, albeit with different kinetics (Fig 2B). Compared to uninfected cells, HSV-1-infected HFFs showed a significant increase in PAD2 and PAD4 protein expression (at 16 and 24 hpi, respectively) but returned to basal conditions soon after (S2B Fig). Of note, PAD3 protein was undetectable in mock-infected HFFs, but it was strongly

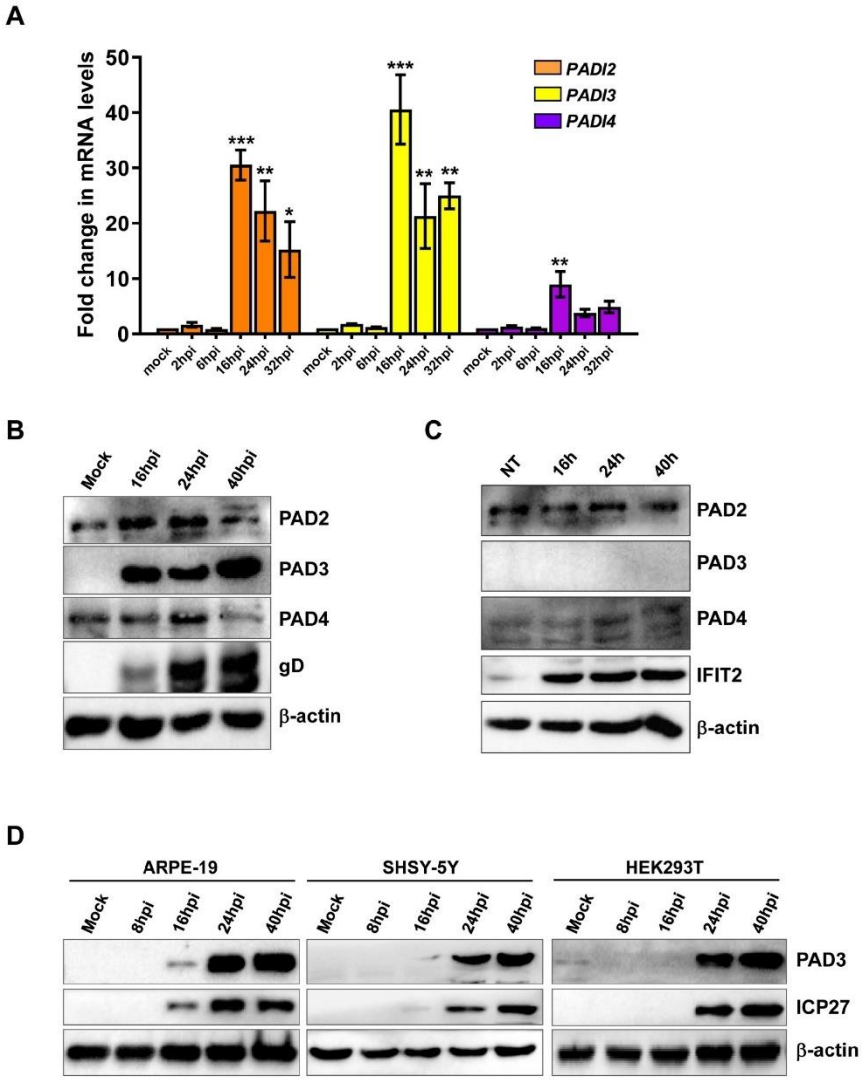

Fig 2. HSV-1 infection upregulates PAD expression in human fibroblasts. (A) mRNA expression levels of *PADI* isoforms by RT-qPCR of HSV-1-infected (8 and 16 hpi) *vs* uninfected (mock) HFFs were normalized to the housekeeping gene glyceraldehyde-3-phosphate dehydrogenase (GAPDH) and expressed as mean fold change ± SEM over mock-infected cells. $^{*}P < 0.05$, $^{**}P < 0.01$, $^{***}P < 0.001$; one-way ANOVA followed by Bonferroni's post test. (**B**) Western blot analysis of protein lysates from uninfected (mock) or infected HFFs (MOI 1) at different time points using antibodies against PAD2, PAD3, and PAD4. An anti-gD antibody was used to assess HSV-1 infection, while β-actin cellular expression was used for protein loading control. (**C**) Western blot analysis of protein lysates from untreated (NT) or IFN-β-treated (500 U/mL) HFFs using antibodies against PAD2, PAD3, and PAD4. An anti-ICP27 antibody was used to assess HSV-1 infection, while β-actin cellular expression was used for protein loading control. **(D)** Western blot analysis of protein lysates from uninfected (mock) or HSV-1-infected (MOI 1) cells at different time points using antibody against PAD3. An anti-ICP27 antibody was used to assess HSV-1 infection, while β-actin cellular expression was used for protein loading control. Representative blots of three independent experiments are shown.

https://doi.org/10.1371/journal.ppat.1011849.g002

expressed in HSV-1-infected cells starting from 16 hpi and persisted at later time points, with a pattern similar to that of the late gD viral protein. Moreover, to rule out the possibility that increased PAD expression in HFFs was induced by an interferon (IFN) response to viral infection rather than HSV-1 infection *per se*, cells were treated with IFN-β (500 U/mL) and harvested at different time points after treatment. IFN-β treatment failed to change the basal expression of PAD proteins at any time compared to untreated cells, whereas the interferon-inducible IFIT2 protein showed a significant increase (Figs 2C and S2E).

Finally, to ascertain whether this phenomenon was restricted to HFFs, we extended our RT-qPCR and Western blot analyses of PAD3 to include ARPE-19 and SHSY-5Y cells. HEK293 cells, which are known to basally express PAD3 [32], were analyzed as well. In all the cell lines tested, PAD3 was upregulated during HSV-1 infection (MOI 1), with minor variations between the cell lines (Fig 2D and S2C Fig). This pattern contrasts with our earlier findings in HCMV-infected HFFs [30] and HCoV-43-infected MRC-5 fibroblasts [26], where PAD3 was undetectable under basal conditions and did not show any signs of upregulation, suggesting that different viruses may induce different PAD isoforms.

PAD3 protein levels are induced through a calcium-independent HSV-1-early mechanism

Having established that PAD3 was the most significantly impacted PAD family member by HSV-1 infection, we sought to determine the mechanism underlying *PADI3* transcriptional upregulation in response to viral infection. To this end, we assessed the promoter activity of *PADI3* gene by transiently transfecting HFFs with luciferase reporter plasmids carrying the wild-type promoter region of *PADI3*. At 24 h post transfection, cells were infected with HSV-1. As shown in Fig 3A, HSV-1 infection led to a robust induction of the luciferase activity driven by *PADI3* promoter (~6 fold) and upregulated viral ICP27 expression at 24 hpi (Fig 3B), indicating once more than early stages of infection are critical for the transcriptional activation of *PADI3* gene. As expected, UV-inactivated HSV-1 infection failed to induce both PAD3 and ICP27 protein expression in HFFs compared to cells infected with wild-type HSV-1 (Fig 3B). Furthermore, treatment of HSV-1-infected HFFs with the protein synthesis inhibitor CHX curbed the induction of PAD2, 3, and 4, as well as ICP27, protein expression and total levels of protein citrullination at 24 hpi, without altering total protein levels (Fig 3C and S2E Fig), indicating that *de novo* gene expression is required for PAD protein upregulation and citrullination profile modification during infection. In contrast, treatment with the viral DNA synthesis inhibitor phosphonoformic acid (PFA) only marginally affected the upregulation of PAD3 despite resulting in a dramatic reduction in the synthesis of the late viral protein gD (Fig 3D). Altogether, these data indicate that one or more viral proteins synthetized during the initial stages of infection are involved in PAD3 transcriptional upregulation.

Finally, as HSV-1 infection is known to increase intracellular calcium levels [33], we asked whether PAD3 overexpression could be ascribable to this calcium influx rather than being a direct consequence of upregulated gene expression induced by HSV-1 viral proteins. To rule out this possibility, we employed thapsigargin (TG), an endoplasmic reticulum (ER) stressor known to elevate intracellular calcium levels by interfering with the sarcoplasmic/endoplasmic reticulum Ca^{2+}-ATPase [34]. Specifically, we treated mock-infected HFFs with two concentrations of TG (1.5 and 5 μM) and evaluated PAD3 expression at both the mRNA (Fig 3E) and protein (Fig 3F) levels after 16 h. We found that, in comparison with HSV-1-infected cells (MOI 1; 16 hpi), TG treatment failed to upregulate PAD3 expression at any of the concentrations tested, whereas it significantly upregulated *ATF-6* gene expression (Fig 3F), confirming its efficacy as an ER stressor at both concentrations.

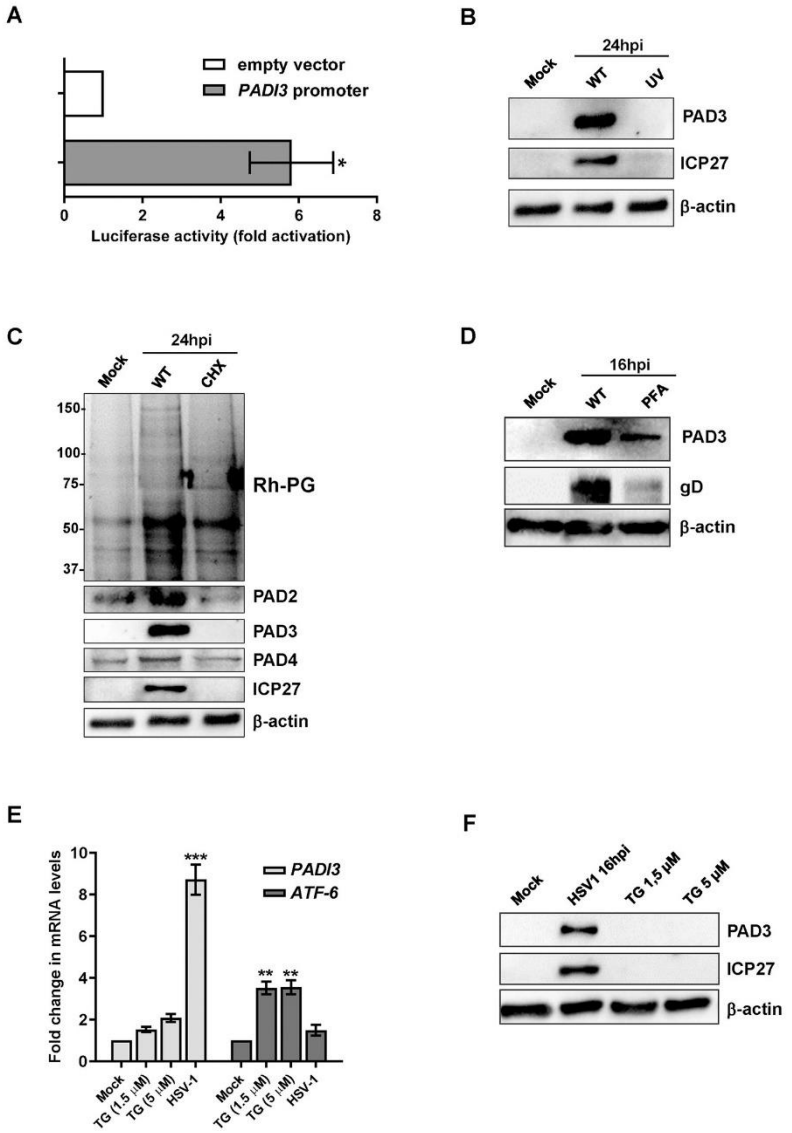

Fig 3. PAD3 induction by HSV-1 early mechanism. (A) HFFs were transiently transfected with luciferase plasmid encoding the wild-type PADI3 promoter region (pGL4.20-PADI3) or the pGL4.20 empty vector. Twenty-four h later, the cells were mock-infected or infected with HSV-1 at an MOI of 1. At 24 hpi, firefly and *Renilla* luciferase activities were measured. Luciferase activity in whole-cell lysates was normalized to *Renilla* luciferase activity and plotted as folds induction relative to infected HFFs carrying the pGL4.20 empty vector (set at 1). Results are shown as means of fold change ± SEM (error bars) of three independent experiments. **(B)** Western blot analysis of protein lysates from uninfected (mock) or infected HFFs with HSV-1 wild-type (WT) or UV-inactivated HSV1 (UV), at 24 hpi (MOI 1). Analysis was performed using antibodies against PAD3, ICP27, or β-actin. One representative blot of three independent experiments is shown. (**C**) Western blot and Rh-PG analysis of protein lysates from uninfected (mock) or HSV1-infected HFFs (MOI 1), treated with 150 μg/ml CHX or left untreated. Analysis was performed using antibodies against PAD2, PAD3, PAD4, ICP27, or β-actin to assess for equal loading. One representative blot of three

independent experiments is shown. **(D)** Protein lysates from uninfected (mock) or infected HFFs (16 hpi) at an MOI of 1 PFU/cell treated with (PFA 250 μM) or vehicle were analyzed by immunoblotting for PAD3, viral protein gD, or β-actin. **(E)** *PAD3* and *ATF-6* mRNA expression levels by RT-qPCR of HSV-1-infected (16 hpi, MOI 1) or mock-infected HFFs treated or not with the indicated amounts of thapsigargin (TG). The results were normalized to the housekeeping gene glyceraldehyde-3-phosphate dehydrogenase (GAPDH) and expressed as mean fold change ± SEM over mock-infected cells. $^{*}P < 0.05$, $^{**}P < 0.01$, $^{***}P < 0.001$; one-way ANOVA followed by Bonferroni's post test. **(F)** Western blot analysis of protein lysates from uninfected (mock), HSV-1-infected (16 hpi, MOI 1) or mock-infected HFFs treated with TG for 16 h. Analysis was performed using antibodies against PAD3, ICP27, or β-actin. Representative blots of three independent experiments are shown.

https://doi.org/10.1371/journal.ppat.1011849.g003

PAD3 targeting impairs HSV-1 replication

Having observed that PAD2, 3, and 4 protein levels increased during HSV-1 infection, we asked whether inhibiting the enzymatic activity of these proteins would affect viral replication. To this end, HFFs were treated with increasing concentrations of the specific inhibitors of the three isoforms (AFM30a for PAD2, HF4 for PAD3, and GSK199 for PAD4) or with equal volumes of vehicle control (DMSO) 1 h before HSV-1 infection (MOI 1) and for the entire duration of the infection. After 24 h of continuous exposure to the PAD inhibitors, we measured total virus production by plaque assay. While AFM30a and GSK199 treatment had no or minimal effect on HSV-1 replication rate at high doses (S3A and S3B Fig, respectively), exposure to HF4 strongly inhibited viral production in a dose-dependent manner, achieving a reduction of almost 3 logs at 5 μM (Fig 4A). To rule out the possibility that this antiviral activity was related to any off-target effects, we confirmed these results with another PAD3-specific inhibitor, namely CAY10727 [35], which showed a very similar efficacy in reducing viral production (Fig 4B). MTT assay excluded cytotoxic effect of drugs under the same treatment conditions (S3C, S3D and S3E Fig). In line with these results, at 24 hpi, infected carrier-treated cells showed a dramatic cytopathic effect, while HF4 and CAY10727 treatments restored a phenotype more similar to that of uninfected cells (Fig 4C). Moreover, immunoblot analysis of total protein extracts showed downregulation of viral late gD protein expression levels at 24 hpi in treated cells, particularly evident in the presence of HF4 and consistent with the inhibition observed in the plaque assay (Fig 4D). To corroborate these findings, we tested the PAD3 specific inhibitors HF4 and CAY10727 in the other cell types included in this study. As shown in Fig 4E and 4F, we observed a reduction in the count of viral particles in all cell lines in a dose-dependent manner, with the concentrations used being non-toxic for the cells (S3C and S3D Fig).

Finally, to confirm these results we knocked down PAD3 expression in HFF cells with a specific cocktail of PAD3-siRNAs and with siRNA control (siCtrl). At 24 h post-electroporation, cells were infected with HSV-1 (MOI 1). Protein lysates were harvested from siRNA-transfected cells at 24 hpi, and the efficiency of cellular gene expression reduction was evaluated at the protein level by Western blot analysis. We noted that PAD3 depletion was accompanied by a significant decrease in gD expression compared to control (Fig 4G). Moreover, the plaque assay on infected and PAD3-silenced HFFs showed a significant reduction of the virus yield by more than 2 logs compared to siCtrl HFFs (Fig 4H), which was confirmed by the complete recovery from the cytopathic effect upon PAD3 silencing (Fig 4I).

Overall, these data suggest that PAD3 activity plays a key role in supporting HSV-1 replication, and that PAD3 might be a promising target for anti-HSV-1 therapy.

Citrullinome analysis reveals IFIT proteins as restriction factors for HSV-1 replication

Next, to identify which cellular and/or viral proteins were citrullinated during infection, we used a citrulline specific probe (biotin-PG) and enriched the HSV-1-associated citrullinome in

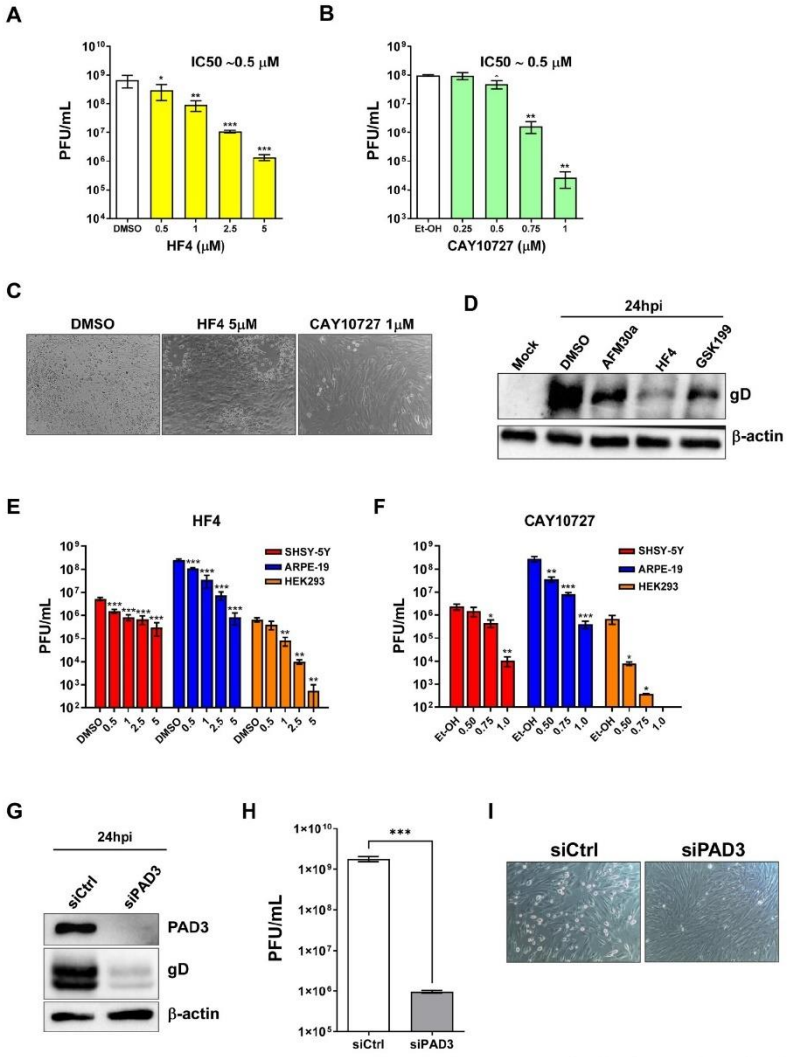

Fig 4. PAD3 targeting impairs HSV-1 replication in human cells. HFFs were infected with HSV-1 (MOI 1) and then treated with increasing concentrations of HF4 **(A)** or CAY10727 **(B)**, two PAD3-specific inhibitors, which was given 1 h prior to virus adsorption and kept throughout the whole experiment. At 24 hpi, viral plaques were microscopically counted, and the number of plaques was plotted as a function of inhibitor concentration. Values are expressed as means ± SEM (error bars) of three independent experiments. Values are expressed as mean ± SEM of three independent experiments, $^{*}P < 0.05$, $^{**}P < 0.01$, $^{***}P < 0.001$; one-way ANOVA followed by Bonferroni's post test. (**C**) Representative images of infected HFFs (24 hpi) at an MOI of 1 PFU/cell and treated with HF4 (5 μM), CAY10727 (1 μM), or vehicle (DMSO). (**D**) Protein lysates from uninfected (mock) or infected HFFs (24 hpi) at an MOI of 1 PFU/cell treated with AFM30a (20 μM), HF4 (5 μM), GSK199 (20 μM) or vehicle (DMSO) were analyzed by immunoblotting to assess for viral expression with an anti-gD antibody; β-actin cellular expression was used for protein loading control. SH-SY5Y, ARPE-19, and HEK293 cells were infected with HSV-1 (MOI 1 PFU/cell) and then treated with increasing concentrations of HF4 **(E)** or CAY10727 **(F)**, which were given 1 h prior to virus adsorption and kept throughout the whole experiment. At 24 hpi, viral plaques were microscopically counted, and the number of plaques was plotted as a function of inhibitor concentration. Values are expressed as means ± SEM (error bars) of four independent experiments, $^{*}P < 0.05$, $^{**}P < 0.01$, $^{***}P < 0.001$; one-way ANOVA followed by Bonferroni's post test.

(G) HFFs were silenced for PAD3 using specific siRNAs (siPAD3), as negative control cells were also similarly transfected with scrambled siRNA (siCTRL). At 24 h post-treatment (hpt), cells were infected with HSV-1 at an MOI of 1 PFU/cell. The efficiency of PAD3 protein depletion at 24 hpi was assessed by immunoblotting using antibodies against PAD3 or β-actin for equal loading. An anti-gD antibody was used to verify HSV-1 infection. Representative blots of three independent experiments are shown. (**H**) PAD3-silenced cells were infected with HSV-1 at an MOI of 1 PFU/cell. Viral supernatants were collected at 24 hpi and analyzed by standard plaque assay. Values are expressed as means ± SEM. Values are expressed as mean ± SEM of three independent experiments, $^{***}P < 0.001$; one-way ANOVA followed by Bonferroni's post test. (**I**) Representative images of infected HFFs (24 hpi) at an MOI of 1 PFU/cell and transfected with the same siCTRL and siPAD3 described in the legend to Fig 3D.

https://doi.org/10.1371/journal.ppat.1011849.g004

HFFs harvested at 16 and 24 hpi through streptavidin-agarose beads. As shown in Fig 5A, and consistent with our earlier findings, we observed a massive increase in overall protein citrullination in HSV-1-infected cells compared to uninfected control cells. In detail, database searches using the SEQUEST algorithm allowed us to identify 297 (126 significant) and 287 (125 significant) citrullinated cellular proteins at 16 and 24 hpi, respectively (S1 Data). In addition, a total of 39 and 35 (28 and 25 significant, respectively) citrullinated viral proteins were also detected at the indicated time points (Fig 5B and S2 Data). Of note, at 16 hpi most of the citrullinated viral proteins were immediate early (IE) genes and enzymes involved in the synthesis of viral DNA, whereas at 24 hpi mainly structural capsid and tegument proteins or envelope glycoproteins were detected. Moreover, through PANTHER software, we were able to identify a wide range of citrullinated host proteins falling into various functional classes, including metabolite interconversion enzymes, RNA and DNA metabolism proteins, chaperones, cytoskeletal proteins, protein-binding activity modulators, protein modifying enzymes, membrane traffic proteins, transporters, and defense/immunity proteins (Fig 5C).

Previously, we demonstrated that during HCMV infection several members of the interferon (IFN)-induced protein with tetratricopeptide repeat (*IFIT*) family were heavily citrullinated, and that IFIT1 lost its restriction factor activity when citrullinated *in vitro* [30]. Consistently, here we found that IFIT1 and IFIT2 were also significantly citrullinated in the HSV-1-associated citrullinome at both 16 and 24 hpi (Fig 5A). Unlike IFIT1 and IFIT2, IFIT3 showed only a slight increase in citrullination during infection, which was not statistically significant ($p = 0.06$). Therefore, we decided to focus on the other two isoforms for further investigation.

To validate these findings, total proteins from mock or HSV-1-infected HFFs at 16 and 24 hpi (MOI 1) were immunoprecipitated with an anti-citrulline antibody and subjected to immunoblotting using antibodies against IFIT1, IFIT2, or the viral protein ICP27. As shown in Fig 5D, IFIT1, IFIT2 and ICP27 proteins were upregulated and, consistent with previous results, citrullinated following infection with HSV-1, especially at 16 hpi. Considering that IFIT family members are significantly upregulated by IFNs, we sought to investigate whether the observed increase in citrullination was a direct consequence of the infection or resulted from the IFN-mediated upregulation in response to the infection. To test whether interferon alone could induce deimination of IFIT1 and IFIT2, we treated HFFs with IFN-β (500 U/mL) for 16 h and 24 h and immunoprecipitated the total proteins with the anti-citrulline antibody. Successively, we performed immunoblotting using antibodies against IFIT1 and IFIT2. As shown in Fig 5E, we found that both proteins were strongly upregulated by IFN treatment, but they did not bind to the anti-citrulline antibody, suggesting that interferon itself is not sufficient to cause deimination of IFIT proteins.

Next, to gain further insight into the role of these genes during HSV-1 infection, we measured viral production in HSV-1-infected HFFs after siRNA-mediated depletion of IFIT1 and IFIT2. Following transfection with specific siRNAs (siIFIT1 and siIFIT2, respectively) and

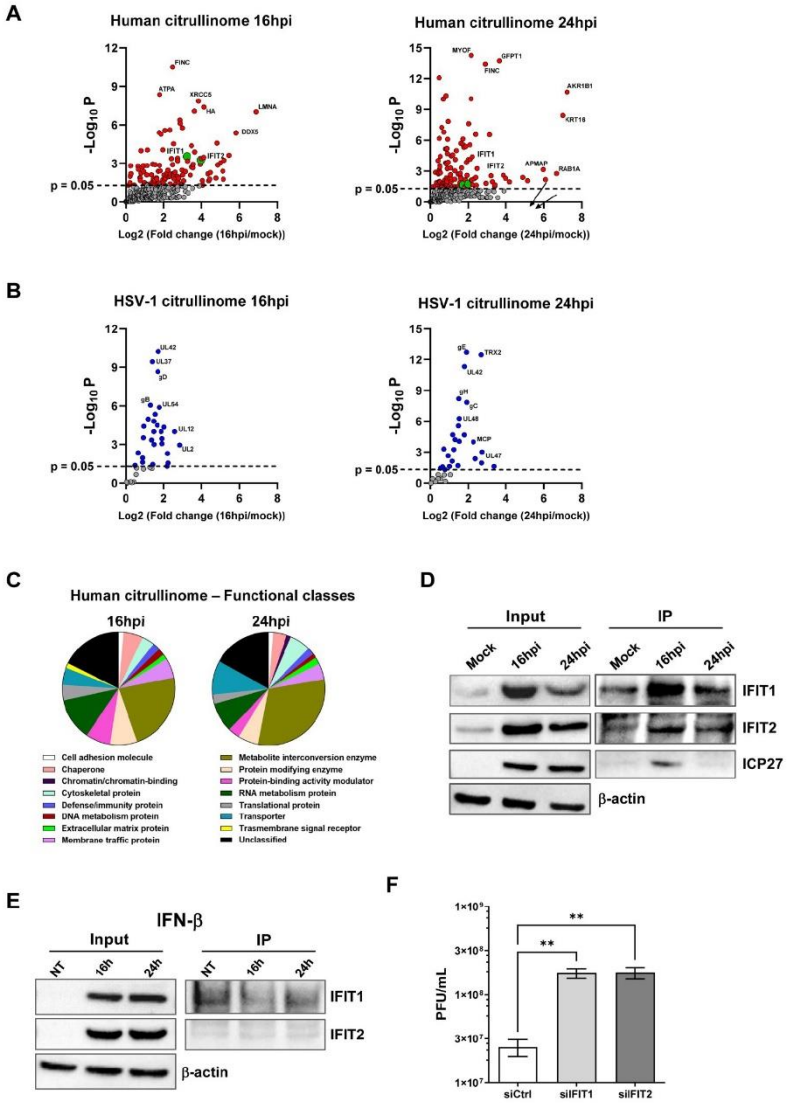

Fig 5. Citrullinome analysis reveals IFIT proteins as restriction factors for HSV-1 replication. **(A-B)** Volcano plot depicting the host (**A**, red dots) and viral (**B**, blue dots) citrullinated proteins of infected cells *vs* mock-infected cells at 16 hpi (left panels) and 24 hpi (right panels). Cell lysates from uninfected (mock) or HSV-1-infected HFFs (MOI 1) were exposed to a biotin-PG to isolate citrullinated proteins on streptavidin agarose. Bound proteins were then subjected to on-bead tryptic digestion and analyzed by LC-MS/MS—in the graph, every identified citrullinated protein corresponds to a dot. The x-axis represents the ratio of citrullination between mock and infected cells at the indicated time points, while the y-axis indicates the statistical significance. Both variables were plotted on a logarithmic scale ($n = 3$). IFIT1 and IFIT2 proteins are reported as green dots, while grey dots represent proteins that do not reach statistical significance. **(C)** The pie charts show the classification of citrullinated cellular proteins at 16 hpi (left) and 24 hpi (right) based on protein classes. Only classes with a representation exceeding 1% are reported. **(D)** Immunoprecipitation (IP) of total cell extracts (Input) from mock or infected HFFs at 24 hpi using an anti-peptidylcitrulline antibody. The IP complexes were analyzed by Western blotting using antibodies against IFIT1 and

IFIT2. An anti-ICP27 antibody was used to assess HSV-1 infection, while β-actin cellular expression was used for protein loading control. The blot shown is representative of three independent experiments. (**E**) Immunoprecipitation (IP) of total cell extracts (input) from untreated (NT) or IFN-β-treated (500U/ml) HFFs using an anti-peptidylcitrulline antibody. The IP complexes were analyzed by Western blot using antibodies against IFIT1 and IFIT2. Equal loading was assessed by β-actin immunoblotting. The blot shown is representative of three independent experiments. (**F**) HFFs were silenced for IFIT1 and IFIT2 using specific siRNAs (siIFIT1 and siIFIT2, respectively). As negative control cells were also similarly transfected with scrambled siRNA (siCtrl. At 24 hpt, cells were infected with HSV-1 at an MOI of 1 PFU/cell. Viral supernatants were collected at 24 hpi and analyzed by standard plaque assay. Values are expressed as means ± SEM of three independent experiments. Representative blots of three independent experiments are shown.

https://doi.org/10.1371/journal.ppat.1011849.g005

subsequent infection with HSV-1 for 24 h, we achieved a nearly complete silencing of both proteins, without affecting the ability of the virus to replicate, as demonstrated by the expression of the ICP27 viral marker (S4A Fig). Rather, silencing either IFIT1 or IFIT2 resulted in significantly higher levels of virus production compared to siCtrl-transfected cells (Fig 5F), suggesting that IFIT1 and IFT2 are potential restriction factors for HSV-1, whose activity can be overcome by virus-induced citrullination.

Discussion

Viruses, unlike other infectious agents, require the molecular machinery of the host to complete their replication cycle. As a result, these pathogens have evolved multiple mechanisms to promote the translation of their transcripts, evade the immune system, and induce host gene expression alterations during infection. These mechanisms are indispensable for the viral life cycle, but they are particularly sophisticated in viruses, such as herpesviruses, that establish latency and persist throughout the host's lifespan. Recent research has unveiled the potential involvement of host-cellular environment manipulation mechanisms in the pathogenesis of autoimmune diseases, as well as tumors and neurodegenerative disorders. A promising strategy to target these evasion mechanisms is to employ host-targeting antiviral agents (HTAs) that interfere with the host factors required for viral replication [36].

Citrullination, a post-translational modification mediated by PAD enzymes, is emerging as a key mechanism that viruses exploit during their replication in host cells. This is supported by an association between viral infection and PAD-mediated upregulation of citrullination, which we and others have reported in various viral and cellular models [25–27,30]. In particular, we have shown that one such virus, HCMV, induces PAD-mediated citrullination of several cellular proteins endowed with antiviral activity, including the IFN-stimulated genes (ISGs) IFIT1 and Mx1, and that blocking this process with the PAD inhibitor Cl-amidine can inhibit viral replication [30]. Here, we extend those findings to a different member of the *Herpesviridae* family, HSV-1, which we demonstrate to be capable of promoting PAD-mediated citrullination *in vitro*. Specifically, we show that HSV-1 infection of human fibroblasts upregulates total protein citrullination, and that this process is required for optimal viral replication.

Despite various viruses being capable of upregulating PAD enzyme expression, which is crucial for optimal viral replication, our findings suggest that each virus displays a preference for specific PAD isoforms. This challenges the assumption that PAD upregulation is a general response to viral infection. For instance, PAD4 is the main isoform regulated by human rhinovirus (HRV) and HCoV [26,27], while PAD2 and PAD4 cooperate in supporting HCMV replication [30]. In the present work, we show that during HSV-1 infection three different PAD isoforms are upregulated: PAD2, 3, and 4. Although PAD2 and PAD4 are also induced upon HSV-1 replication, PAD3 seems to play a major role, as shown by the fact that its promoter is robustly induced by HSV-1 infection and that its targeted inactivation

through specific inhibitors or silencing by siRNAs has a detrimental effect on HSV-1 replication. Noteworthy, during HSV-1 infection PAD3 consistently displayed similar kinetics to that of the viral protein ICP27, regardless of the cell model used, suggesting that the variations in permissiveness among cells, and consequently, the different kinetics of viral replication, rather than the different basal expression of PAD3, influence the kinetics of PAD expression. Hence, developing specific inhibitors for this particular isoform could improve the efficacy and mitigate the toxicity of HSV-1 antiviral treatments. This underscores the overarching need to identify which isoforms are specifically involved in different viral infections to design more effective HTAs [37].

In this study, we have also identified the cellular and viral proteins deiminated during HSV-1 infection, thus determining the citrullinome of the infected cells. We show that several members of the interferon (IFN)-induced protein with tetratricopeptide repeat (*IFIT*) family, such as IFIT1 and IFIT2, are robustly citrullinated, similar to what we observed in HCMV-infected cells. This is of particular interest because IFIT family members, primarily known for their antiviral activity against RNA viruses [38,39], have recently been linked to the innate immune response against DNA viruses, including two other members of the herpesvirus family, namely KSHV and HCMV [30,40]. More specifically, the antiviral function of IFIT3—which in our analysis was not significantly citrullinated—against HSV-1 is known, as is the ability of the virus to evade this function via the UL41 protein [41]. However, the roles of the other two members, IFIT1 and IFIT2, in HSV-1 infection have not been previously reported. Our research shows that silencing of either IFIT1 or IFIT2 results in increased virus production, while ectopic expression of IFIT1 inhibits viral growth, which agrees with previous findings in KSHV and HCMV-infected cells [30,40]. In terms of viral proteins, our study reveals that citrullination follows the natural replication cycle of the virus, with IE, E, and L proteins undergoing citrullination in a sequential order. Importantly, both viral structural and catalytic proteins show citrullination, underscoring the need to understand how this modification impacts their functions and whether it is involved in the assembly of new virions. In this regard, the substantial presence of citrullinated cellular and viral proteins observed in our analysis indicates that infection-induced citrullination is critically involved in multiple stages of HSV-1 replication throughout its life cycle. Therefore, PAD family members represent promising candidates for antiviral drug targeting, as their inhibitors can effectively block the replication of HSV-1 through various mechanisms.

It is however worth pointing out that although some substrates of PADs are IFN-inducible proteins, citrullination *per se* is not an IFN-dependent phenomenon. We show that, in mock-infected cells exposed to interferon, IFIT1 and IFIT2 proteins are upregulated but not over-citrullinated, and that the expression levels of PAD enzymes are unchanged. These findings, along with the fact that PADs are only upregulated in cells infected with functional HSV-1 but not in cells infected with UV-treated HSV-1, imply that viral IE protein production regulates PAD protein expression, as we observed in HCMV-infected cells [30].

Overall, our results clearly demonstrate that PAD induction and subsequent citrullination profile alteration are virus-specific phenomena. However, it is highly likely that the over-citrullinated host proteins in the course of infection are closely dependent on the infected tissue, just as the citrullinome is strictly linked to the gene expression profile of host cells prior to infection [42]. Consequently, it is highly probable that the effects of citrullination induced by an infection will vary depending on the specific tissue and organ affected, rather than simply being influenced by the type of virus involved.

Altogether, our findings suggest the intriguing scenario that conditions where citrullination contributes to a pathological state may be triggered by a viral infection that initially disrupts PAD activity.

Materials and methods

Cell lines and viruses

Human foreskin fibroblasts (HFFs; ATCC, SCRC-1041), African green monkey kidney Vero cells (Sigma-Aldrich, 84113001), the human neuroblastoma cell line SH-SY5Y (ATCC, CRL-2266), human embryonic kidney cells HEK293 (ATCC, CRL-1573) and retinal pigment epithelial cell (ARPE-19; ATCC, CRL-2302) were grown in Dulbecco's Modified Eagle Medium (DMEM; Sigma-Aldrich) supplemented with 1% (v/v) penicillin/streptomycin solution (Euroclone) and heat-inactivated 10% (v/v) fetal bovine serum (FBS) (Sigma-Aldrich). The medium of SH-SY5Y cells was also supplemented with non-essential amino acids (NEAA, Sigma-Aldrich). The clinical isolate of HSV-1 was grown in Vero cells and titrated by standard plaque assay as described previously [43].

Reagents and treatments

The PAD inhibitors Cl-amidine (Cl-A), BB-Cl-amidine (BB-Cl), GSK199, CAY10727, and AFM30a—also known as CAY10723—were obtained from Cayman Chemical (Ann Arbor). CHX and foscarnet (phosphonoformic acid, PFA) were from Sigma-Aldrich. All these compounds were reconstituted in dimethyl sulfoxide (DMSO) or ethanol accordingly to their solubility. HF4 and Thapsigargin were kindly provided by Dr. P. Thompson and Dr. M. Corazzari, respectively. Immediately before use, the inhibitors were diluted in the cell medium to their final concentrations. For the PADs inhibitors experiments, cells were pre-treated with the inhibitors for 1 h and then infected (MOI 1) by adding the virus without changing the medium. Following virus adsorption (2 h), the viral inoculum was removed, and a new medium with fresh inhibitor was added. After that, no more medium or inhibitor was added until the samples were collected.

Cell viability assay

Cells were seeded at a density of $3*10^4$/well in a 96-well plate. After 24 h, the cells were treated with the indicated concentration of the different inhibitors or mock-treated using the vehicle alone (DMSO or ethanol). After 48 h, cell viability was determined using the 3-(4,5-dimethylthiazol-2-yl)-2,5-diphenyltetrazolium bromide (MTT, Sigma) method as described previously [30].

In vitro antiviral assay

Cells were cultured in a 24-well plate for 1 day and then treated as described in 3.2. Briefly, they were incubated with the aforementioned PAD inhibitors at the indicated concentration for 1 h and subsequently infected with HSV-1 at a MOI of 1. Following virus adsorption (2 h at 37˚C), the viral inoculum was removed, and the cell cultures were maintained in a medium containing the indicated treatment for 24 h. DMSO or ethanol were used as a negative control. Next, the cells and supernatants were harvested, pooled, and then lysed by two freeze-thaw cycles. The extent of virus replication was then assessed by titrating the infectivity of the sample by standard plaque assay on Vero cells.

Plaque assay

Vero cells were seeded at a density of $3*10^4$/well in a 96-well plate and inoculated 24 h later with 10-fold serial dilutions of the HSV-1 production. After 48 h, cells were fixed and stained with crystal violet solution, and plaques were counted on each well to determine the virus titer,

which was determined by counting the number of immunostained foci on each well using the following formula: virus titer (PFU/ml) = number of plaques * 0.1 ml/dilution fold.

DNA and RNA isolation and quantitative nucleic acid analysis

Total DNA and RNA were extracted using the NucleoSpin RNA kit (Macherey-Nagel, Düren, Germany), and 1 μg of RNA was retrotranscribed using the Revert-Aid H-Minus FirstStrand cDNA Synthesis Kit (Thermo Fisher Scientific, Waltham, USA), according to the manufacturer's instructions. Comparison of mRNA expression between samples (*i.e.*, infected *vs.* untreated) was performed by SYBR green-based RT-qPCR using a Biorad CFX96 apparatus, using the primers reported in S1 Table. To determine the number of viral DNA genomes, viral DNA levels were measured by quantitative PCR on a Biorad CFX96 apparatus (Stratagene, San Diego, USA). To create a standard curve for each analysis, genomic DNA mixed with a gE2-encoding plasmid (Addgene pAcUW51-gE2) was serially diluted from 109 to 1 copy and analyzed in parallel. The amount of human GAPDH gene amplified per reaction mixture was used to normalize the HSV-1 DNA copy numbers.

Western blot analysis

Cells were treated with the indicated compound or equal volumes of DMSO solvent 1 h before infection and throughout the entire duration of the infection as previously described in point 2.2. Cells were infected with HSV-1 at an MOI of 1 and harvested at the indicated time points. Cell lysates were prepared with RIPA buffer, quantified by Bradford method, and subjected to Western blot analysis. The primary antibodies were as follows: anti-PAD1 (Abcam, ab181791); anti-PAD2 (Cosmo Bio, SML-ROI002-EX); anti-PAD3 (Abcam, ab50246); anti-PAD4 (Abcam, ab128086); anti-PAD6 (Abcam ab16480); anti-actin (Sigma-Aldrich, A2066), anti-gD (Virusys, HA025-1), anti-ICP27 (Virusys, P1113), anti-IFIT1 (Invitrogen PA5-31254), anti-IFIT2 (Proteintech, 12604-1-AP), anti-IFIT3 (Proteintech 15201-1-AP).

Detection of citrullination with rhodamine-phenylglyoxal (Rh-PG)

Whole-cell protein extracts were prepared as described in the previous paragraph. Equal amounts of protein were diluted with 80% trichloroacetic acid and incubated with Rh-PG (final concentration 0.1 mM) for 30 min [44]. The reaction was quenched with 100 mM L-citrulline, then centrifuged at 21,100xg for 10 min, washed with ice-cold acetone, and resuspended in 2X SDS loading dye for gel electrophoresis. Gels were imaged (excitation = 532 nm, emission = 580 nm) using a Biorad Chemidoc Imaging System, stained with brilliant blue G-colloidal solution (Sigma-Aldrich).

PAD3 vector construction

The 5' flanking region of *PADI3* gene was amplified by PCR using the Q5 High-Fidelity DNA polymerase (New England Biolabs, Ipswich, USA), the human genomic DNA from HFFs as a template, and the PAD3 primers containing *Xho* I and *Hind* III restriction enzymes sites (see primers sequences listed in S1 Table). The resulting amplification products were digested with *Xho* I and *Hind* III (Thermo Fisher Scientific, Waltham, USA) and cloned into the pGL4.20 [luc2/Puro] vector (Promega, Madison, USA), which encodes the luciferase reporter gene *luc2* (*Photinus pyralis*) with no other regulatory elements. The resulting pGL4.20-PADI3prom construct was purified using the PureYield Plasmid Miniprep System (Promega, Madison, USA) and verified by restriction mapping and complete sequencing. The resulting chromatograms were analyzed using Chromas software 2.6.6 (Technolysium Ltd.).

Dual-luciferase reporter assay

HFFs were seeded into 12-well plates and, after 24 h of incubation, transiently transfected with 1 μg of pGL4.20 or pGL4.20-PADI3 plasmids together with 0.1 μg of Renilla reporter plasmid (pRL-SV40, to correct for transfection efficiency) using Lipofectamine 2000 Transfection Reagent kit (Thermo), according to the manufacturer's instruction. After 24h, cells were infected with HSV-1 (MOI of 1 PFU/ml), and 24 hpi the Dual-luciferase Reporter Assay System (Promega, USA) was used to detect Firefly and *Renilla* luciferase activities and recorded using GloMax 96 Microplate Luminometer (Promega, USA). Firefly luciferase activity from the luciferase reporter vector was normalized to *Renilla* luciferase activity from the pRL-SV40 vector and plotted as folds of induction relative to infected HFFs expressing the pGL4.20 empty vector (set at 1).

Pull-down experiments

Uninfected or HSV-1-infected cells (MOI of 1 PFU/ml) were washed with 1X PBS and lysed in radioimmunoprecipitation assay (RIPA) buffer (50 mM Tris pH 7.4; 150 mM NaCl; 1 mM EDTA; 1% nonidet P-40; 0.1% SDS; 0.5% deoxycholate; protease inhibitors). Proteins (200 μg) were then incubated with 2 μg of anti-citrulline monoclonal antibody (Cayman Chemical, 30773) or with an isotype antibody as negative control (62–6820; Thermo Fischer Scientific, Waltham, USA) for 1 h at room temperature with rotation followed by overnight incubation at 4˚C with protein G-sepharose (Sigma-Aldrich, Milan, Italy). Immune complexes were collected by centrifugation and washed with RIPA buffer. The sepharose beads were pelleted and washed three times with RIPA buffer, resuspended in reducing sample buffer (50 mM Tris pH 6.8; 10% glycerol; 2% SDS; 1% 2- mercaptoethanol), boiled for 5 min and resolved on an SDS-PAGE gel to assess protein binding by immunoblotting.

Citrullinome analysis by mass spectrometry: Sample preparation

Sample preparation in technical triplicates followed the procedure outlined in [45]. Equal amounts of cell lysates from each experimental group (300 μg) were diluted in buffer (100 mM HEPES pH 7.6) to a final concentration of 1 μg/μL and incubated with 20% trichloroacetic acid (TCA) and 0.5 mM biotin-PG [46] for 30 min at 37 ˚C. Labeled proteomes were precipitated on ice for 30 min. Samples were pelleted through tabletop centrifugation (21,100xg, 15 min) at 4 ˚C. The supernatants were discarded, and the pellets were washed with cold acetone (300 μL). After drying for 5 min, the pellets were resuspended in 1.2% SDS in PBS by bath sonication and heating. Samples were then transferred to 15 mL screw cap tubes and diluted in 1X PBS to a 0.2% SDS final concentration. Samples were incubated with streptavidin agarose slurry (Sigma Aldrich, 170 μL) overnight at 4 ˚C and for an additional 3 h at 25 ˚C. After discarding the flow through, the streptavidin beads were washed with 0.2% SDS in PBS (5 mL) for 10 min at 25 ˚C. The beads were then washed three times with 1X PBS (5 mL) and three times with water (5mL) to remove any unbound proteins. Beads were then transferred to a screw cap microcentrifuge tube and heated in 1X PBS with 500 μL 6 M urea and 10 mM DTT (65 ˚C, 20 min). Proteins bound to the beads were then alkylated with iodoacetamide (20 mM, 37 ˚C for 30 min). The beads were successively pelleted by centrifugation (1,400 x *g* for 3 min) and the supernatant was removed. The pellet was resuspended in a premixed solution of 2 M urea, 1 mM $CaCl_2$ and 2 μg Trypsin Gold (Promega, Madison, USA) in PBS. These were shaken overnight at 37 ˚C. The supernatant was collected, and the beads were washed twice with water (50 μL), each time collecting the supernatant. The fractions were combined, acidified with formic acid (5% final concentration) and stored at -20 ˚C until use.

Mass spectrometry

Liquid chromatography-mass spectrometry/mass spectrometry (LC-MS/MS) analysis was performed with an LTQ-Orbitrap Discovery mass spectrometer (Thermo Fisher Scientific, Waltham, MA, USA) coupled to an Easy-nLC HPLC (Thermo Fisher Scientific, Waltham, MA, USA). Samples were pressure loaded onto a 250-μm fused-silica capillary hand packed with 4-cm Aqua C18 reverse phase resin (Phenomenex). Samples were separated on a hand packed 100-μm fused-silica capillary column with a 5-μm tip packed with 10 cm Aqua C18 reverse phase resin (Phenomenex). Peptides were eluted using a 10-h gradient of 0–100% Buffer B in Buffer A (Buffer A: 95% water, 5% acetonitrile, 0.1% formic acid; Buffer B: 20% water, 80% acetonitrile, 0.1% formic acid). The flow rate through the column was set to ~400 nL/min, and the spray voltage was set to 2.5 kV. One full MS scan (FTMS) was followed by 7 data-dependent MS2 scans (ITMS) of the n^{th} most abundant ions. The tandem MS data were searched by the SEQUEST algorithm using a concatenated target/decoy variant of the human and viral UniProt database. A static modification of +57.02146 on cysteine was specified to account for alkylation by iodoacetamide. SEQUEST output files were filtered using DTASelect 2.0.

Database search

Raw data were processed and searched using Maxquant 1.6.14 and its integrated Andromeda search engine using the Swiss-Prot human (downloaded 04/09/2019) and Uniprot HCMV (downloaded 02/27/2021). Search parameters were as follows: tryptic digestion with up to 2 missed cleavages; peptide N-terminal acetylation, methionine oxidation, N-terminal glutamine to pyroglutamate conversion were specified as variable modifications. The monoisotopic mass increment of the triplex dimethyl labels, light, medium and heavy dimethyl label at 28.0313, 32.0564 and 36.0757 Da, respectively, were set as variable modification on the peptide N-termini and lysine residues. Carbamidomethylation of cysteines was set as static modification. Main search tolerance was 6 ppm, and the first search tolerance was 50 ppm. Both the protein and peptides identification false discovery rates (FDR) were $< 1\%$. Protein grouping, dimethyl ratio calculations and downstream statistics were performed in Scaffold Q+S 4.8.9 (Proteome Software, Portland, OR).

siRNA-mediated knockdown

HFFs were transiently transfected with a Neon Transfection System (Thermo Fischer Scientific) according to the manufacturer's instructions (1200 V, 30 ms pulse width, one impulse) with a pool of small interfering RNAs targeting PAD3 (Sigma-Aldrich, EHU012711), IFIT1 (Qiagen S102660777), IFIT2 (Invitrogen AM16708) or control siRNA (siCTRL, Qiagen 1027292) as negative control.

Statistical analysis

All statistical tests were performed using GraphPad Prism version 9.5.1 for Windows (GraphPad Software, San Diego, USA). The data were presented as means ± standard error of mean (SEM). Statistical significance was determined by using unpaired t test (two-tailed), one-way or two-way analysis of variance (ANOVA) with Bonferroni's, or Dunnett's post-tests. Differences were considered statistically significant for $P < 0.05$ ($^{*}P < 0.05$; $^{**}P < 0.01$; $^{***}P < 0.001$). The half-maximal inhibitory concentration (IC_{50}) was calculated by Quest Graph IC50 Calculator (AAT Bioquest, Inc, https://www.aatbio.com/tools/ic50-calculator).

Supporting information

S1 Fig. Uninfected HFFs, ARPE-19, and SHSY-5Y were treated with the indicated concentrations of Cl-A (**A**) and BB-Cl (**B**) for 24 h, and the number of viable cells was determined for each concentration using the MTT assay. Values are expressed as means ± SEM of three independent experiments. SH-SY5Y (**C**) and ARPE-19 (**D**) were infected with HSV-1 (MOI 1 PFU/cell) and then treated with increasing concentrations of Cl-A, which were given 1 h prior to virus adsorption and kept throughout the whole experiment. At 24 hpi, viral plaques were microscopically counted, and the number of plaques was plotted as a function of inhibitor concentration. Values are expressed as means ± SEM (error bars) of three independent experiments, $^{*}P < 0.05$, $^{**}P < 0.01$, $^{***}P < 0.001$; one-way ANOVA followed by Bonferroni's post-test. **(E)** Protein lysates from uninfected (mock) or infected HFFs (24 hpi) at an MOI of 1 PFU/cell treated with Cl-A (100 μM), BB-Cl (2.5 μM) or vehicle (DMSO) were exposed to an Rh-PG citrulline-specific probe (left panel) and subjected to gel electrophoresis to detect citrullinated proteins. Equal loading was assessed by Coomassie blue staining (right panel). (**F**) Representative images of infected HFFs (24 hpi) at an MOI of 1 PFU/cell and treated with Cl-A (100 μM), BB-Cl (2.5 μM), or vehicle (DMSO).
(TIF)

S2 Fig. **(A)** mRNA expression levels of *PADI* isoforms by RT-qPCR of HSV-1-infected (8 and 16 hpi) *vs* uninfected (mock) HFFs were normalized to the housekeeping gene glyceraldehyde-3-phosphate dehydrogenase (GAPDH) and expressed as mean fold change ± SEM over mock-infected cells. $^{*}P < 0.05$, $^{**}P < 0.01$, $^{***}P < 0.001$; one-way ANOVA followed by Bonferroni's post test. **(B)** Densitometric analysis of three independent experiments, values are expressed as fold change in PAD2 and PAD4 expression normalized to α-tubulin. **(C)** mRNA expression levels of *PADI3* isoforms by RT-qPCR of HSV-1-infected (6, 16 and 24 hpi) *vs* uninfected (mock) cells were normalized to GAPDH and expressed as mean fold change ± SEM over mock-infected cells. $^{*}P < 0.05$, $^{**}P < 0.01$, $^{***}P < 0.001$; one-way ANOVA followed by Bonferroni's post test. (**D**) Western blot analysis of protein lysates from untreated (NT) or IFN-β treated (500 U/mL) HFFs using antibodies against PAD1 or PAD6. β-actin cellular expression was used for protein loading control. One representative gel of three independent experiments is shown. **(E)** Blu Coomassie staining of the same protein extracts used in the experiments shown in Fig 2D (protein lysates from uninfected (mock) or HSV1-infected HFFs, treated with 150 μg/ml CHX or left untreated).
(TIF)

S3 Fig. **(A-B)** HFFs were infected with HSV-1 (MOI 1 PFU/cell) and then treated with increasing concentrations of AFM30a (A), GSK199 (B) and CAY10727 (C), which were given 1 h prior to virus adsorption and kept throughout the whole experiment. At 24 hpi, viral plaques were microscopically counted, and the number of plaques was plotted as a function of inhibitor concentration. Values are expressed as means ± SEM (error bars) of three independent experiments, $^{*}P < 0.05$, $^{**}P < 0.01$, $^{***}P < 0.001$; one-way ANOVA followed by Bonferroni's post test. (**C-E**) Uninfected HFF, SHSY-5Y, ARPE-19 or HEK293 cells were treated with the indicated concentrations of HF4 (C), CAY10727 (D), AFM30a, or GSK199 (E) for 24 h and the number of viable cells was determined for each concentration by MTT assay. Values are expressed as means ± SEM of three independent experiments.
(TIF)

S4 Fig. **(A)** The efficiency of IFIT1 or IFIT2 protein depletion at 24 hpi was assessed by immunoblotting using antibodies against IFIT1 or IFIT2, or against β-actin to check for equal loading. An anti-ICP27 antibody was also used to verify HSV-1 infection. Representative blots of

three independent experiments are shown.
(TIF)

S1 Table. Oligonucleotide primer sequences for qPCR and PADI3 promoter cloning.
(PDF)

S1 Data. List of the host citrullinated proteins of infected *vs* mock-infected HFFs at 16 hpi and 24 hpi.
(XLSX)

S2 Data. List of the viral citrullinated proteins of infected *vs* mock-infected HFFs at 16 hpi and 24 hpi.
(XLSX)

Acknowledgments

We thank Marcello Arsura for critically reviewing the manuscript, and Dr. M. Corazzari and Dr. Romina Monzani (CAAD Center, University of Piemonte Orientale, Novara) for providing reagents and expertise for the experiments with thapsigargin.

Author Contributions

Conceptualization: Selina Pasquero, Francesca Gugliesi, Paul R. Thompson, Santo Landolfo, Marco De Andrea.

Data curation: Selina Pasquero, Francesca Gugliesi, Camilla Albano, Stefano Raviola, Sen Sudeshna, Marco De Andrea.

Formal analysis: Camilla Albano, Greta Bajetto, Linda Trifirò, Bianca Brugo, Qiao Yang, Sen Sudeshna, Leonard Barasa, Hafeez Haniff.

Funding acquisition: Francesca Gugliesi, Matteo Biolatti, Valentina Dell'Oste, Marco De Andrea.

Investigation: Selina Pasquero, Francesca Gugliesi, Camilla Albano, Greta Bajetto, Gloria Griffante, Linda Trifirò, Bianca Brugo, Davide Lacarbonara, Qiao Yang, Sen Sudeshna, Leonard Barasa.

Methodology: Selina Pasquero, Francesca Gugliesi, Matteo Biolatti, Valentina Dell'Oste, Camilla Albano, Greta Bajetto, Bianca Brugo, Stefano Raviola, Sen Sudeshna.

Project administration: Marco De Andrea.

Resources: Paul R. Thompson.

Software: Selina Pasquero, Francesca Gugliesi, Greta Bajetto, Gloria Griffante, Linda Trifirò, Davide Lacarbonara, Qiao Yang, Sen Sudeshna, Leonard Barasa, Hafeez Haniff, Paul R. Thompson.

Supervision: Matteo Biolatti, Valentina Dell'Oste, Paul R. Thompson, Marco De Andrea.

Validation: Selina Pasquero, Francesca Gugliesi, Matteo Biolatti, Valentina Dell'Oste, Stefano Raviola, Sen Sudeshna, Hafeez Haniff.

Visualization: Selina Pasquero, Francesca Gugliesi, Gloria Griffante, Leonard Barasa, Hafeez Haniff.

Writing – original draft: Selina Pasquero, Francesca Gugliesi, Valentina Dell'Oste.

Writing – review & editing: Paul R. Thompson, Santo Landolfo, Marco De Andrea.

References

1. Yousuf W, Ibrahim H, Harfouche M, Abu Hijleh F, Abu-Raddad L. Herpes simplex virus type 1 in Europe: Systematic review, meta-analyses and meta-regressions. BMJ Global Health. 2020; 5: 1–15. https://doi.org/10.1136/bmjgh-2020-002388 PMID: 32675066
2. Rechenchoski DZ, Faccin-Galhardi LC, Linhares REC, Nozawa C. Herpesvirus: an underestimated virus. Folia Microbiologica. 2017; 62: 151–156. https://doi.org/10.1007/s12223-016-0482-7 PMID: 27858281
3. Itzhaki RF. Herpes and Alzheimer's Disease: Subversion in the Central Nervous System and How It Might Be Halted. Journal of Alzheimer's Disease. 2016; 54: 1273–1281. https://doi.org/10.3233/JAD-160607 PMID: 27497484
4. De Chiara G, Piacentini R, Fabiani M, Mastrodonato A, Marcocci ME, Limongi D, et al. Recurrent herpes simplex virus-1 infection induces hallmarks of neurodegeneration and cognitive deficits in mice. PLoS Pathogens. 2019; 15: 1–30. https://doi.org/10.1371/journal.ppat.1007617 PMID: 30870531
5. Krishnan R, Stuart PM. Developments in Vaccination for Herpes Simplex Virus. Frontiers in Microbiology. 2021; 12. https://doi.org/10.3389/fmicb.2021.798927 PMID: 34950127
6. Sadowski LA, Upadhyay R, Greeley ZW, Margulies BJ. Current drugs to treat infections with herpes simplex viruses-1 and -2. Viruses. 2021; 13:1–12. https://doi.org/10.3390/v13071228 PMID: 34202050
7. Badia R, Garcia-Vidal E, Ballana E. Viral-Host Dependency Factors as Therapeutic Targets to Overcome Antiviral Drug-Resistance: A Focus on Innate Immune Modulation. Frontiers in Virology. 2022; 2: 1–17. https://doi.org/10.3389/fviro.2022.935933
8. Cakir M, Obernier K, Forget A, Krogan NJ. Target Discovery for Host-Directed Antiviral Therapies: Application of Proteomics Approaches. mSystems. 2021; 6. https://doi.org/10.1128/mSystems.00388-21 PMID: 34519533
9. Witalisom E, Thompson R, Hofseth L. Protein Arginine Deiminases and Associated Citrullination: Physiological Functions and Diseases Associated with Dysregulation. Curr Drug Targets. 2015; 16:700–10. https://doi.org/10.2174/1389450116666150202160954 PMID: 25642720
10. Mondal S, Thompson PR. Protein Arginine Deiminases (PADs): Biochemistry and Chemical Biology of Protein Citrullination. Accounts of Chemical Research. 2019; 52: 818–832. https://doi.org/10.1021/acs.accounts.9b00024 PMID: 30844238
11. Valesini G, Gerardi MC, Iannuccelli C, Pacucci VA, Pendolino M, Shoenfeld Y. Citrullination and autoimmunity. Autoimmunity Reviews. 2015; 14: 490–497. https://doi.org/10.1016/j.autrev.2015.01.013 PMID: 25636595
12. Vossenaar ER, Zendman AJW, Van Venrooij WJ, Pruijn GJM. PAD, a growing family of citrullinating enzymes: Genes, features and involvement in disease. BioEssays. 2003; 25: 1106–1118. https://doi.org/10.1002/bies.10357 PMID: 14579251
13. Acharya NK, Nagele EP, Han M, Coretti NJ, DeMarshall C, Kosciuk MC, et al. Neuronal PAD4 expression and protein citrullination: Possible role in production of autoantibodies associated with neurodegenerative disease. Journal of Autoimmunity. 2012; 38: 369–380. https://doi.org/10.1016/j.jaut.2012.03.004 PMID: 22560840
14. Sokolove J, Brennan MJ, Sharpe O, Lahey LJ, Kao AH, Krishnan E, et al. Brief Report: Citrullination Within the Atherosclerotic Plaque: A Potential Target for the Anti-Citrullinated Protein Antibody Response in Rheumatoid Arthritis. Arthritis & Rheumatism. 2013; 65: 1719–1724. https://doi.org/10.1002/art.37961 PMID: 23553485
15. Yang L, Tan D, Piao H. Myelin Basic Protein Citrullination in Multiple Sclerosis: A Potential Therapeutic Target for the Pathology. Neurochemical Research. 2016; 41: 1845–1856. https://doi.org/10.1007/s11064-016-1920-2 PMID: 27097548
16. Yuzhalin AE. Citrullination in Cancer. Cancer Research. 2019; 79: 1274–1284. https://doi.org/10.1158/0008-5472.CAN-18-2797 PMID: 30894374
17. Masutomi H, Kawashima S, Kondo Y, Uchida Y, Jang B, Choi EK, et al. Induction of peptidylarginine deiminase 2 and 3 by dibutyryl cAMP via cAMP-PKA signaling in human astrocytoma U-251MG cells. Journal of Neuroscience Research. 2017; 95: 1503–1512. https://doi.org/10.1002/jnr.23959 PMID: 27704563
18. Ishigami A, Masutomi H, Handa S, Nakamura M, Nakaya S, Uchida Y, et al. Mass spectrometric identification of citrullination sites and immunohistochemical detection of citrullinated glial fibrillary acidic protein in Alzheimer's disease brains. Journal of Neuroscience Research. 2015; 93: 1664–1674. https://doi.org/10.1002/jnr.23620 PMID: 26190193

19. Knight JS, Subramanian V, O'Dell AA, Yalavarthi S, Zhao W, Smith CK, et al. Peptidylarginine deiminase inhibition disrupts NET formation and protects against kidney, skin and vascular disease in lupus-prone MRL/ *lpr* mice. Annals of the Rheumatic Diseases. 2015; 74: 2199–2206. https://doi.org/10.1136/annrheumdis-2014-205365 PMID: 25104775

20. Willis VC, Gizinski AM, Banda NK, Causey CP, Knuckley B, Cordova KN, et al. N-α-Benzoyl-N5-(2-Chloro-1-Iminoethyl)-l-Ornithine Amide, a Protein Arginine Deiminase Inhibitor, Reduces the Severity of Murine Collagen-Induced Arthritis. The Journal of Immunology. 2011; 186: 4396–4404. https://doi.org/10.4049/jimmunol.1001620 PMID: 21346230

21. Causey CP, Jones JE, Slack J, Kamei D, Jones LE, Subramanian V, et al. The development of o-F-amidine and o-Cl-amidine as second generation PAD inhibitors. J Med Chem. 2011; 54: 6919–6935. https://doi.org/10.1021/jm2008985.The

22. Falcão AM, Meijer M, Scaglione A, Rinwa P, Agirre E, Liang J, et al. PAD2-Mediated Citrullination Contributes to Efficient Oligodendrocyte Differentiation and Myelination. Cell Reports. 2019; 27: 1090–1102.e10. https://doi.org/10.1016/j.celrep.2019.03.108 PMID: 31018126

23. Muth A, Subramanian V, Beaumont E, Nagar M, Kerry P, McEwan P, et al. Development of a Selective Inhibitor of Protein Arginine Deiminase 2. Journal of Medicinal Chemistry. 2017; 60: 3198–3211. https://doi.org/10.1021/acs.jmedchem.7b00274 PMID: 28328217

24. Lewis HD, Liddle J, Coote JE, Atkinson SJ, Barker MD, Bax D, et al. HHS Public Access. 2015; 11: 189–191. https://doi.org/10.1038/nchembio.1735.Inhibition

25. Arisan ED, Uysal-Onganer P, Lange S. Putative roles for peptidylarginine deiminases in COVID-19. International Journal of Molecular Sciences. 2020; 21: 1–29. https://doi.org/10.3390/ijms21134662 PMID: 32629995

26. Pasquero S, Gugliesi F, Griffante G, Dell'Oste V, Biolatti M, Albano C, et al. Novel antiviral activity of PAD inhibitors against human beta-coronaviruses HCoV-OC43 and SARS-CoV-2. Antiviral Research. 2022; 200: 105278. https://doi.org/10.1016/j.antiviral.2022.105278 PMID: 35288208

27. Casanova V, Sousa FH, Shakamuri P, Svoboda P, Buch C, D'Acremont M, et al. Citrullination Alters the Antiviral and Immunomodulatory Activities of the Human Cathelicidin LL-37 During Rhinovirus Infection. Frontiers in Immunology. 2020; 11. https://doi.org/10.3389/fimmu.2020.00085 PMID: 32117246

28. Trier NH, Holm BE, Heiden J, Slot O, Locht H, Lindegaard H, et al. Antibodies to a strain-specific citrullinated Epstein-Barr virus peptide diagnoses rheumatoid arthritis. Scientific Reports. 2018; 8: 3684. https://doi.org/10.1038/s41598-018-22058-6 PMID: 29487382

29. Pratesi F, Tommasi C, Anzilotti C, Puxeddu I, Sardano E, Di Colo G, et al. Antibodies to a new viral citrullinated peptide, VCP2: fine specificity and correlation with anti-cyclic citrullinated peptide (CCP) and anti-VCP1 antibodies. Clinical & Experimental Immunology. 2011; 164: 337–345. https://doi.org/10.1111/j.1365-2249.2011.04378.x PMID: 21413944

30. Griffante G, Gugliesi F, Pasquero S, Dell'Oste V, Biolatti M, Salinger AJ, et al. Human cytomegalovirus-induced host protein citrullination is crucial for viral replication. Nature Communications. 2021; 12: 1–14. https://doi.org/10.1038/s41467-021-24178-6 PMID: 34162877

31. Bicker KL, Thompson PR. The protein arginine deiminases: Structure, function, inhibition, and disease. Biopolymers. 2013; 99: 155–163. https://doi.org/10.1002/bip.22127 PMID: 23175390

32. U KP, Subramanian V, Nicholas AP, Thompson PR, Ferretti P. Modulation of calcium-induced cell death in human neural stem cells by the novel peptidylarginine deiminase-AIF pathway. Biochim Biophys Acta. 2014; 1843: 1162–1171. https://doi.org/10.1016/j.bbamcr.2014.02.018 PMID: 24607566

33. Cheshenko N, Del Rosario B, Woda C, Marcellino D, Satlin LM, Herold BC. Herpes simplex virus triggers activation of calcium-signaling pathways. J Cell Biol. 2003; 163: 283–293. https://doi.org/10.1083/jcb.200301084 PMID: 14568989

34. Quynh Doan NT, Christensen SB. Thapsigargin, Origin, Chemistry, Structure-Activity Relationships and Prodrug Development. Curr Pharm Des. 2015; 21: 5501–5517. https://doi.org/10.2174/1381612821666151002112824 PMID: 26429715

35. Jamali H, Khan HA, Stringer JR, Chowdhury S, Ellman JA. Identification of Multiple Structurally Distinct, Nonpeptidic Small Molecule Inhibitors of Protein Arginine Deiminase 3 Using a Substrate-Based Fragment Method. 2015.

36. Hartenian E, Nandakumar D, Lari A, Ly M, Tucker JM, Glaunsinger BA. The molecular virology of coronaviruses. J Biol Chem. 2020; 295: 12910–12934. https://doi.org/10.1074/jbc.REV120.013930 PMID: 32661197

37. Martín Monreal MT, Rebak AS, Massarenti L, Mondal S, Šenolt L, Ødum N, et al. Applicability of Small-Molecule Inhibitors in the Study of Peptidyl Arginine Deiminase 2 (PAD2) and PAD4. Frontiers in Immunology. 2021; 12: 1–11. https://doi.org/10.3389/fimmu.2021.716250 PMID: 34737738

38. Vladimer GI, Górna MW, Superti-Furga G. IFITs: Emerging roles as key anti-viral proteins. Frontiers in Immunology. 2014; 5: 1–6. https://doi.org/10.3389/fimmu.2014.00094 PMID: 24653722

39. Mears H V., Sweeney TR. Better together: The role of IFIT protein-protein interactions in the antiviral response. Journal of General Virology. 2018; 99: 1463–1477. https://doi.org/10.1099/jgv.0.001149 PMID: 30234477

40. Li D, Swaminathan S. Human IFIT proteins inhibit lytic replication of KSHV: A new feed-forward loop in the innate immune system. PLoS Pathogens. 2019; 15: 1–27. https://doi.org/10.1371/journal.ppat.1007609 PMID: 30779786

41. Jiang Z, Su C, Zheng C. Herpes Simplex Virus 1 Tegument Protein UL41 Counteracts IFIT3 Antiviral Innate Immunity. Journal of Virology. 2016; 90: 11056–11061. https://doi.org/10.1128/JVI.01672-16 PMID: 27681138

42. Lee CY, Wang D, Wilhelm M, Zolg DP, Schmidt T, Schnatbaum K, et al. Mining the human tissue proteome for protein citrullination. Molecular and Cellular Proteomics. 2018; 17: 1378–1391. https://doi.org/10.1074/mcp.RA118.000696 PMID: 29610271

43. Luganini A, Caposio P, Landolfo S, Gribaudo G. Phosphorothioate-modified oligodeoxynucleotides inhibit human cytomegalovirus replication by blocking virus entry. Antimicrob Agents Chemother. 2008; 52: 1111–1120. https://doi.org/10.1128/AAC.00987-07 PMID: 18180342

44. Bicker KL, Subramanian V, Chumanevich AA, Hofseth LJ, Thompson PR. Seeing citrulline: development of a phenylglyoxal-based probe to visualize protein citrullination. J Am Chem Soc. 2012; 134: 17015–17018. https://doi.org/10.1021/ja308871v PMID: 23030787

45. Tilvawala R, Nguyen SH, Maurais AJ, Nemmara VV., Nagar M, Salinger AJ, et al. The Rheumatoid Arthritis-Associated Citrullinome. Cell Chemical Biology. 2018; 25: 691–704.e6. https://doi.org/10.1016/j.chembiol.2018.03.002 PMID: 29628436

46. Lewallen DM, Bicker KL, Subramanian V, Clancy KW, Slade DJ, Martell J, et al. Chemical Proteomic Platform To Identify Citrullinated Proteins. ACS Chemical Biology. 2015; 10: 2520. https://doi.org/10.1021/acschembio.5b00438 PMID: 26360112

Manuscript #	COMMSBIO-23-2411A
Current Revision #	1
Other Version	COMMSBIO-23-2411-T
Submission Date	19th Dec 23
Current Stage	Under Review
Title	Human cytomegalovirus infection triggers a paracrine senescence loop in renal epithelial cells
Manuscript Type	Article
Collection	N/A
Corresponding Author	Professor Marco De Andrea (University of Turin, Medical School)
Contributing Authors	Dr Stefano Raviola , Dr Gloria Griffante , Dr Andrea Iannucci , Dr Shikha Chandel , Dr Irene Lo Cigno , Dr Davide Lacarbonara , Dr Valeria Caneparo , Dr Selina Pasquero , Dr Francesco Favero , Dr Davide Corà , Dr Elena Trisolini , Professor Renzo Boldorini , Dr Vincenzo Cantaluppi , Dr Santo Landolfo , Dr Marisa Gariglio
Authorship	Yes
Abstract	Human cytomegalovirus (HCMV) is an opportunistic pathogen causing severe diseases in immunosuppressed individuals. To replicate its double-stranded DNA genome, HCMV induces profound changes in cellular homeostasis that may resemble senescence. However, it remains to be determined whether HCMV-induced senescence contributes to organ-specific pathogenesis. Here, we show a direct cytopathic effect of HCMV on primary renal proximal tubular epithelial cells (RPTECs), a natural setting of HCMV disease. We find that RPTECs are fully permissive for HCMV replication, which endows them with an inflammatory gene signature resembling the senescence-associated secretory phenotype (SASP), as confirmed by the presence of the recently established SenMayo gene set, which is not observed in retina-derived epithelial (ARPE-19) cells. Although HCMV-induced senescence is not cell-type specific, as it can be observed in both RPTECs and human fibroblasts (HFFs), only infected RPTECs show downregulation of LAMINB1 and KI67 mRNAs, and enhanced secretion of IL-6 and IL-8, which are well-established hallmarks of senescence. Finally, HCMV-infected RPTECs have the ability to trigger a senescence/inflammatory loop in an IL-6-dependent manner, leading to the development of a similar senescence/inflammatory phenotype in neighboring uninfected cells. Overall, our findings raise the intriguing possibility that this unique inflammatory loop contributes to HCMV-related pathogenesis in the kidney.
External Editor	Assigned
Subject Terms	Health sciences/Diseases/Infectious diseases/Viral infection Biological sciences/Microbiology/Virology/Virus–host interactions
Show Author Information	Allow Reviewers to see Author information.
Research Square author dashboard	I understand that my manuscript and associated personal data will be shared with Research Square for the delivery of the author dashboard.
Preprint Deposition	No, my co-authors and I would not like to benefit from *In Review*
Competing interests policy	There is **NO** Competing Interest.
Applicable Funding Source	No Applicable Funding
Transparent peer review	No, I do not want to participate in transparent peer review
Previous Interactions	None of the above

Human cytomegalovirus infection triggers a paracrine senescence loop in renal epithelial cells

Stefano Raviola,[a,b] Gloria Griffante,[b] Andrea Iannucci,[a,b,#] Shikha Chandel,[b] Irene Lo Cigno,[b] Davide Lacarbonara,[a,b] Valeria Caneparo,[a] Francesco Favero,[c,d] Davide Corà,[c,d] Elena Trisolini,[e] Renzo Boldorini,[e] Vincenzo Cantaluppi,[f] Santo Landolfo,[g] Marisa Gariglio,[a,b,¶] Marco De Andrea,[a,g,¶,*]

[a]Intrinsic Immunity Unit and [c]Bioinformatics Unit, CAAD - Center for Translational Research on Autoimmune and Allergic Disease, University of Eastern Piedmont, Novara, Italy

[b]Molecular Virology Unit, [d]Bioinformatics Unit and [f]Nephrology and Kidney Transplantation Unit, Department of Translational Medicine, University of Eastern Piedmont, Novara, Italy

[e]Pathology Unit, Department of Health Sciences, University of Eastern Piedmont, Novara, Italy

[g]Viral Pathogenesis Unit, Department of Public Health and Pediatric Sciences, University of Turin, Medical School, Turin, Italy.

[#]Current address: Department of Biomedicine and Prevention, University of Rome "Tor Vergata", Rome, Italy

[¶]These authors equally contributed to the study

*Corresponding author

Email: marco.deandrea@unito.it (MDA)

Short Title: HCMV drives cellular senescence

Abstract

Human cytomegalovirus (HCMV) is an opportunistic pathogen causing severe diseases in immunosuppressed individuals. To replicate its double-stranded DNA genome, HCMV induces profound changes in cellular homeostasis that may resemble senescence. However, it remains to be determined whether HCMV-induced senescence contributes to organ-specific pathogenesis. Here, we show a direct cytopathic effect of HCMV on primary renal proximal tubular epithelial cells (RPTECs), a natural setting of HCMV disease. We find that RPTECs are fully permissive for HCMV replication, which endows them with an inflammatory gene signature resembling the senescence-associated secretory phenotype (SASP), as confirmed by the presence of the recently established SenMayo gene set, which is not observed in retina-derived epithelial (ARPE-19) cells. Although HCMV-induced senescence is not cell-type specific, as it can be observed in both RPTECs and human fibroblasts (HFFs), only infected RPTECs show downregulation of *LAMINB1* and *KI67* mRNAs, and enhanced secretion of IL-6 and IL-8, which are well-established hallmarks of senescence. Finally, HCMV-infected RPTECs have the ability to trigger a senescence/inflammatory loop in an IL-6-dependent manner, leading to the development of a similar senescence/inflammatory phenotype in neighboring uninfected cells. Overall, our findings raise the intriguing possibility that this unique inflammatory loop contributes to HCMV-related pathogenesis in the kidney.